Advanced Cure Monitoring and Analysis for Optimization of Thermoset Resin Processes

---

A dissertation submitted in partial fulfillment of
the requirements for the degree of

Doctor of Philosophy

(Material Science)

by

Javier C. Cruz

Adviser:

Prof. Dr. Tim A. Osswald

University of Wisconsin – Madison - 2008

Dissertation: Präzise Kontrolle und Analyse des Aushärtungsvorgangs zur Optimierung der Duroplastharzverarbeitung

(Advanced Cure Monitoring and Analysis for Optimization of Thermoset Resin Processes)

Verfasser: Javier C. Cruz, doctoral dissertation
University of Wisconsin at Madison

Kurzfassung

Die Möglichkeit einer kinetischen Verhaltenskontrolle für Duroplastwerkstoffe wird zur Optimierung von Verarbeitungsbedingungen und zum tieferen Verständnis der im fertigen Teil enthaltenen, endgültigen Materialeigenschaften beitragen. Die Eigenschaften eines Duroplasts sind vom Umsetzungsniveau abhängig, welches wiederum von mehreren Material- und Prozessparametern abhängt, was die Aushärtereaktion zu einem wesentlichen Schritt in der In-Line-Prozesssteuerung macht.

Zur Prozessoptimierung für Duroplaste und deren endgültigen Materialeigenschaften wurden Methoden zur Kontrolle des Aushärtungsvorgangs untersucht. Eine neue Methode wurde entwickelt, die sich durch die Verwendung eines dispersiven Raman-Systems mit kontaktfreier Optik auszeichnet. Die zur Anwendung gebaute Ausrüstung besteht aus einem Druckreaktor, in dem die Aufheizgeschwindigkeit einer kleinen Probe durch ein auf kleine Veränderungen in der Probetemperatur reagierendes Regulierungssystem gesteuert wird. Die Reaktion wird gleichzeitig durch Aussenden eines Laserstrahls in die Kammer kontrolliert. Der Reaktionsvorgang einer ungesättigten Hochleistungspolyestermasse (Pultrusionsqualität) mit einem Epoxidharz (Beschichtungsqualität) wurde mit dem so entwickelten System kontrolliert. Beim Durchlauf ungesättigter Polyester DSC Proben ergab sich eine nichtsteuerbare Überhitzung. Dagegen wurden die Überhitzungseffekte minimiert bzw. beseitigt, als der gleiche Werkstoff in der konstruierten Kammer erprobt wurde.

Die Auswirkungen von Druck auf Reaktionsgeschwindigkeiten und endgültige Materialeigenschaften wurden untersucht. Die Druckerhöhung führte bei der Reaktion von ungesättigten Hochleistungspolyestern zu einer Konkurrenzwirkung auf die Reaktionsgeschwindigkeit. Die endgültigen Materialeigenschaften zeigen ein ähnliches Verhaltensmuster. Bei den Epoxidharzen wurde die Reaktionskinetik durch Druck beschleunigt; dennoch wurden keine Unterschiede in den endgültigen Materialeigenschaften festgestellt.

Darüber hinaus wurde durch die Anwendung von Aushärtungskontroll- und –optimierungstechniken eine spezielle Anwendung zur Imprägnierung von Holz entwickelt. Diese Anwendung setzt eine genaue Aushärtungsregelung für die erfolgreiche Funktion voraus. Das für dieses Verfahren gewählte Material war ein Epoxidharz auf Linsensaatbasis. Dieser neue Werkstoff ist für imprägnierende Anwendungen noch nie ausgewertet worden. Es ergaben sich synergetische Holz-Harz-Wirkungen, die im Verbund zu weitaus überlegeneren Eigenschaften führten, als die eigenen der Einzelmaterialien. Wesentliche Erhöhungen hinsichtlich Härte und Moduls wurden für die imprägnierten Teile erreicht. Obwohl weitere Untersuchungen zur Anwendung abgeschlossen werden müssen, lässt die Anwendung von Aushärtekontrolle und -optimierung die Holzimprägnierung durch Epoxidharz auf Linsensaatbasis als eine realisierbare Technik erscheinen, wodurch die Eigenschaften von Weichholz auf das Niveau von Harthölzern angehoben werden können.

Abstract

Being able to monitor the kinetic behavior of thermosetting materials will aid in the optimization of processing conditions and in understanding the final material properties obtained within a part. The properties of thermosets are a function of the degree of conversion, which itself is a function of multiple material and process variables, making the curing reaction an essential stage to control during processing.

Cure monitoring methods developed for the optimization of thermoset processes and final mechanical properties were studied. A new method consisting of the use of a dispersive Raman system with non-contact optics has been developed. The equipment built for the application consists of a pressure reactor in which the heating rate of a small sample is controlled with a control system that reacts to direct changes in sample temperature. Simultaneously, reaction is monitored by emitting a Raman laser into the chamber. The reaction progress of accelerated unsaturated polyester pultrusion grade resin and coating grade epoxy resin was monitored with the developed system. When running unsaturated polyester DSC samples uncontrollable overheating was obtained. In contrast, when the same material was tested with the designed chamber, overheating effects were minimized or eliminated.

Effects of pressure on reaction rates and final mechanical properties were studied. For accelerated unsaturated polyester reactions, increasing pressure resulted in a competing effect on the reaction rate. The final mechanical properties exhibited a similar behavior. For epoxy, reaction kinetics were accelerated by pressure, although no final mechanical property differences were determined.

Furthermore, using cure monitoring and optimization techniques, a special wood impregnation application has been developed. In this application, precise control of the curing behavior is essential for the process to work successfully. A linseed based epoxy resin was the material selected for the process. This new resin has never been evaluated for impregnation applications. It was found that synergistic effects between the wood and the resin lead to far superior properties as a composite than as individual materials. Substantial hardness and modulus increases were obtained for impregnated parts. Although more research has to be completed for the application, using cure monitoring and optimization techniques, made impregnation of wood with linseed epoxy resin a viable technique to greatly improve properties of softwoods to the level of expensive hardwoods.

Schlagwörter: Aushärtungskinetik, Duroplaste, Raman-Spektroskopie, DSC

keywords: Curing Kinetios, thermosets, Raman –Spektroskopy, DSC

Acknowledgements

First of all, I would like to thank God for his guidance through all these years of work and for giving me the strength to do my best. I also want to thank my family, especially my parents Carlos and Nilda for all unconditional support they have always offered me in anything I have attempted to do.

I would like to thank my wife Migna for all her support and for accepting to leave from beautiful Puerto Rico and move to Wisconsin to help me pursue my dream. She has always been there for me and I could not be more grateful.

I would like thank my professor, advisor and friend Tim Osswald whom I have great respect and admiration both as a professional an individual. Tim has been a mentor to me in these changing periods of my life and has provided an excellent example of how to balance family and obligations.

I would like to thank my PhD committee, Prof. Lih-Sheng Turng, Prof. A. Jeffrey Giacomin, Prof. Xiaochun Li, and Prof. Padma Gopalan for all their time and continued support. I would also like to thank the GERS program for their financial support, and the companies and individuals from, Teel Plastics, Kaiser Optical Systems, Forest Products Laboratories and IF Technologies that were willing to provide us with materials, equipment and personal knowledge to make this research possible.

I am very grateful for all my friends with whom I have learned to enjoy Madison and the cold weather, especially Pedro and Betsy for being like a family for me and my wife here in Madison. I have been blessed to be able to meet so many great people within the college of engineering and all the members of the Polymer Engineering Center. I would like to thank Diana Rhoads for all her help which she willingly provided from the first day I entered the Materials Science Program.

I would like to thank all my friends who spent their extra time revising this dissertation and providing input and ideas throughout all my years here at UW. In addition, I would like to thank the undergraduates, Steven K. Esch, Andrea Emmons, Moritz Ruoff, Stefanie Knauf and Rob Pickens for their efforts.

I have been blessed to have met so many wonderful people these last four years which unfortunately are too many to list, but luckily know who they are.

Table of Contents

List of Abbreviations

α_I	Kinetically Controlled Region
α_{II}	Accelerated Reaction Period
α_{III}	Diffusive Reaction Period
BMC	Bulk Molding Compound
BORR	Based-on-Renewable-Resource
C=C	Carbon-Carbon Double Bond
C_p	Heat Capacity
DDM	4,4′-Diaminodiphenylmethane
DGEBA	Di-Glycidyl Ether of Bisphenol A
DMA	Dynamic Mechanical Analysis
DSC	Differential Scanning Calorimetry
E’	Youngs Modulus
EP	Epoxy
FTIR	Fourier Transform Infra-Red
HPLC	Performance Liquid Chromatography
H_v	Vickers Hardness
IR	Infra- Red
LIM	Liquid Injection Molding
LN_2	Liquid Nitrogen
MEK-P	Methyl ethyl ketone peroxide
MMA	Methyl Methacrylate
N-IR	Near Infra-Red
PMMA	Polymethyl Methacrylate
PP	Polypropylene
$R^{\bullet}$	Free- Radical
RTM	Resin Transfer Molding
SEC	Size Exclusive Characteristic

SEM	Scanning Electron Microscopy
SMC	Sheet Molding Compound
SYP	Southern Yellow Pine
TBA	Torsion Braid Analysis
TBPB	Tert-Butyl Perbenzoate
TC	Thermo Couple
TEPA	Tetraethylenepentamine
TETA	Triethylenetetramine
T_f	Furnace Temperature
T_g	Glass Transition Temperature
TGA	Thermal Gravimetric Analysis
T_gT_p	Conversion-Temperature-Property Diagram
TMA	Thermal Mechanical Analysis
T_s	Sample Temperature
TTT	Time-Temperature-Transformation (isothermal)
UP	Unsaturated Polyester
UV	Ultra Violet

List of Figures

List of Tables

1 Introduction

Thermosets may be defined as a polymeric material where individual polymeric molecules have been joined through covalent bonds within particular regions on the molecules. Covalent bonds may be created by energetically exciting other polymeric molecules, end-groups, specific functional groups or by use of monomers. The joining of the molecules, also known as cross-linking, produces a unique behavior that leads to their name “thermo-set”. These materials have a much higher thermal stability than thermoplastics because the rigidity of the macrostructure is maintained through links between the polymers that prevent flow of molecules past each other. As seen in Figures 1-1 and 1-2, when testing a thermoset under shear or tension, as the temperature is increased the decrease of shear modulus or tensile strength is not as significant as with thermoplastics.

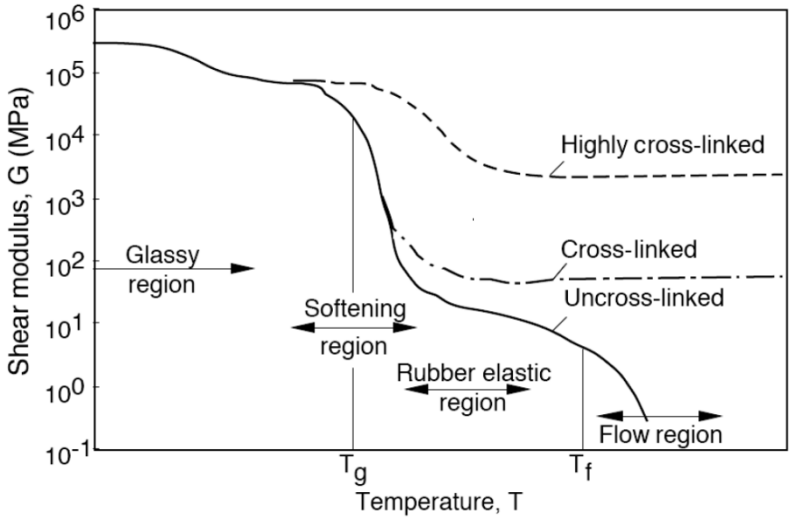

Figure 1-1. Shear modulus as a function of temperature for uncross-linked and cross-linked polymers [1].

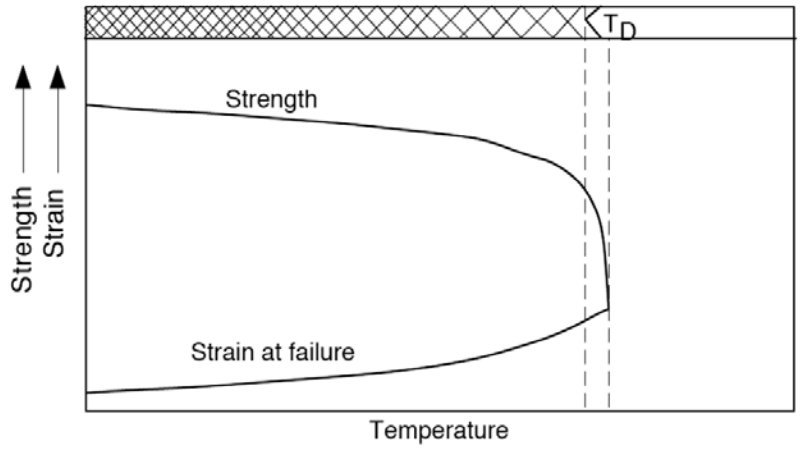

Figure 1-2. Tensile strength and strain at failure as a function of temperature for typical thermosets [1].

At higher temperatures, energy within molecules increases, i.e., mobility increases, leading to greater material deflection but being one big macro-molecule, flow is not possible. For the general case, if a thermoset is maintained well under the thermal degradation temperature, as cross-link density increases the less notable are the reductions in mechanical properties due to temperature increase. Other unique characteristics that make thermosets very attractive for many high-end applications include their bonding capabilities, strength, thermal and chemical stability, and minimal creep. Unfortunately, these excellent physical and chemical properties are dependent on the processing conditions and on the cross-linking reaction occurring during the process.

Before presenting thermosets used in structural engineering applications, it is worth mentioning that over 50% of thermosets are not applied for engineering uses but are processed for other specific methods such as gluing, spraying, powdering, coating, varnishing, impregnation, and agglomeration. A large portion of the polyurethanes,

accounting for approximately 20% of all thermosets are foamed [2]. As illustrated in Figure 1-3 unsaturated polyester and epoxy resins account for only 20% of the production market.

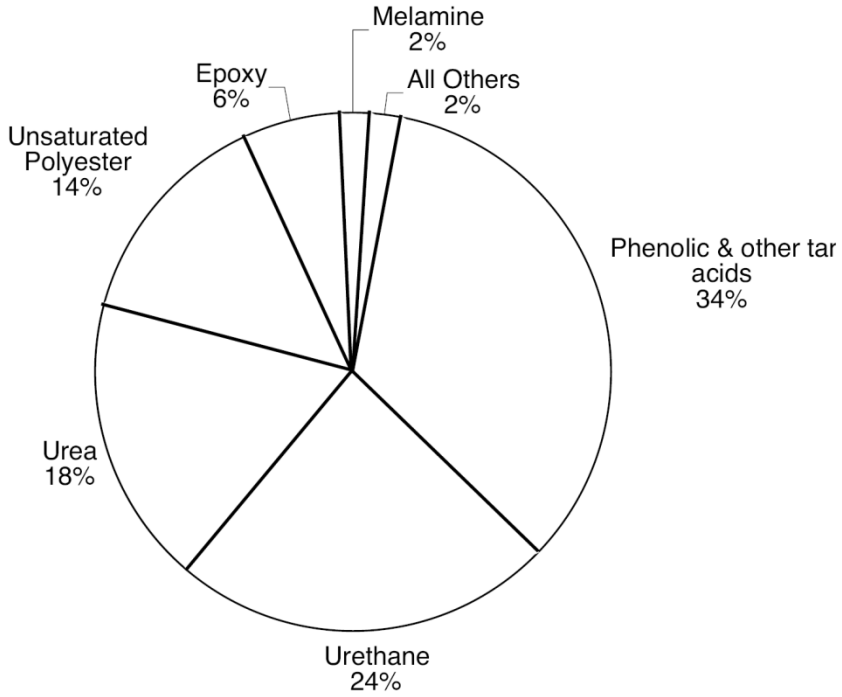

Figure 1-3. Break-down of US thermoset production into common types [1].

In order to better understand thermoset applications it is appropriate to include the various consumer market sectors. Table 1-1 provides market share distributions for thermosets estimated in 2003 [2].

Table 1-1. Market shares for eight main thermoset application sectors

Market	% Market Share
Paints, adhesives, cements	53
Automotive and transportation	14
Building and civil engineering	7
Electricity and electronics	7
Furniture and bedding	7
Consumer goods	4
Mechanical and industrial	2
Packaging	1
Others	5

Small changes may be noted within five years but not as significant as to make the general distribution inaccurate. Thermoset application sectors are significantly different than that of thermoplastics. It is estimated that one of the biggest market sectors for plastics is packaging, accounting for about 40% of all plastics made. For thermosets, packaging only accounts for about 1% of the market. The largest thermoset market sector is found on solutions and emulsions such as paints, adhesives and cements. Setting aside this market sector, the other large thermoset applications are found in transportation, civil engineering and electronics. As with plastics, thermosets are not used as a single substance but they are always combined with other substances in order to obtain the desired properties. Resins may contain different additives to work as, stabilizers, shrinkage controllers, toughening agents, lubricants, flame retardants, adhesion improvers, conductivity modifiers, and mechanical property enhancers. When considering structural applications, most thermoset resins are used as matrix or binding material for high-strength fibers such as glass, carbon, and aramid fibers to form a composite structure. The benefit of a composite structure is that they will typically

combine the ductility, forgiveness and toughness of a matrix with the load carrying capability of the reinforcing material.

As a composite structure, thermosets may provide a very strong and consistent material leading to parts with incomparable strength-to-weight ratios [3, 4]. When analyzing a composite structure the properties of the fibers or reinforcing material itself may easily be identified since fibers are stable throughout most processes. However, due to the curing reaction occurring around them by the matrix, which itself is very dependent on processing conditions, the parts properties also become very dependant on processing parameters. Since the excellent properties of composites are attained through the synergistic effect of the combination of materials, the resin, also known as the matrix or adhesive material, becomes key in the final mechanical properties. Three inter-related elements may be shown to influence the performance of a resin: its own strength obtained through intrinsic material characteristics, the degree of cure and the interaction or bonding strength between the resin and the fibers. Good consistency of the matrix is obtained by creating a well mixed low void resin base and by applying an adequate and stable process. This will provide desired properties through efficient matrix interaction and a well cross-linked molecular structure.

Some of the most common methods for processing thermosets include compression molding, resin transfer molding (RTM), extrusion, liquid injection molding (LIM) and for some special cases injection molding. Some thermosets such as melamine-phenolics are prepared in such a way that they may be formed into granules and injection molded, but

for the most common cases, thermosets are found to be in liquid to high-viscous liquid state. All these processes have unique benefits and are particular to the applications and the type of resin being processed. For example, sheet molding compounds (SMC) and bulk molding compounds (BMC) are prepared by combining sheets or chopped fibers with the resin creating a high viscous paste which may then be compression molded and heat cured into particular geometries. Therefore, each process is designed to tailor individual material characteristics of the different thermosetting composites available today. As there are numerous processes for curing thermosets, there are plenty of options available for thermoset materials.

Figure 1-4 illustrates approximate market shares of the main composite matrices including polypropylene (PP), a thermoplastic that has also been vastly used as composite matrix material [2].

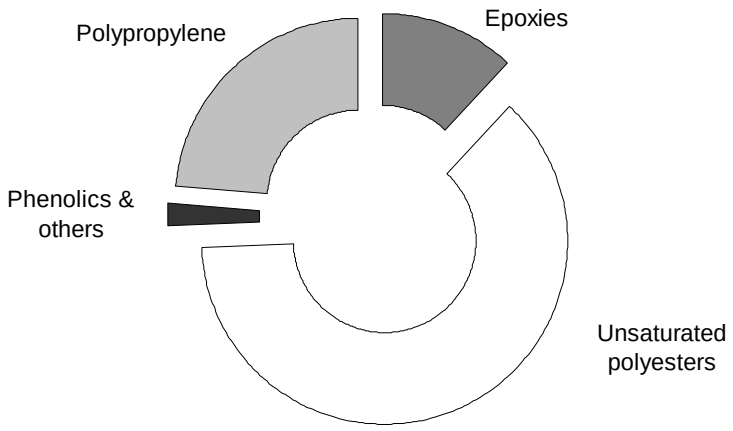

Figure 1-4. Market shares for some of the main composite matrices.

This figure is an estimate and may vary according to different geographical regions and is constantly evolving with time. Numerous matrices as well as reinforcing materials are constantly being developed for composites, including materials made from renewable resources and even biodegradable materials. One of these new materials recently developed in Germany is an epoxy resin based on linseed extract, known as a BORR (Based-on-renewable-resource) resin. Chapter 5 will introduce the new material and present a unique application for the resin. As demonstrated in Figure 1-4, two of the main thermosets used as composite matrices are unsaturated polyester (*UP*) and Epoxy (*EP*). This research will be focused on the study of these two materials. *UP* and *EP* are thoroughly described in section 2.2. Both unsaturated polyester and epoxy posses excellent properties. The properties of any particular resin vary widely based on the different formulations, curing agents and cross-linking density, but for the general case, mechanical and thermal properties of epoxies are typically higher as compared to *UP*, but the price tag is higher too. Table 1-2 provides a comparison of some basic properties of *UP* and *EP*. A key benefit of epoxies is their lower water absorption, especially for applications where parts will be exposed to high humidity environments or immersed in water. For such applications *UP* usually requires the use of gel coats and other protective coatings to repel the water from the material which in turn, induces additional costs. Table 1-3 shows a comparison of resin versus key additive prices. As may be observed, not only the price of the epoxy is higher, but the hardener is usually as much as twice the price of the resin.

Table 1-2. Basic Properties of unsaturated polyester and epoxy resins [5, 6].

		Material	
Properties	ASTM	Unsaturated Polyester	Epoxy
Tensile Modulus (MPa)	D638	2070 – 4140	2415 – 5520
Tensile Strength at Break (MPa)	D638	4.1 – 90	30 – 90
Flexural Strength (yield) (MPa)	D790	60 – 160	90 – 145
Elongation at Break (%)	D638	< 2.6	3 – 6
Deflection Temperature under flexural load, °C, 1.82MPa	D648	60 – 200	50 – 290
Water Absorption 24hr (%)	D570	0.15 – 0.6	0.08 – 0.15

Table 1-3 Comparative prices between resins and additives [5, 6].

Polymer	Resin Cost $/lb (€/kg)	Additive	
		Type	Cost $/lb (€/kg)
Epoxy	3.6 – 18 (5 – 25)	Hardener	14 – 29 (20 – 40)
Unsaturated polyester	0.7 – 5 (1 – 7)	Gelcoat	1.4 – 22 (2 – 30)
		Styrene thinner	5 – 5.8 (7 – 8)
		Wax	14 (20)

In order to prolong shelf-life most resins will provide separate curing or hardening agents. Although depending on the application one-component systems are also very common. When considering a process, time is cost. Therefore, the reduction of steps during the process will reduce overall costs. A basic example of this situation is BMC parts where everything including resin, curing agents, stabilizers, reinforcing material, and other additives have all been prepared together as a one-component system.

For any thermoset system there will be a time in the process that the material has to be reacted in order to create the cross-linked molecular structure. This curing period is

critical because it will not only affect your process but also the final mechanical properties of your part. Creating alternatives to monitor cure will help understand and control these complicated curing behaviors. Molecules may inter- and intra-connect generating very unique performance characteristics such as higher temperature range and minimal creep. The curing process is highly dependent on the processing environment (time, temperature, pressure, and concentrations). Not only processing conditions, but also geometry of the part may play a significant role in cure. For example, variations in thicknesses will cause changes in the heat transfer and release, affecting the reaction rates and curing times. Final mechanical properties, chemical resistance and long-term behavior of thermosets are dependant on the degree of cure. Therefore, a thorough understanding of the curing process has to be met to assure excellent quality of the parts. This brings us to the core of this research.

The properties of thermosets are a function of the degree of conversion which itself is a function of the initiators, catalysts, thickness, heating rate and other process conditions making the curing reaction an essential stage to control during processing. Not only is it important to monitor and control the curing during the reaction stages but also the degree of cure of the final part. A part that is not properly or fully cured results in inferior properties and may also contain harmful monomers that will slowly diffuse out of the part. In general, a thermoset will have a higher strength if it has reached full conversion. For example, a standard unsaturated polyester resin has been determined to produce a ratio of 2:1 styrene to unsaturated polyester [7]. Conditions can be altered by increasing or decreasing the concentration of styrene monomer and adjusting the pressure and

temperature. An excess of styrene causing a larger monomer ratio will lead to a brittle part.

Many methods are constantly being developed to monitor, understand and control curing reactions. The objective of this research will be to address methods of monitoring curing reactions for a pultrusion grade unsaturated polyester and a standard coating grade epoxy. A Raman spectroscopy method for curing analysis has been implemented in order to better control highly accelerated curing reactions. The method may be applied to monitor many different thermosetting reactions and may allow for online reaction monitoring. Properties of the materials at different processing conditions will also be addressed. Also, a wood impregnation process for a new linseed based epoxy resin will be developed by studying the curing stages of the material.

Chapter 2 presents a literature review and discusses the general aspects of thermoset cure. The chapter will cover the materials studied and some of the many curing analysis methods that are being used today including their benefits and pitfalls. The issue of the need for monitoring techniques will be addressed and a detailed description of the two monitoring techniques used in this research (Raman Spectroscopy and Differential Scanning Calorimetry) will be presented.

Chapter 3 will introduce the monitoring method of Raman Spectroscopy. The chapter will begin providing a set of preliminary results obtained by differential scanning calorimetry (DSC) that describe a basic overheating problem found when monitoring

highly accelerated curing reactions—the problem that created the interest of designing an accurate cure monitoring device. The chapter will include the design and creation of a reaction vessel designed to be used in conjunction with Raman equipment for cure monitoring. Section 3.4 will describe the spectra for *UP* and *EP* and illustrate how cure monitoring by gathering spectra in time may be performed. Finally, the chapter will conclude by providing curing analysis results obtained by our Raman cure monitoring system, comparing them to DSC results and presenting various applications where using such a system might be beneficial.

Chapter 4 begins providing some background information of previous research addressing the topic of pressure effects on the curing reaction. Following the review, results for pressure effects on the curing of our highly accelerated *UP* resins and coating grade epoxy are reported. The chapter proceeds to describe how the reactor vessel designed for cure monitoring was modified to create samples for mechanical testing. Pressure effects on final mechanical properties of *UP* and *EP* resins are presented. The chapter concludes by describing some of the benefits of understanding cure in order to apply such information into curing diagrams and models.

Chapter 5 presents a real world application where it is necessary to fully understand the curing process and material behavior in order to make an efficient process. The chapter will introduce with the motivation and some background information that will aid in understanding the complexity and variability of the process. A short description of the BORR resin used for the application will be included. The development of the

impregnation process will be described including DSC and viscosity analyses used to determine the process window. The chapter ends with results from the infiltration process, mechanical testing results for the samples, and a proposal for directions of future research on the topic.

Chapter 6 summarizes the conclusions of the research reported on this dissertation.

2 Cure Monitoring of Thermosetting Materials

2.1 Thermoset Cure

The term curing of thermosets refers to the action of creating a network polymer from individual polymeric chains and/or monomers. When curing happens a macro-molecule is formed. Figure 2-1 depicts the basic difference between a thermoplastic and a thermoset. As seen, thermoset polymeric molecules have been inter-connected.

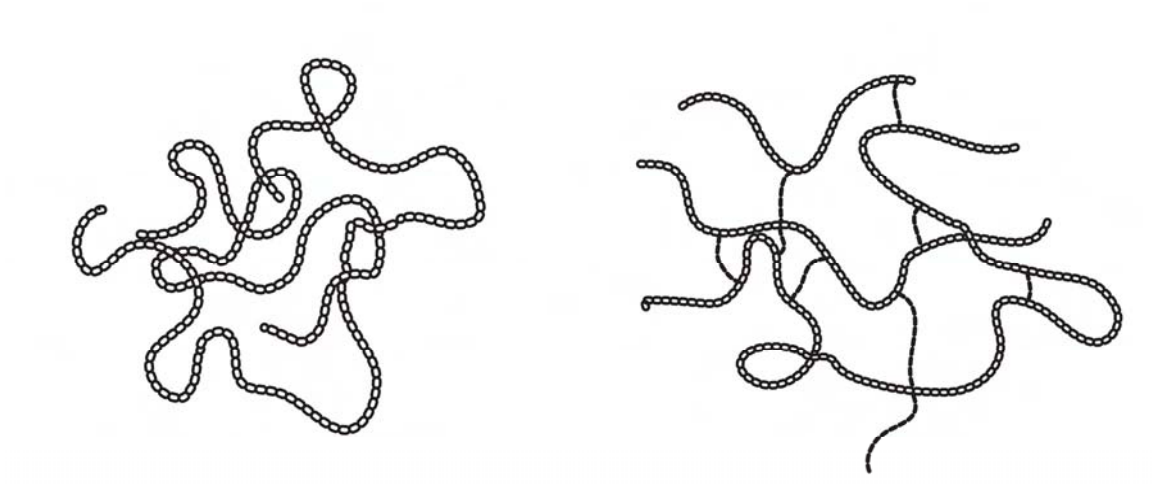

Figure 2-1. Simplified representation of the molecular configurations of a thermoplastic (left) and a thermoset (right).

These networks may be formed through the same polymeric material or by reaction with a different monomer or polymeric species. It is all dependent on the chemistry and the reactive sites available within molecules. The molecular structure of a thermoset

possesses distinctive benefits, but creating it involves a great understanding of the kinetics of the material and of all the variables that affect the process.

Temperature, time and mass are critical variables to consider when dealing with polymeric reacting systems. The temperature dependence of thermoset reactions, for all intents and purposes, behaves in a traditional Arrhenius relationship [6]. Consequently, it can be assumed that temperature of the material will have much influence on the curing rate. The solidification process of most thermosets such as unsaturated polyester, phenolics, epoxies and polyurethanes is governed by an exothermic chemical reaction [8] where usually some kind of monomer or functional cross-linking agent bonds the polymeric molecules together through branches known as cross-links. Reaction kinetics for any chemical require some sort of excitation of the molecules to induce the breaking of a chemical bond followed by a release of energy to bond with a neighboring molecule. The most basic energy absorption mechanism used in most thermosetting reactions is induced heat, but other methods such as UV-radiation are also common. Activation energy has to be surpassed to initiate the reaction process. If the release of energy for bonding is greater than the energy absorbed to break the initial bond sites (activation energy), which is the usually the case for most commercially available thermosets, a negative activation volume [9] or high releases of energy (exothermic heat) are created within the part [10, 11]. This excessive heat generation that is proportional to the conversion of reactive sites in time and the low conductivity of the polymer, greatly increases the glass-transition (T_g) and viscosity hindering the final cure. Many times this effect also leads to high shrinkage and internal stress build-up [12-14]. For these reasons

the mass of material becomes critical during cure. If heat cannot be released because material thickness is too large, variations in heat between the center and walls of the part will occur. In many cases the temperature in the center of the part will continue to rise causing excessive overheating. As shown, curing directly affects the properties of your final part therefore a thorough understanding of the reaction is necessary when developing and working with such materials.

Most thermoset reactions can be described as nonlinear step-growth or chain-growth polymerizations. Step polymerizations refer to reactions that occur simultaneously between mutually reactive functional groups within your mixture. Step-polymerizations include polycondensation and polyaddition reactions. Examples of materials that undergo these types of cross-linking polymerizations include multifunctional phenol, urea or melamine to formaldehyde, multifunctional amines to epoxy and polyurethanes. The term multifunctional is the key to the creation of a cross-linked structure. The greater the functionality, the easier it will be to create a higher cross-link density within the structure. Molecular functionality refers to the number of reactive moieties per mole of reactant [6]. In other words, a molecule that has a functionality of two has the potential to react at two different points (reactive sites). Cross-linked non-linear step polymerizations occur by reacting molecules with functionality greater than two [15].

In order to understand the basic difference between a step-growth versus a chain-growth polymerization it is beneficial to consider a standard linear polymerization process. Figure 2-2 provides an illustration. As demonstrated in the figure, for a group of bi-

functional (f=2) monomers reacting together there will be a greater options for reactions to occur between monomers on a step-growth polymerization due to the kinetic behavior of the different polymerization mechanisms. On a step-growth reaction there are two different ways to create a tetramer or a pentamer. Three different reaction steps can create a hexamer and a heptamer, and so forth. In contrast, during chain-growth polymerizations the monomers can only react with active sites forcing the reaction to proceed by only one method.

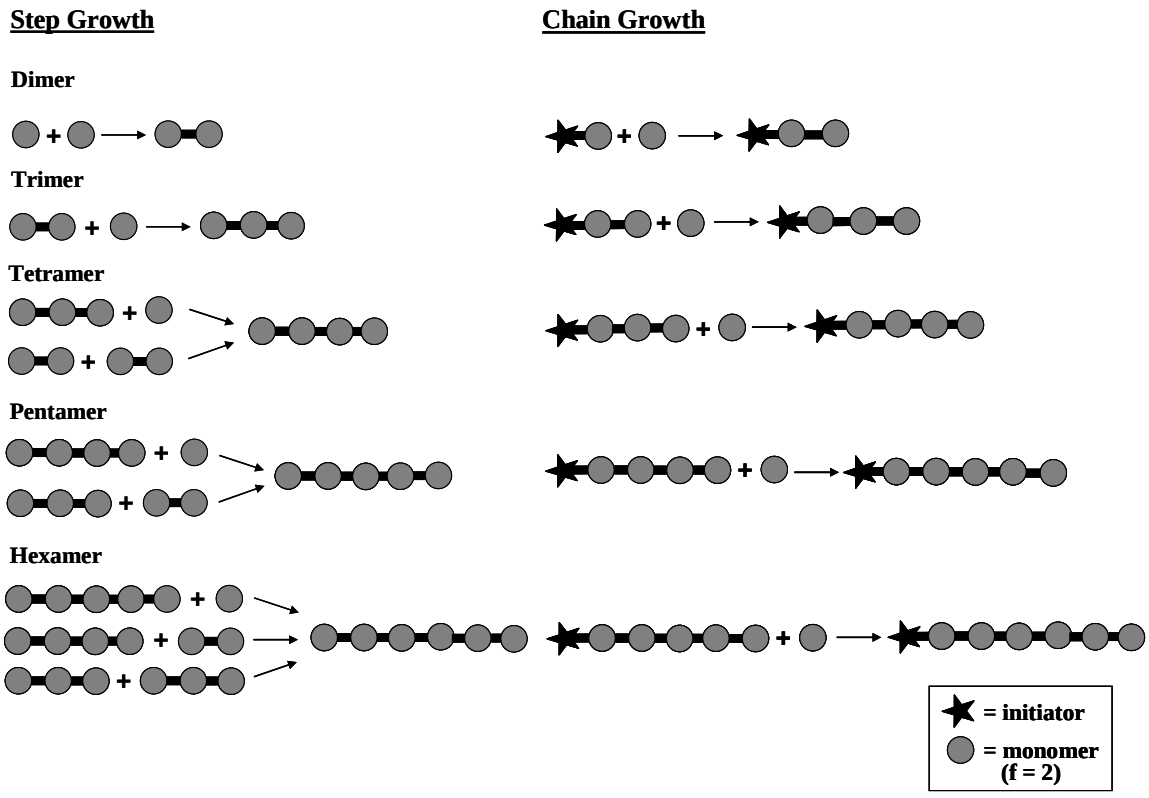

Figure 2-2. Comparison between a step-growth and chain growth polymerization.

The same relations are observed for molecules reacting by non-linear cross-linking polymerizations. For chain-growth, only initiated molecules could join to other molecules to create cross-links. Conversely, during step-growth reactions, like those found in epoxies, any two functional groups could react with each other. The most common chain-growth polymerizations are free-radical reactions. An example for these is unsaturated polyester resin cross-linked with styrene. During chain-growth polymerizations monomers react with functional groups activated by an initiator. An electron transfer occurs during the initiation step, activating the molecule, and inducing further reaction propagation. Reaction rates on these materials are dependent on the amount of free radicals present in solution. The general understanding of the basic reaction mechanisms undergone for unsaturated polyester and epoxy resins will provide a better understanding of the behaviors of these materials observed during this research. Whether an initiation step is required or the reaction occurs naturally, reactive systems have been created in such a way that there can be some control over the curing of the material. For this reason, many thermosets may react within a certain period of time after reactive species are mixed together. The field of thermoset materials is extensive. Therefore, the presented research has been focused on two of the most common types of resins. Resins which are liquid prior to cure and react by heat absorption, and slower reacting liquid resins which activate when reactive substances are mixed together.

2.2 Materials

2.2.1 Unsaturated Polyester

Unsaturated polyesters (*UPs*) are usually produced by a condensation polymerization of dicarboxilic acids, glycols and anhydrides of dicarboxilic acids[16]. In general the *UP* structure varies, but will be defined by the repetitive carbon-carbon double bond between carbonyl groups. *UP* polymers have number average molecular weights within the range of 800-3000 units. A generalized representation of the *UP* structure may be seen on Figure 2-3(a).

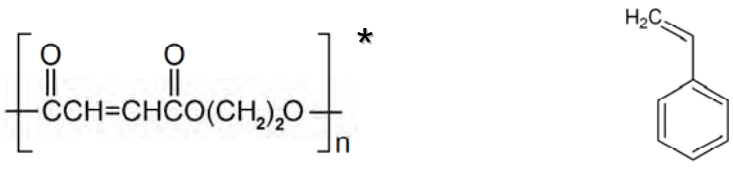

(a) **(b)**

Figure 2-3 (a) Generalized structure for an unsaturated polyester molecule before cross-linking. (b) Styrene molecule: Active site is the C=C bond external to the ring.
***general form: *UP* structures vary**

Unsaturated polyesters co-polymerize with monomers having olefinic unsaturation much more rapidly than they homo-polymerize. Therefore, most *UPs* are used as mixtures with reactive, usually liquid monomers [6]. *UP* polymeric molecules are typically cross-linked by the use of a styrene monomer (Figure 2-3(b)) in a free radical co-polymerization.

Styrene has the benefits of having a low cost, of polymerizing very actively with *UP* both at room temperature and at elevated temperatures, and of having a low viscosity. Other monomers that are used to induce co-polymerization of *UPs* and their respective applications are shown on Table 2-1.

Table 2-1. Examples of some non-styrene monomers used in *UPs* [6].

Monomer	Application
Methyl methacrylate (MMA)	Enhanced weather resistance
Butyl acrylate (BA)	Enhanced weather resistance
Butyl methacrylate (BMA)	Enhanced weather resistance
Alpha methyl styrene (AMS)	"Cooler" cure, reduced exotherm
Vinyl toluene (VT)	Less volatility, higher flash point
Para-methyl styrene (PMS)	Less volatility, higher flash point
Diallyl phthalate (DAP)	Very low volatility, prepregs
Diallyl isophthalate (DIAP)	Very low volatility, prepregs
Octyl acrylamide (OAA)	Solid monomer, molding compounds
Trimethylol propane triacrylate (TMPT)	UV and electron beam cures
Triallyl cyanurate (TAC)	High heat deflection
Triallyl isocyanurate (TIAC)	High heat deflection
Diallyl maleate (DAM)	High heat deflection
Diallyl tetrabromophthalate	Fire retardance

For the case of commercial unsaturated polyester, the resin refers to the complete combination of components into one batch. These components will include the *UP*, the styrene that also acts as diluent to control the initial viscosity, and any additives including shrinkage controllers, flame retardants, dyes and stabilizers. The resin may be a one or two-component system, but in general, most resins are two-component systems in order to extend shelf life. One part consists of the batch resin while the other component contains the precursor, initiator or catalyst. For most resin systems the initiator is a

peroxide molecule. A basic illustration of the cross-linking polymerization is described on Figure 2-4.

(a) **(b)**

Figure 2-4. (a) Schematic of the cross-linking reaction between styrene and unsaturated polyester initiated by a free radical. (b) Schematic of the network formation after certain amount of cross-linking has occurred.

When the initiator is heat activated a free radical ($R^{\bullet}$) forms which may interact with the unsaturated carbon double bonds (C=C) in *UP* and styrene molecules creating new radicals. These new free radicals can then react with other C=C sites propagating the reaction and creating junctions that will lead to a cross-linked network. Termination steps may occur in several ways: by joining two styrene radicals, by joining of a styrene and *UP* radical, by joining a styrene or *UP* radical with an initiation radical or by fully reacting the monomer.

The ratio of unsaturated polyester to styrene becomes very important in the curing of the material and affects the properties of the final part. Most general purpose resins have ratios of styrene to *UP* double bonds ranging from 2-4. This does not mean that there is an absolute control over the styrene to *UP* ratio during cross-linking, but only that the theoretical ratios have been estimated during the preparation of the resin. Many times, due to external processing conditions, materials have to be tested by trial and error to find the optimal mixing ratio that will provide the desired properties within the part. In general, there are combinations of situations that may occur. Some single styrene molecules may create bridges between *UPs*. In other places two or three molecules may be found. On some instances, styrene molecules may simply create branches which terminate and never join to another *UP* molecule. It has even been proposed that for high styrene concentrations, regions of low molecular weight polystyrene may be formed [17] and for low styrene concentrations, joining of *UP* molecules may occur without styrene [18].

For this research a pultrusion grade unsaturated polyester resin (COR31-DA-470) from Interplastic Corporation provided by Teel Plastics, Inc. has been used. Our *UP* pultrusion grade resin was made through a combination of maleic anhydride, poly(ethylene terephthalate), and a mix of glycols and determined to have been diluted in 30% styrene by weight. Pultrusion processing conditions require fast reactions to achieve optimal properties as soon as the material exits the die. Hence, three different initiators were used to perform the reaction. The first initiator is di-(4-t-butylcyclohexy)peroxydicarbonate known as Perkadox 16, with initiation temperatures between 45°C-95°C. This low

temperature initiator assures that the reaction will begin at a low enough temperature in order to reach the gel point fast enough to maintain better structural rigidity of the part during fiber impregnation. The second initiator was a mixture of 75% tert-amyl-peroxy-2-ethylhexanoate and 25% butyl benzyl phthalate known as Trigonox 121-BB75, with initiation temperatures between 85°C-125°C. The third initiator was t-butylperoxy benzoate known as Trigonox C, a high temperature initiator covering the range of 135°C-170°C. By the combination of these three initiators the whole temperature range in which the *UP* Resin will cure during pultrusion process is covered and reactions will be highly accelerated. For a second set of experiments, that would help validate the results with data from Skrifvars [19], MEK-P provided by Jamestown Distributor was used as an initiator. MEK-P with a reaction range between room temperature and 130°C allowed for slow, controlled and well monitored reactions.

2.2.2 Epoxy

Epoxy (*EP*) resins are usually composed of short polymeric molecules, known as oligomers, containing a minimum of two epoxide groups and a respective curing agent. The curing agent, also known as the hardener, is commonly an amine. Amines will react with the epoxide functional groups through a ring-opening addition polymerization. Due to the size of the oligomers and the high functionality of most systems, hardened epoxies may come to be very compact and densely cross-linked structures.

An epoxy resin may contain cyclic or internal epoxide groups, but most of the time they are found to be terminal. Figure 2-5 presents two of the most common epoxide groups found in epoxy resins. These are terminal glycidyl groups and 1,2 epoxy.

Figure 2-5. Molecular structure of a glycidyl group (left) and 1,2 epoxy (right)

An example of an epoxy that possesses internal epoxide groups is the BORR resin studied in chapter 5. Such a material which contains at least two internal epoxide groups will cross-link by attaching molecules internally to one another immediately creating branches that may extend into cross-linked networks. In contrast, for bi-functional terminal group epoxies the hardener is the key material in creating the cross-links. Hardeners are required to have functionalities greater than two in order to generate branching that may lead to cross-linking.

The epoxide resin diglycidyl ether of bisphenol-A (DGEBA) is one of the most common epoxide resins, and is produced by the reaction of bisphenol-A with epichlorohydrin in the presence of sodium hydroxide. The general structure of the DGEBA is shown on Figure 2-6.

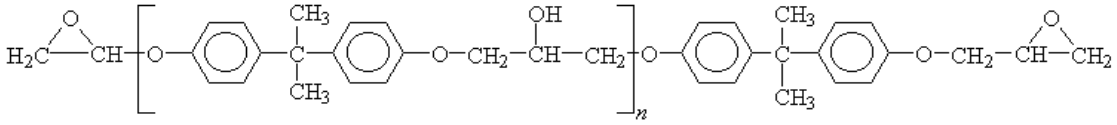

Figure 2-6. DGEBA molecular structure showing polymeric repeating unit '*n*'

Variations of standard bisphenol-A resins are common. One familiar modified bisphenol resin that is also widely used, which is based on bisphenol-F, is shown on Figure 2-7.

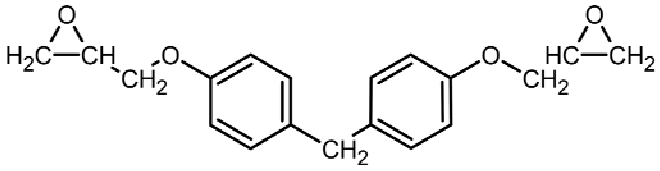

Figure 2-7. Molecular structure of bisphenol-F based resin

It may be noticed that there is a higher degree of complexity for DGEBA as compared to a standard *UP* resin. *EP* resins are constantly made with very different molecular structures in order to achieve the appropriate chemistry for the application. The variation in molecular structure provides their unique characteristics. Depending on the molecular structure, formulations may be available as both liquids and solids. Epoxies are similar to vinyl esters with reactive sites at either end. However, in the epoxy resin, the reactive sites are formed by epoxy groups, like those shown on Figure 2-5, instead of ester groups. The benefit of having epoxide groups rather than ester groups may be seen in the increased water resistance of epoxy. It can also be noted that for DGEBA the repeating unit contains two ring groups which provide better mechanical and thermal behavior as

compared to linear groups. Backbone rings such as these generally give very good stiffness, toughness and heat resistant properties. DGEBA possesses a functionality of two (the two epoxide rings on the ends). Therefore, in order to obtain a cross-linked structure it is required that the hardener be of functionality of three or higher. For this reason, is that usually molecules such as secondary amines are used as hardeners. By attaching two epoxide sites to each amine site highly complex three-dimensional structures can be formed. Primary and secondary amines are highly reactive with epoxy. Tertiary amines are generally used as catalysts, commonly known as accelerators for cure reactions.

Figure 2-8 shows the molecular structure of 4,4'-bis-(diaminodiphenyl) methane (DDM), a secondary amine commonly used as hardener for DGEBA resin. Other very widely used amines are triethylenetetramine (TETA) and tetraethylenepentamine (TEPA). In many situations TETA and TEPA are used to form aliphatic polyamines that have excellent electrical and chemical resistance. For DDM, the functional sites are the two hydrogen atoms on each amine leading to four reactive sites. Provided the right energy for reaction to advance, nitrogen groups will interact with the epoxide rings opening them and creating new bonds as illustrated on Figure 2-9.

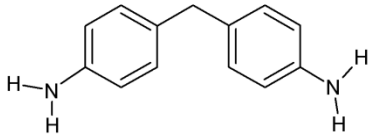

Figure 2-8. Molecular structure of 4,4'-bis-(diaminodiphenyl) methane (DDM)

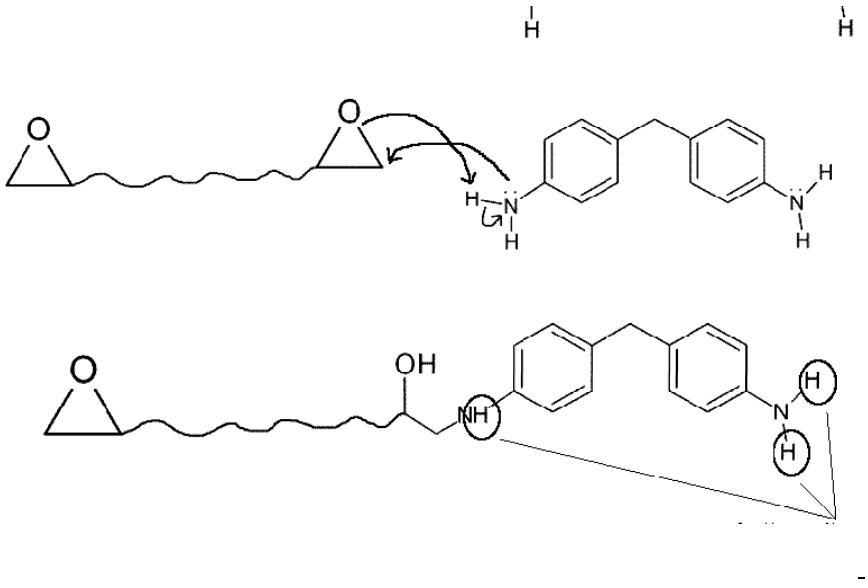

Figure 2-9. Single reaction step of DGEBA to DDM

As illustrated, a single hydrogen is consumed leaving three more available to create a highly cross-linked structure. As the cross-linking process is occurring amine molecules co-react with epoxides in a fixed ratio, therefore, it is crucial that the correct mix ratio is obtained between resin and hardener. Incorrect ratios will lead to unreacted resin or

hardener left within the solid material which will be detrimental to the final properties of the part.

In most cases, epoxy resins and their respective curing agents form low viscosity systems prior to cure. *EP* may be cured at various temperature ranges usually ranging from 5°C to 180°C. The curing temperature and rate is very dependent on the hardener used. Curing may occur very fast leading to high exotherms and large temperature rises. One of the most advantageous properties of epoxies is their low shrinkage during cure, which minimizes composites fabric 'print-through' and residual stresses.

Most of the various methods to cure *EP*s are also dependant on the hardener used. The main curing agents used for epoxies may be divided into three categories: Compounds with active hydrogens, ionic initiators and hydroxyl coupling agents [20]. Active hydrogens include the previously described amine (DDM). Amines are usually used in room temperature curing but many other applications are also seen. Table 2-2 includes some examples of various amines including polymeric amines used for cure.

Table 2-2. Hardening amines [6, 20-22]

Compound	Description
Ethylene diamine	Fast curing, low viscosity
Diethylenetriamine	Fast curing, low viscosity
Hexamethylene diamine	Slower curing, needs elevated temperature, flexible materials
Diethylaminopropylamine	Elevated temperature cure, adhesives
Menthane diamine	Elevated temperature cure, long potlife
Tetraethylenepentamine (TEPA)	Ambient-slow cure, high viscosity
Triethylenetetramine (TETA)	Ambient-fast cure, low viscosity
N-aminoethyl piperazine	Fast Curing
Polymercaptopolyamines	Used in combination with customary amine hardeners [23]
Olefin oxide polyamine adducts	Fast curing, low toxicity
Glycidyl ether polyamine adducts	Fast curing
Ketimines	Low viscosity, long potlife, latent hardening catalysts
Polyethylene-polyamine	Fast curing, high viscosity, flexible adhesives
4,4′-Diaminodiphenylmethane (DDM)	Mid-to-High temperature cure, high viscosity, chemical resistant materials
4,4′-Diaminodiphenylsulfone (DDS)	Very high temperature cure, high viscosity, chemical resistant materials

Ionic curing includes cationic and anionic polymerizations. Anionic curing is not so common in industry due to the usual slow rate of cure and inferior final material properties as compared to other methods [20]. Quite the opposite, cationic polymerizations may be very fast and have therefore gained great interest in industry. Hydroxyl groups are also rather varied. Phenols and organic acids are some examples, although these are usually not used as individual curing agents. Both are mainly used as reactive accelerators for other curing agents. Another example which has been used very successfully for curing epoxy resins are cyclic anhydrides [6]. Anhydride hardeners are increasingly found in aerospace and electronic applications. Cure with anhydrides

generally exhibits epoxies with improved high-temperature stability and excellent physical and electrical properties [22]. In electronics, these formulations are used to encapsulate electronic parts which are sensitive to shock, abrasion, temperature and moisture. Another consideration is the cure temperatures of these materials which should not be as high as to damage the object being encapsulated. Since most anhydrides cure relatively slow and require high temperature for cure, catalysts which permit faster and lower temperature curing are used [24].

As with unsaturated polyesters, epoxies may be cured by various methods being heat and room temperature mixing most common for composites. Due to the wide use of epoxies in coatings, adhesives and printing inks curing by ultraviolet light is also very common. The main benefit of photo-initiated cures is the extremely fast polymerization. Often reactions can be completed within less than one second [25]. Besides photo curing, curing with γ-rays and electron beams is an alternative. Another type of accelerated curing that has gained great interest in the aerospace and microelectronics applications is microwave cure. The main benefit of microwave curing is that energy is directly absorbed by the resin without the need of heat transport as with thermal curing, requiring less energy and time for cure.

Epoxies find uses as adhesives, caulking compounds, casting compounds, sealants, varnishes and paints, as well as laminating resins for a variety of industrial applications. The largest application for *EP* is currently in coatings. Epoxy resin coatings are designed to adhere to many kinds of surfaces. Their increased adhesive properties and resistance to

water degradation make these resins ideal for use in boat building applications. Epoxies generally out-perform most other resin types in terms of mechanical properties and resistance to environmental degradation, which leads to their increased use in aircraft components [26]. This also leads to their extensive use in many other composite applications. Epoxies are corrosion resistant and have excellent resistance to many chemicals including acids, bases, organic and inorganic solvents, salts, and other chemicals [20].

Final mechanical properties of epoxy resins can be traced back to the processing conditions, hardeners and monomers used to create them. The resin properties depend on the chemistry and flexibility of the segments, the cross-linking density and the percent conversion. For purposes of this research we will limit our cure study to a general purpose epoxy resin commonly used in composite structures and as a coating for boat-building applications. The resin is a two-part epoxy provided by West System, Inc. Part-A-105 resin is a bisphenol-A type epoxy resin including less than 20% bisphenol-F based resin. Part-B-205 hardener consists of a combination of commonly used hardeners such as those mentioned on Table 2-2 including, polyethylene-polyamide, TETA, TEPA, and certain reaction products with these. A 5:1 ratio of resin to hardener is suggested with curing temperatures around 25°C. Initiator activation temperature range is between 0°C-32°C when fully mixed.

2.3 Cure Monitoring Techniques

The desire to be able to monitor and understand reaction processes has been a subject that has always been very important in chemical industries. Reactions are very sensitive to processing parameters and slight variations can drive a reaction the wrong way. A temperature and pressure miscalculation or a difference in stoichiometric ratios may significantly change your products. Not to mention any impurities or uncontrolled reaction rates that can lead to huge faults. No different should be considered the case of reacting thermoset materials. Thermoset materials undergo a chemical reaction in order to create a molecularly cross-linked structure. Processing conditions, such as temperature, pressure and concentration, all affect the chemical reaction taking place. In addition, the degree of cross-linking, which is dependent on the reaction, affects the final properties of a part. Being able to monitor and control the curing process taking place will help obtain steady and positive results.

During cure, thermosetting resins exhibit three distinct phases: viscous liquid, gel, and solid. Each phase is marked by dramatic changes in thermo-mechanical properties of the resin [27]. As reaction occurs two competing effects happen simultaneously: viscosity reduction due to temperature rise and viscosity rise due to rise in the T_g of the sample as it cures. When the material reaches the gel-point (gelation), it may be considered as a high molecular weight network and consequently, viscosity reaches infinity. As the reaction progresses the material continues to react, and the T_g increases, creating a solid rigid structure after which the final conversion occurs as a diffusion controlled process—

a well observed stage if monomers take part in the reaction [12]. Physical and chemical changes are simultaneously occurring as the material cures. These changes may be evaluated by using different techniques currently on the market. Most of the techniques have not been directly designed to be used for monitoring a curing reaction, but due to the inherent changes occurring within the material as it cures they have been found to be very effective for this application.

The first stage of a curing reaction, where the material is reacting as a viscous liquid, may be studied by using rheometers. As the curing progresses the viscosity will increase and this increase may be related to the percent conversion increase. For such an evaluation a determination of cure at gelation or another key point in the reaction has to be determined or the data cannot be related to an actual conversion value. In most cases, viscometers are used to study cure when the property of interest is not the percent conversion. A good example is the optimization of an impregnation process, like the one described in chapter 5, where the property of interest is not the actual percent cure but the viscosity value and gelation point of the material as it cures. Any rheometer could potentially be used with thermosets if it allows for multiple data collection in time but it is important to consider that some may be permanently damaged since the material is reacting and viscosity is increasing until eventually reaching the gel-point and hardening. Therefore, cone-plate rheometers are recommended because they permit the use of a small sample size that may be cleaned-up much easier. Haake rotational viscometers have also been successfully used but require larger sample sizes. Since most commercially available thermosets

undergo exothermic reactions the larger sample size may lead to variations in temperature within the sample and undesired sample overheating.

Another method that has recently been used to study the cure of resins below gelation is high performance liquid chromatography (HPLC). The method allows the cure to be followed by determining the appearance or disappearance of reactive materials. The main drawback of the method is the tedious sample preparation which requires special dilutions that are dependent on the material being reacted. It has been shown by Dopico-Garcia et al., that HPLC may be used to monitor the reaction of bisphenol-A based epoxy resin by following the disappearance of epoxy monomer using the area of the DGEBA chromatographic peak [28]. They were also able to show how the method may not only be used for monitoring the pre-gel state of the reaction but the whole curing until full conversion. A demonstration of how the method may be used to determine extent of residual monomers was also discussed. The basis of the method consists of two steps. For the pre-gel state, size-exclusion chromatography may be used to track monomer consumption. After gelation, material has to be reacted prior to analysis and reaction inhibited by liquid nitrogen cooling. Dilution is done on samples with different cure times then reversed-phase HPLC using a UV-detector may be used to compare the samples against each other. Residual monomers can be determined in a similar way, by extraction of the monomer in the final part using a chloroform methanol mixture. As it may be expected, the post-gelation material analysis is very tedious with this method. For that reason, other methods such as spectroscopy are preferably considered to analyze the later stages of the reaction.

After gelation occurs within the material, the visco-elastic properties come about while further hardening occurs. Physical and chemical properties are still rapidly changing at this state and as a result, additional properties may be evaluated. Dynamic mechanical analysis (DMA) [29-32] and Torsion braid analysis (TBA) [33-35] are examples of some methods commonly used to determine cure properties post-gelation. A benefit of these methods is that with the proper preparation technique they may also be used to determine key properties of the pre-gel and post-gelation states such as the transition into gelation and glass transition temperature (T_g).

TBA is a method that has been very well studied and characterized by John K. Gillham for characterizing cure and properties of thermosetting composites [34, 35]. With TBA a key benefit is the high sensitivity due to the use of a freely oscillating torsion pendulum. With this resonance technique, measurements are made at the resonant frequency of the pendulum. The technique is able to determine minor material transitions versus temperature and follow small changes in moduli versus time. Both DMA and TBA are excellent in following the gelation and vitrification which are the main events encountered in the curing of thermosets.

DMA dynamically tests the mechanical response of a sample. As the sample cures, the loads required to create a certain very small plastic deformation increase and may be related to the cure of the sample. Tests such as tension, compression, and bending may all be performed. TBA works in a similar manner but only under torsional loads. TBA

method is specific for resins which may be impregnated on a braid. Considering that most thermosetting resins are low viscosity before cure, when gelation occurs, a sudden increase in mechanical properties may be observed which may easily be tracked by these systems. Unfortunately, due to the low viscosity of the resin, DMA tests usually have to be done by creating a composite structure by impregnating a braid or working with fiber filled materials. In these cases a baseline of the properties of the structural material itself must be created. In any case, actual percent conversion is not always needed, but the mechanical properties obtained during cure are. With DMA, the mechanical properties can be directly monitored to assure that the process is providing the necessary mechanical properties for your application. Cho, et al. [32] demonstrated how the DMA method may be very accurately used to determine cure percentages, based on variations in storage modulus. Their samples consisted of glass braids impregnated with resin. They also demonstrated the capacity of the DMA for determining T_g by monitoring changes in tan δ. It is usually more common to use DMA to determine final overall properties for systems that have been reacted under varying conditions. Cure time for pre-cured composites that have already been prepared as a highly viscous solid such as pre-preg, SMC or BMC sample, is also common. Samples for such cases will require minimal preparation and generally, the overall composite response is the variable of interest. An example where DMA was used to monitor the final cure properties of a standard DGEBA/TETA epoxy with different stoichiometric ratios of hardener was published by Wu et al [29]. They reported that DMA has been found to be more sensitive in monitoring T_g than differential scanning calorimetry (DSC) and explained how DMA

may be used to compare the effects of diverging from theoretical stoichiometric ratios on the properties of the material.

The final step of the reaction, when the material has reached very high conversions and is highly cross-linked is also individually studied. As previously mentioned HPLC has been used to characterize this region by looking into any residual monomers. Mechanical testing methods (DMA, TBA) are also used by performing post-cure and verifying if any significant increase in properties is noted. Spectroscopy (individual spectra) and thermogravimetry analysis (TGA) are two other methods widely used for these cases. In a highly reacted part curing is hindered due to the solid state of the material and reduction in mobility of the already cross-linked molecules. A slow curing is sustained through a diffusion controlled process. With any type of spectroscopy method used vibrations particular to specific molecular bonds are detected and may be used to determine concentrations of unreacted species. Spectroscopy techniques generate a spectrum of the material that may be considered unique to that material. In the spectrum, every peak corresponds to vibration created by a molecular bond, which may be used to identify the complete molecules. By looking at particular peaks in the spectrum residual substances may be identified.

When using TGA, volatile species that remain unreacted will be released under the heat imposed and an estimation of residual substances can be generated. TGA is also used to monitor the curing reaction but this application is not very common. Monitoring the extent of reaction with TGA is limited to materials that release by-products during

reaction such as phenolics that undergo a condensation reaction where the rate of release of water may be followed through the mass loss of the sample and related to the cross-linking rate.

All the methods previously discussed provide very good information on the property changes during cure and allow an estimation of the percent cure. Unfortunately, since some material properties are dependent on more than one variable these methods may not be accurate. For example, mechanical properties of resins vary with composition and any change in composition will affect the results. Also, some of the methods previously described, such as viscometers, may not be used to monitor all the reaction stages of the material. As for approximating cross-linking percent (i.e. a chemical change) to property changes, many times, the chemical reactions are not linearly related to the physical variation. In addition, an interest that has been growing significantly is the ability to do online or real-time cure monitoring which is not possible with these lab-scaled methods. For these reasons, other monitoring techniques are considered more appropriate for the intended cure monitoring application. Some examples of these include dielectric measurements, differential scanning calorimetry (DSC) and a variety of different spectroscopic techniques. For purposes of this research two monitoring techniques, Raman spectroscopy and DSC have been selected and will be described in depth in sections 2.3.2 and 2.3.1 respectively. Both analysis methods directly relate to molecular behavior (conversion). DSC is a laboratory technique which based on the number of publications is considered the most popular technique for monitoring exothermic curing reactions. Raman, although not as popular, has gained much interest in recent years

because of new technological developments which have made it more affordable. The main benefit of Raman in this research is the sensitivity to carbon-carbon double bonds consumed during the unsaturated polyester reaction and the possibility, of under certain circumstances, using Raman spectroscopy as an online cure monitoring device.

Dielectric cure monitoring involves monitoring changes in the viscosity (hardening) of a thermosetting resin system through variations in the dielectric properties of the material. Therefore, dielectric cure monitoring does not directly relate to the chemical conversion. It is still very popular due to the ability of using remote dielectric sensors that allow for real-time measurements to be made in actual processing environments such as presses, autoclaves, and ovens. A relatively new application which is becoming well accepted consists of adapting the measurement devices to control systems so that a thermoset tool can communicate with press controls. This technology is now used in injection and compression molding units where sensors are flush mounted onto the surface of the tool and cure cycles can be optimized on a shot to shot basis [36].

In order to understand the dielectric cure monitoring technique it is important to understand how electrical current is transferred through materials. A dielectric material is a “non-conducting” substance. Dielectric materials have high resistivity (impedance, for alternating current), which is resistance to the flow of current. Essentially, a dielectric measurement is done by measuring the voltage and current between a pair of electrodes in order to determine the conductance and capacitance between those electrodes. For dielectric cure monitoring, the conductance of the material is the variable of interest.

Conductance is a measure of the ability of a material to “carry” or transfer an electrical current, which is the inverse of resistance. Ions carry electrical charges through materials. Since almost all materials contain ions, when a voltage is applied between electrodes, the electric field created will create an orientation on these ions. Mobility of the ions will be dependent on the viscosity of the material. Ionic movement is essentially easier through a low viscosity media. It takes time to displace molecular dipoles into the field direction. The more viscous the surrounding medium, the longer it takes. Ions encounter viscous drag as they flow through a medium densely packed with molecules. In other words the higher the viscosity the higher the resistivity. The resistivity or impedance can therefore be directly related to the viscosity and relative cure degree. One important detail of dielectric measurements is that after the material has reached gelation dielectric technique continues to provide reliable information for tracking the cure. During a cross-linking polymerization there is still molecular mobility occurring, even if it is a diffusion controlled process for the later stages of the reaction. This molecular movement keeps affecting ionic motion which may be detected through the dielectric monitoring. As a result, with proper interpretation, dielectric measurements are useful throughout the entire cure; not only for determining changes in viscosity and rigidity, but also, for determining the end of cure and kinetic cure parameters. Kalenda [37], demonstrated how it is possible to obtain kinetic parameters that can be used in curing models from electrical resistance measurements on an unsaturated polyester resin.

Spectroscopic techniques have been previously mentioned as a way to determine residual monomers or other unreacted substances in your part. Although, there is much more to

these techniques than simply looking at the fully cured samples. Spectroscopic methods may be used to monitor the whole reaction and provide a real insight of the cross-linking reaction at the molecular level including reactant consumption in time, material identification, and tracking of materials consumed and formed in a reaction. Spectroscopy itself may be described as the science of measuring and describing the emission and absorption of different wavelengths (spectra) of visible and non-visible light on materials. Due to the vast range of light frequencies covering the whole electromagnetic spectrum, spectroscopic methods have been subdivided among the frequency region covered. Spectroscopy has traditionally been used in the physical sciences to determine composition and concentration of materials ranging from individual atoms to complex molecular structures. Spectroscopy can essentially be done using most wavelengths in the electromagnetic spectrum (Figure 2-10) although energy level at the different frequencies will result in very different effects on matter. Table 2-3 provides examples of some different spectroscopic techniques covering the different regions of the electromagnetic spectrum. On the lower side of the spectrum, the larger wavelengths (or smaller wavenumber; wavenumber being the inverse of the wavelength) do not have much energy to create a significant change in the molecular vibrations, rotations or translations.

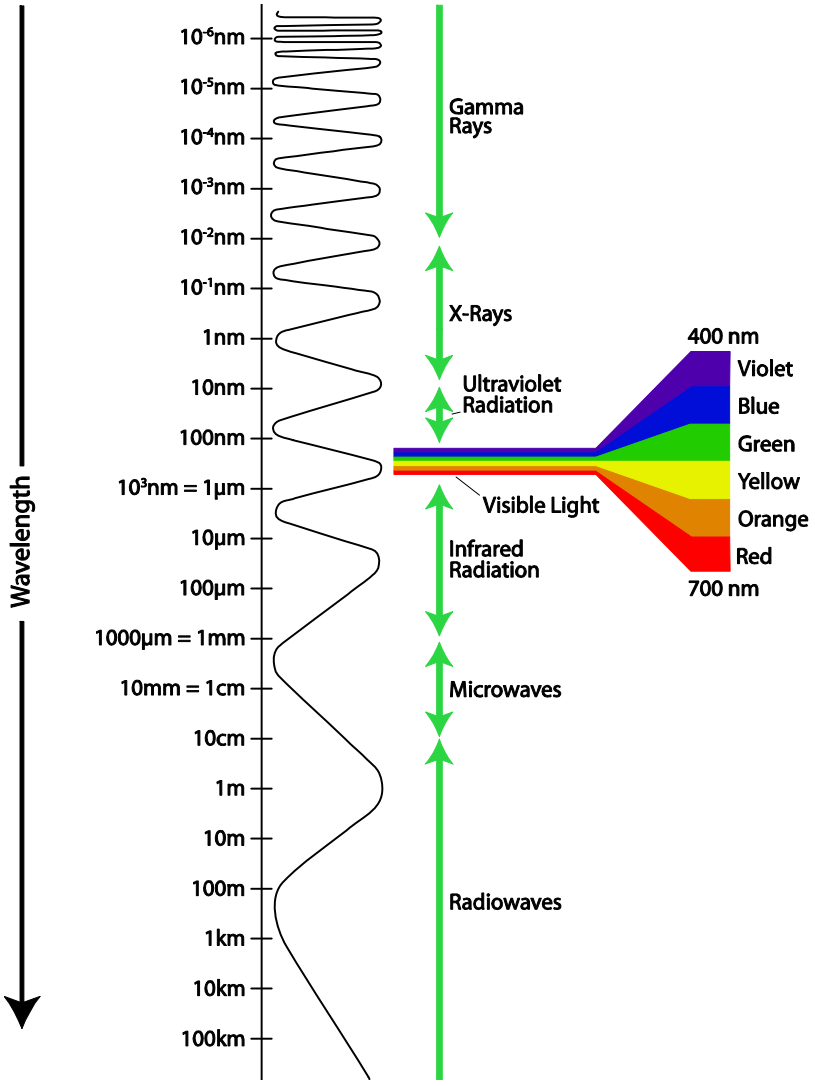

Figure 2-10. Electromagnetic Spectrum [38]

Similarly on the other side of the spectrum for example for the case of X-rays, wavelengths are so small that the higher frequencies (energy) can be strong enough to cause an ejection of inner-shell electrons in atoms. For these reasons, depending on the application and what is desired to be obtained, the proper wavelength regions have to be studied. For purposes of cure monitoring and in terms of necessity, cost, and ease of use, the infrared region has been found to be most effective.

Table 2-3. List of various spectroscopic techniques

Technique	Remarks
X-ray Fluorescence Spectrometry (XRF)	High energy, ejection and transfer of electrons causing secondary x-ray emission
Energy-dispersive Spectrometry (EDS)	High energy, secondary x-ray emission, qualitative or quantitative assessment
Ultraviolet-visible Spectroscopy (UV-vis)	wavelength range from UV to visible, 200 to 700 nm, energy causes electronic molecular transitions
Color Spectroscopy	Measures reflected visible wavelength range 360 to 750 nm on material, used for measurement of colors, fading, pigment identification
Near infrared spectroscopy (near-IR)	Measures IR wavelength absorption near visible-red region. Enough energy to penetrate tissue with no harmful effects
IR spectroscopy and Fourier transform infrared (FTIR) spectroscopy	Mid-infrared region, wavenumber range 4000 to 600 cm -1; absorption spectrum, Lower energy to induce low frequency mode vibrations
Raman Spectroscopy	Visible, near infrared, or near ultraviolet range. Inelastically scattered light spectrum; vibrational, rotational, and other low-frequency modes

Infrared spectroscopy has gained great popularity in the analytical sciences because the amounts of energy are not excessive leading to the generation of stable low frequency modes on molecules. The absorption of infrared (IR) radiation (wavelengths above ~ 1 μm) distorts a dipole in the molecule, inducing molecular vibrations with energy shifts. These modes are usually described as rotational and vibrational stretching, bending, and rocking motions between bonded molecules. The term vibration is mostly used when analyzing the molecular motions. Since the energy levels are low, energy imparted into the sample during testing does not induce any adverse effects. A low incident energy system, also means, less complex lower priced systems. Therefore, for most material analyses, infrared spectroscopy is usually considered as a first step to more complete

identification using other techniques. In polymeric cure monitoring, IR is also one of the most popular spectroscopic techniques and due to the vast use as an analysis system today, databases have been built in order to ease the spectral identification analysis from the user.

An IR system works by passing a beam of infrared light through the sample. Examination of the transmitted light reveals how much energy was absorbed at each wavelength. This can be done with a monochromatic beam, which changes in wavelength over time, or by using a Fourier transform (FTIR) instrument to measure all wavelengths at once. FTIR separates superimposed waves using Fourier transformations allowing for faster spectral creation and improvement in sensitivity, since all wavelengths are collected simultaneously and averaged together. Most modern infrared spectrometers are FTIR instruments. After the transmittance or absorbance intensities have been collected for each wavelength a spectrum can be produced. Peaks in the spectrum show at which IR wavelengths the sample absorbs and the absorptions at these different energy levels are particular to the vibrational energy of the molecules. As a result the spectrum of absorptions may be used as a chemical “fingerprint” to identify the sample. By generating multiple spectrums in time and monitoring spectral changes, molecular changes such as cross-linking may be easily followed. Similar to IR, Raman spectroscopy is also analyzed in a similar manner although it relies on inelastic scattering, or Raman scattering of the incident light imparted on the sample, rather than the transmittance and absorbance of light by the sample. Raman scattering may be seen with visible, near infrared, or near ultraviolet light, but usually, infrared light is used. Both IR and Raman should be

considered complimentary. In general, based on the theory behind the analysis and generation of the spectral data, when IR has a weak sensitivity Raman has good intensity.

2.3.1 Differential Scanning Calorimetry (DSC)

Heat cured thermosetting resins undergo an exothermic chemical reaction during cure. The quantity of heat released is particular to the amount and rate at which bonds are being consumed in time. In other words, reacting molecules release energy (heat) and the amount of energy released based on the activation energy of the molecules will be representative for that particular bond. During a curing reaction there is a high concentration of reacting molecules therefore, the heat released at a given time is basically the sum of the amount of heat being released by each and every one of the molecules that are cross-linking. This total heat in time also known as the rate of heat released is proportional to the amount of molecules bonding, i.e. the cure percent. Differential scanning calorimetry has the ability to quantify this amount of heat release providing an analysis value that is directly related to the consumption of molecular bonds in the reaction. The benefit of having a monitoring technique that creates a direct relation of the monitored variable to the cross-linking, but that does not require any direct understanding of the molecular behavior, has made DSC the most common method of monitoring curing reactions.

Figure 2-11 depicts the inside components of a DSC equipment. The main components of a DSC system are the sample and reference, the heat sensors (thermocouples), and the temperature control system.

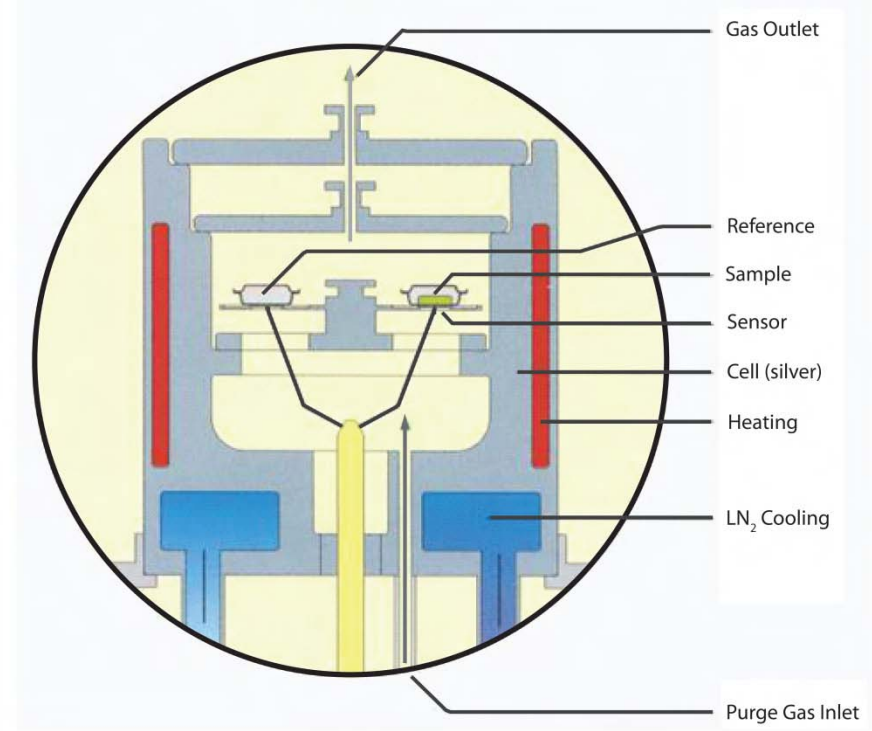

Figure 2-11. Netzsch Thermal Analyzer – NETZSCH – Geratebau; Illustration of the DSC system used for this research. Note the position of the sensors, furnace and cooling lines.

The name differential scanning calorimetry basically describes the functionality of the system. A DSC scans in time for differences in heat required to increase (dynamic) or maintain (isothermal) the temperature value between the sample and the reference pans constant. In order for this to work appropriately, very good thermocouple sensors have to be placed in the system. The location of the sensors is critical for proper heat transfer.

Samples have to be placed on pans that when seated might not have good surface contact. This only, may already create a heat transfer delay between surfaces before heat reaches the thermocouple. Having a reference sample to compare changes in released or absorbed heat is very beneficial because it provides a baseline to eliminate errors from all the other heat transfer surfaces or materials in contact with the sample. Both the sample and reference are maintained at nearly the same temperature throughout the experiment. Controls systems are designed such that heat inputs are done very consistently such that for dynamic runs the sample pan temperature increases perfectly linear in time. It is also critical that the reference which would be the empty pan for most cases have a well-defined heat capacity over the range of temperatures tested.

A DSC system has the ability to identify many thermodynamic transitions points or molecular changes that a material undergoes which lead to heat release or absorption. Some examples of important parameters identified include: T_g, phase transformations such as melting, solidification and evaporation, crystallization, chemical reaction energy and even, chemical decompositions. For purposes of exothermic cross-linking reactions the term of interest is the heat released in time when a molecular covalent bond occurs. The heat released in time may be expressed as '*Q*' and the cure degree (*C**) at any point in time defined as [8],

$$C^* = \frac{Q}{Q_T} \tag{2-1}$$

where Q_T is the total amount of heat released during complete reaction. When a DSC experiment is performed for an exothermic curing reaction an output curve is produced such as the one shown on Figure 2-12, where a peak of heat release will be generated. The total area under the peak for material cured to full extent is Q_T.

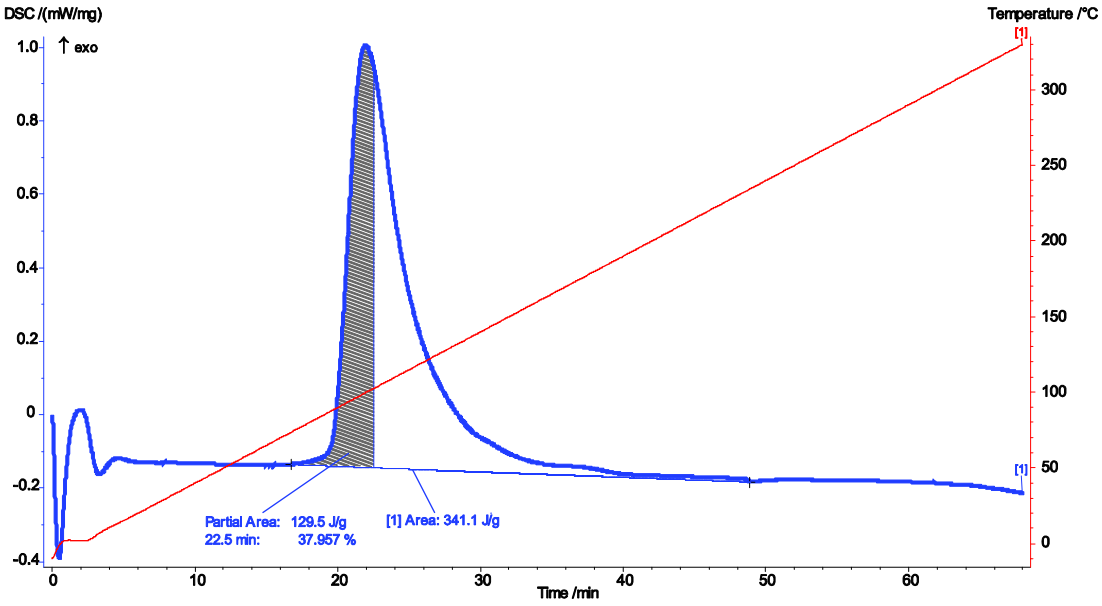

Figure 2-12. DSC output curve for a pultrusion grade unsaturated polyester resin heated dynamically at a rate of 5K/min.

To determine Q a similar idea follows, where the area under an exotherm curve up to a specific time t represents the cure degree up to that time. Consequently, the cure degree may be defined as,

$$C^* = \frac{\int_0^t \dot{Q} dt}{Q_T} \tag{2-2}$$

where $\dot{Q}$ represents the exothermic rate. As demonstrated on Figure 2-12 in order to determine cure percent, a dynamic scan is executed to a high enough temperature and time (over maximum T_g) where the area under the curve may be assumed to be full conversion.

A disadvantage of this evaluation method when compared to equipment such as Raman spectroscopy is that reactions are dependent on ratios of reactive species. Therefore, in some instances reactions will stop but not necessarily after reaching a good cross-linking. DSC does not provide sufficient information, but only averages of what is happening kinetically at the molecular level. This might not only lead to errors, but make it very hard to fully understand reaction mechanisms in order to be able to develop accurate kinetic models [39]. For example, if there is an error in ratios and too little hardener is added to an epoxy resin, the hardener will be consumed and reaction will go to completion but properties will not be optimal and residual unreacted epoxide groups will remain present. For this case, if the reaction were monitored using spectral peaks it would be easy to identify the unreacted substances, and as a result the error in ratios. In a plot of conversion generated by DSC everything is normalized with respect to an experimentally determined total area, which might have been obtained with a run that never really reached 100% conversion. Actually, most reactions never do reach 100% conversion.

This is very common for slow reacting substances that take extremely long periods of time to cure at high conversion levels due to the rigidity of the material, which limits the molecular movement to a diffusion controlled process. One other limitation of the analysis is that in order to determine the exothermal heat of reaction, the sample material has to be in a very controlled environment, as a result, the technique does not allow for online measurements during processing.

Even so, due to the ease of use DSC has found much growth in analysis of curing reactions. From kinetic studies and evaluation of models, to studies of cure changes caused by variations in ratios, heating rates and concentrations of catalysts and initiators, DSC has been applied in almost all.

Many researchers [12, 40-48], use differential scanning calorimetry (DSC) to continuously monitor the curing kinetics of *UP* resins and epoxies for low temperature reactions isothermally and at constant heating rates. Others like Huang and Chen [11, 49] have described variations in curing at different comonomer compositions for medium and high temperature reactions combining and comparing DSC and IR spectroscopy. Bilyeu etal. [50] demonstrated how the DSC may be used at high heating rates to obtain accurate clean results for glass transition temperature of epoxies by eliminating the overlap of exotherm and glass transition. DSC has been widely used for studying the behavior of thermoset material as it cures when varying initiators, catalysts, hardeners and additives [29, 42, 51-53]. A wide approach has been to combine DSC with SEM in morphological studies [9, 52]. By looking at SEM images an understanding of the cross-linking behavior

and structure formation are obtained. With DSC, the morphological results may be related to respective curing levels, rates, and kinetic changes. Gorovaya and Korotkov [10] have analyzed quick cure of thermoset composites through a one-dimensional heat transfer model and applied DSC to evaluate the model. For quick reactions that lead to high exotherms during the process overshoots of temperature in the sample may alter the isothermal temperatures or linear heating rates assumed during cure and create errors in final kinetic results. Heat conduction effects which are directly related to the temperature rise in the sample have been modeled by Barone and Caulk [54] for curing of fiber reinforced unsaturated polyester resin during compression molding. They describe how non-uniform temperature distributions may be seen in thick parts, how rapid cure can result in a reaction time comparable to the time scale of thermal diffusion, and how progressing cure as it couples with heat conduction may lead to non-uniform curing in parts and excessive temperature rises. In order to characterize the curing of a material, kinetic models such as the Kamal and Sourour model [47] have been created in which dependant constants have to be derived for a particular material from experimental results. Examples of different procedures to use in order to apply such models with DSC have been provided by Salla and Ramis [55]. Models have been shown to be applicable to many different thermosetting reactions, conditions and materials. Other kinetic models such as the Kissinger and Ozawa have been used alternatively for both unsaturated polyesters and epoxies [33, 44, 55, 56] and have been found to be satisfactory even with the difference in polymerization mechanisms found on an addition versus a free-radical co-polymerization. For the case of most thermosetting resins the main models developed maybe divided into two types: phenomenological and mechanistic. Phenomenological

models are not reliable though when reaction pathways are not simple. Mechanistic models on the other hand, may be much more accurate but may become extremely complicated. As a consequence, they require certain assumptions or justified hypotheses such as steady state equilibrium allowing the reduction of unknown parameters [39]. A mechanistic model for the case of a free-radical cross-linking reaction such as that seen in *UP* resin considers the different reaction stages (initiation, propagation, termination) and may even include effects occurring at high cure levels where molecular mobility becomes an issue. One important consideration is that in order to appropriately provide reaction parameters for models assumptions have to hold true when these parameters are evaluated. A simple case is the assumption of constant heating rates in samples where any deviation from a linear heating rate will provide the wrong parameters which will cause errors in models when compared to experimental behaviors.

Janeschitz-Kriegl et al. [57, 58] described how there is a thermal delay between the sample, pan and surface-to-thermocouple which has to be accounted for in order to obtain accurate and correct heating rates of samples. In addition, polymeric materials have a very low thermal conductivity that has to be taken into account when heating a sample and more over when heat is being released from the sample. For fast exothermic reactions temperature rises within the sample may be significant enough to cause isothermal or constant heating rates of the sample to deviate from their true values. Chapter 3 demonstrates a situation for unsaturated polyester where this erroneous effect was observed and had to be accounted by developing an alternate cure method to monitor highly accelerated reactions.

2.3.2 Raman Spectroscopy

Many methods available to monitor the curing reactions are based on observing changes in the physical properties of a sample and correlating them to the degree of cure. As discussed, many include strength, viscosity, heat-release and impedance changes recorded as a function of time. These techniques do not provide any kind of direct insight to what is actually occurring molecularly in the curing process, but are only means to help determine stages of the curing process or physical and mechanical properties of the part [7]. To have the ability to directly study the molecular chemical reaction of a thermosetting resin, spectroscopic methods have been used. Techniques including, IR, N-IR, FT-IR and Raman have all been found to provide valuable information of chemical structure, composition, and reaction progress. Raman, although not as popular in the plastics industry as IR, due to recent advances in technology has gained greater acceptance within all these practical methods for analysis of reactions [59]. All of the different spectroscopy equipments have unique benefits depending on the application for which they are being used and they should all be considered tools to better understand molecular structures and behaviors.

Raman spectroscopy systems similar to IR use a laser beam that energetically excites the molecules in the sample but measures the difference in the inelastically scattered light caused by the molecular vibrations to that of the laser incoming light. The best way to

describe Raman spectroscopy is to consider what happens to a beam of monochromatic light on a material. Some will be reflected, some absorbed, and some transmitted. Most of scattered or reflected light will have the same wavelength as the incident light but a small fraction may be shifted in wavelength by the molecular vibrations and rotations of the molecules of the sample. This wavelength shifted light (i.e. inelastically scattered light) is what is seen in a Raman spectrum [60]. Approximately one in every 10^7 photons is scattered at optical frequencies (energy) different and generally lower than the incident photons. Remembering the basic energy relation (eq. 2-3) that relates wavelength and frequency, allows for the use of each alternatively.

$$\lambda = \frac{c}{\nu} \tag{2-3}$$

In this equation, *c* is the speed of light, λ is the wavelength and ν the frequency. Molecular bonds also vibrate at certain frequencies. The specific difference in energy between the incident photon and the Raman scattered photon is equal to the energy of a vibration of the scattering molecule, which allows the identification of a particular molecular bond. The spectrum is then a plot of intensity of scattered light versus energy difference or frequencies at which the particular vibrations are happening. Each peak in the spectrum resembles a molecular vibration that caused a shift in the wavelength of the scattered or reflected light. The intensity of the peak is directly proportional to the concentration of the species in the sample.

Two terms are commonly used to describe the emitted or scattered light; Rayleigh scattering and Raman scattering. Rayleigh scattering represents the light that is emitted at the same energy level of the incoming radiation, whereas Raman radiation is shifted in frequency and thus energy. The scattering effects can be represented with an energy level diagram such as the one show on Figure 2-13.

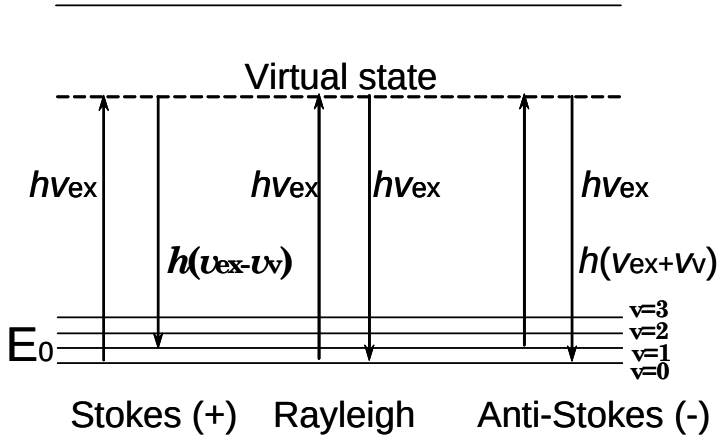

Figure 2-13. Energy level diagram that shows Stokes, Anti-stokes and Rayleigh scattering.

The common Raman spectral region covers wavenumbers of shifted light from 200cm^{-1} to as much as 4000cm^{-1} in both positive and negative directions based on the molecules absorbing or releasing energy. As may be seen in Figure 2-13, Rayleigh scattering is an elastic scatter. Therefore, the energy level of the molecule does not change from an initial to a final state. Raman scattering on the contrary includes both Stokes and Anti-Stokes scatterings. Raman is a measure of the wavelength and intensity of inelastically scattered light where a molecule may end in a higher or lower energy level. In particle physics, inelastic scattering is a fundamental scattering process in which the momentum of an

incident particle is not conserved. In this scattering process, the energy of the incident particle is lost or gained. During Stokes scatter the final energy level of the molecule is higher than the initial (some energy is retained) and during an anti-Stokes scatter vibrations lead to an energy release. At room temperature the excited states of most molecules are lower than at higher temperatures. This means there is a higher tendency for a molecule to absorb energy. As a result, the molecule would emit scattered photons at a lower energy that the incident light, resulting in a Stokes scatter. Similarly, as temperature is raised anti-Stokes scatters become greater. The ratio of anti-Stokes to Stokes intensity at any vibrational frequency is relative to the temperature of the material. There is believed to be symmetry in Stokes and anti-Stokes vibrations but that is not necessarily the case considering a molecule may not lower to a lower level of energy that is its lowest state [60, 61]. Even so, based on this idea, anti-Stokes Raman scattering is used for contactless thermometry. Disregarding the differences, Raman equipment generally reports only the Stokes scatter.

One of the main benefits of Raman spectroscopy that leads to its vast possibilities in polymeric reactions is that the Raman signal is strong in long polymer chains, where the dipole moments, which are the basis for IR detection, are in many occasions canceled out [60]. The Raman scatter is dependent on changes in polarizability thus being quite sensitive to vibrations in symmetrical molecules and larger atoms [59]. IR measurements are recording the absorption that arises due to a direct resonance between molecular vibrational frequency and IR radiation. This resonance interaction leads to a change in dipole moment. Therefore, when an IR photon encounters the molecule, it is absorbed,

and the molecule is elevated to a higher energy level relative to the photon energy absorbed [61]. Raman scattering on the other hand involves two steps. First, is when the photon impacts the sample, and the second, when the emitted radiation which contains the Raman scattering leaves the sample and is collected. During Raman scattering there is a change in the polarizability of the molecule but a dipole moment is not required because it is being induced by the interaction of the polarizability and the incoming radiation [61]. A good way to define polarizability is to describe it as a measure of the "ability to" or ease with which the electron cloud around a molecule can be distorted. Polarization is the force that light can apply to an electron cloud which will result perpendicular to the light direction. For Raman scattered light the polarization will be in the same direction as the changing polarizability caused by the induced dipole moment on the electron cloud. For example, if the incoming light causes an electron cloud movement in the same direction it is coming, then the polarizability will be in the same direction as the incoming light and will not induce a Raman scatter because the scattered light will have the same polarization as the incident light and there will be no induced dipole. If the electron cloud is moved in a different direction (induced dipole) then the scattered light will have a different polarization as the incident light and therefore, will contain Raman scattering. For our particular case of study where reactions of unsaturated polyester and epoxy resin are being considered, Raman technology appears to be very valuable due to the sensitivity of specific carbon-carbon double bond vibrations and epoxide ring opening reactions.

Raman Spectroscopy equipment has recently improved substantially due to the ability of filtering unwanted elastic scatter which has greatly improved sensitivity and reduced noise. By considering that most of the scattering generated by a material is elastic, it is clearly demonstrated that the key to a good Raman system involves the filtering techniques. Figure 2-14 presents a schematic overview of a typical dispersive Raman instrument.

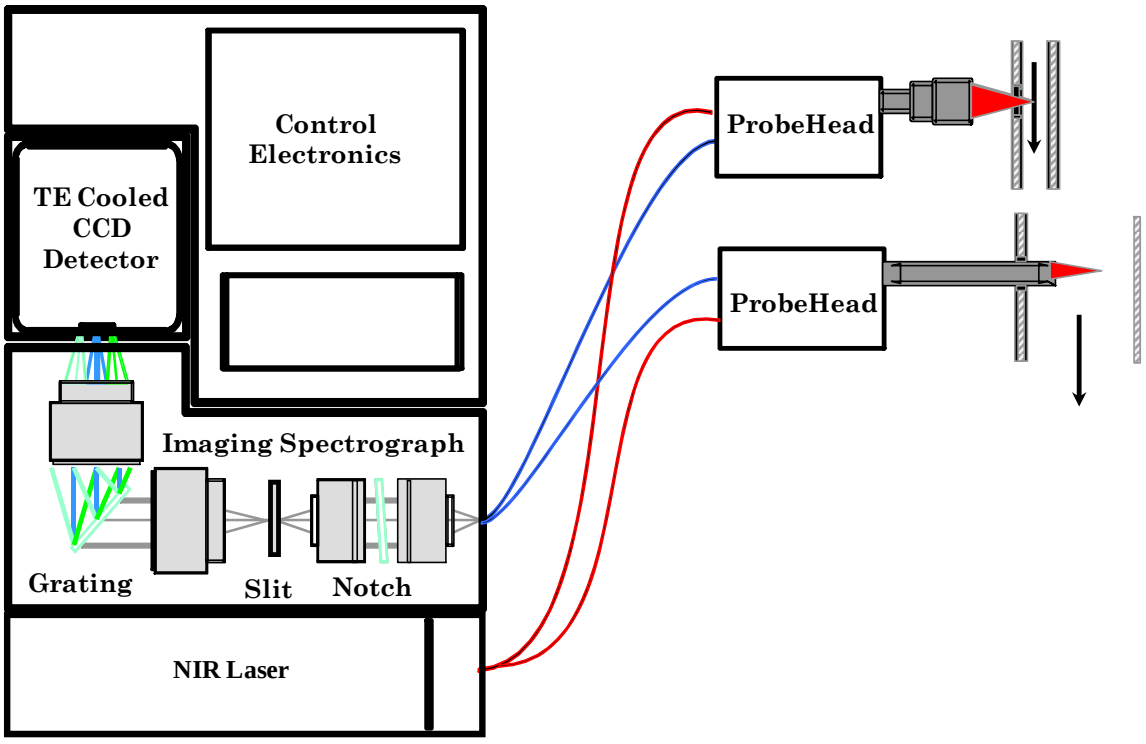

Figure 2-14. Schematic of a typical dispersive Raman instrument.

For the research presented on this dissertation a comparable equipment to the one illustrated was used. As seen in Figure 2-14 the main components of a dispersive Raman

spectrograph include the laser, the fiber optic sampling device, a notch filter, the grating, and the CCD Detector.

Two of the most common types of Raman instruments are FT-Raman and dispersive-Raman. FT-Raman uses the same idea previously mentioned for IR in section 2.3 where all wavelengths are measured simultaneously and decoupled by use of Fourier transformations. FT-Raman allows for good reproducibility and avoids fluorescence well. The main disadvantage of this system is that the sample is more susceptible to overheating or even burning—a great concern when monitoring exothermic curing reactions. Most researchers [62-67] have used FT-Raman for thermosetting cure analysis but dispersive Raman may provide some added benefits. Dispersive Raman uses optical CCD and grating techniques by implementing lenses and cameras. The main benefit of this technique is that although there may be some fluorescence, the equipment is known to provide much better response for dynamic systems such as fast reactions, and the signal-to-noise ratio is very good. The laser power may be well controlled to minimize overheating. For any Raman system calibrations are required and can be tedious, especially if they are required for every run. Fortunately, new equipment has the benefit of automated continuous calibrations, which for some cases, where normalizations will be performed, they may not even be required. Another benefit of dispersive Raman is that equipment does not require moving parts which might suffer wear and mechanical damage. Raman systems incident radiation is provided by use of a laser. Table 2-4 includes some of the lasers commonly used. For this research a 785-nm NIR laser was

selected. NIR laser are most commonly used today because they provide much better fluorescence rejection, thus reducing noise, but still allowing the use of CCDs.

Table 2-4. Lasers commonly used for Raman Spectroscopy

Laser Frequency	Remarks
1064-nm	Nd:YAG laser FT Instrumentation, Out of range for CCDs
830-nm	Not common but could help avoid fluorescence
785-nm	Diode laser, Most common laser used for Raman work Good compromise between fluorescence and Raman efficiency Stable and Electronically efficient
633-nm	He-Ne laser Longer lifetime
532-nm	Nd:YAG laser High-efficiency low-power, Errors of fluorescence common, temperature sensitive
514-nm	Ar-ion laser
488-nm	Ar-ion laser
UV-lasers	Resonance Raman Expensive

Curing analysis using Raman has only recently grown with most publications emerging after the 1970's. The main reason is the latest technological developments that have made the systems less expensive and much more user friendly. Most of the publications on cure have been done by the use of FT-Raman rather than dispersive Raman and if any, they have not been specified as being dispersive method. Even with the benefit of such an accurate analysis method almost none of the publications have proposed the use of Raman for the determination of kinetic parameters. A reason for this may be that the main focus of the method has been the application as an online cure monitoring tool. By accurately determining the real temperature of the material and degree of cure, parameters for modeling may accurately be determined.

Koenig and Shih [7] studied the structure and followed the cure of a slow curing and low temperature unsaturated polyester resin reaction. They provided the basis for undergoing a Raman analysis for *UP*, including very important information involving the understanding and representation of particular peaks in the spectrum to molecular bonds in the polyester and monomer. They were able to follow the whole cure of the material and determine the average ratio of styrene to *UP* fumarate bonds to be a 2:1 ratio. They also described good methods which may be applied to aid in the determination of peaks which might vary in position due to interaction of neighboring molecules. A similar analysis were the curing analysis was performed and peaks determined, but for an epoxy resin, was presented by Lu and Koeing [68].

An area of Raman research that is of great interest is the ability to perform online monitoring. Researchers [19, 62, 65, 69-73] have attempted many different situations in which they may monitor the reaction of a thermosetting resin *in-situ*. The benefit of Raman is that scattered light is what is measured; therefore, it may easily be done by use of fiber optics. A recent study presented by Musto [73], shows an application of the technique for analyzing effects of changes in molar ratios and compares the Raman results to dynamic mechanical properties. Lyon et al. [70] used fiber optic Raman spectroscopy to monitor the room temperature cure of an epoxy *in situ.* The idea was to use a small fiber optic probe that could be immersed in the sample and could be left there prior to cure. They monitored the cure by relating the concentration of epoxide groups to the intensity of peak 1240cm^{-1}. This peak has been assigned as a vibrational mode of the oxirane (epoxide) ring and is the peak mainly used by every other researcher. Although

the peak may undergo certain shifts depending on the specific molecular structure of the epoxy analyzed, it is always found within the same region. The spectrum of DGEBA was compared to that of FTIR to provide a comparison for analysis. For composites, a similar idea was suggested where the small probe can be left within the part after cured. Testing directly on composites has also been reported. Aust et al. [69] presented the idea of *in situ* monitoring for a glass fiber reinforced composite with an epoxy matrix. Rose et al. [71] introduced a similar example, but while directly working inside an autoclave system, and compared the results to DSC method. Farquharson et al. [62] did a similar *in situ* testing by using FT-Raman for an epoxy composite cured under high temperatures and demonstrated how through the use of fiber optic probes high temperature monitoring is possible. In addition, he demonstrated how the molecular structure of that particular resin may be correlated to the mechanical properties of the material. Skrifvars et al. [19] not only demonstrated how curing of laminates with glass-fibers could be followed by Raman, but they also studied surface coatings such as gel-coats, and demonstrated the extensive cure times that are usually required to reach a high cure level on these materials.

Some other investigations have been introduced for cure monitoring by using Raman spectroscopy. An area that has been well accepted has been its use in the determination of cure in dimethacrylate dental resins, where the $1635cm^{-1}$ C=C band similar to the $1632cm^{-1}$ found in unsaturated polyester may be related to cure [74]. A remarkable investigation was presented by Musick et al. [75]. Their research presented a new approach to monitoring cure of unsaturated polyesters used in coatings. Many coatings

are sprayed in the form of micro-particles thus the cure at these conditions due to heat transfer effects and such will be much different than that of a contained batch resin. By using a special technique of optical levitation using forces generated by a focused laser, they stabilize and single micro-droplet and analyze its chemical composition. In this case, the system is similar to a non-contact optic where resin never touches any part of the device, since it is being levitated. The composition of individual C=C bonds of styrene and *UP* are monitored and peaks used for analysis are presented. Another interesting publication was presented by Rose et al. [76]. They presented a new method in which they could monitor the full extent of cure and determine viscosity changes such as gelation. The method consisted of adapting a Raman probe into the upper fixture of a rotational rheometer. They presented results for an epoxy resin, and although not mentioned, provided all the necessary techniques to obtain all the basic curing information usually illustrated in a TTT-phase diagram. Such a diagram has been recently created by use of Raman equipment in combination with other techniques [63].

As demonstrated throughout all the publications, monitoring cure with Raman is an area that in recent years has been growing extensively. With Raman, evaluations of unreacted substances, chemical composition, degradation, and reaction ratios have been determined successfully. It has also been demonstrated how *in-situ* monitoring may be performed. Based on these investigations, this dissertation will present two new approaches using dispersive Raman technique and innovative non-contact optics. The method will allow accurate monitoring of highly accelerated reactions and an evaluation of pressure effects on a curing resin.

2.4 Curing Analysis and Methods

The reasoning behind developing different methods to properly describe the curing of a resin is to be able to gain some useful insight that may help improve material properties, processing conditions, storage and final properties of parts. Other than chemical structure-property studies, the main analysis methods that have been developed for the study of thermoset resins may be divided into three main areas: phase diagrams, morphological studies and curing models. Each of these methods, provide particular information of the material and the curing behavior and serve as means to describe properties and kinetics.

Phase diagrams for thermoset materials are developed in order to provide information on the main transitions that resins undergo during cure. The two transitions considered most important when processing thermosets are gelation and vitrification. Gelation represents the time and temperature where the material changes phase from a liquid into a gel-like structure because sufficient covalent bonds are formed to create a three dimensional network. Vitrification corresponds to the solidification of the material to the glassy state, which occurs when the glass transition temperature of the resin rises to the processing temperature. At this point the reaction changes into a diffusion dominated process. The most common phase diagram is the isothermal time-temperature-transformation (TTT) diagram developed by Enns and Gillham [77], which relates iso-conversion curves with

temperature and time. A representation of a generalized TTT-diagram is shown on Figure 2-15. The many different phases a thermoset material passes through during cure are illustrated by different shadowed areas. The vitrification phenomenon is also depicted in this diagram as the “S” shape curve.

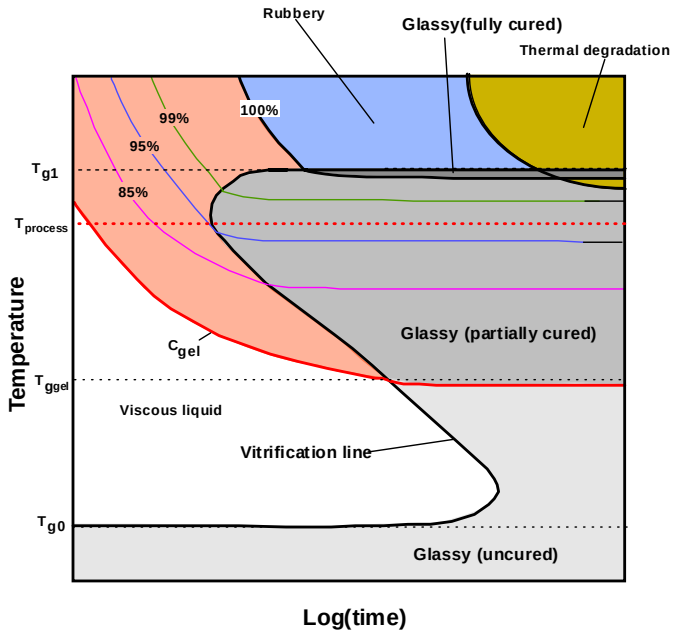

Figure 2-15. Time-Temperature-Transformation (TTT) diagram for thermosets

The temperature of the process has purposely been set lower than T_{g1} to demonstrate the problem encountered with a process temperature that is too low and will not allow a high cure degree. The different possible stages include: liquid, solid-gel rubber, gel-rubber (rubbery), solid-gel glass (glassy partially cured), solid glass (glassy uncured), gel-glass (glassy fully cured), and charcoal (thermal degradation). At temperatures below T_{g0} is the solid glass region, where the resin will not cure due to immobilization of the molecules at this low state of energy. Below $T_{g(gel)}$ the resin will slightly crosslink, but still on a low

energy level, thus reaction will be slow and material will remain as a viscous liquid. Above the gel point the material has the ability to begin curing at higher rates if given the right amount of energy. Finally at T_{g1} (also known as $T_{g\infty}$), the material will vitrify reaching the highest levels of cure. When the viscosity of a material increases so much as to solidify (vitrify), the molecular movement reduces greatly thus the reaction rate also reduces into a diffusion step. If a material reaches the vitrification point before having reached a high conversion it will be very difficult for it to ever gain high enough conversion.

The TTT-diagram is only one of the many diagrams that have been developed to describe thermosets during cure. Other relationships may also be used to design time-temperature cure paths to optimize processes and properties [35, 78]. Even so, no diagrams have been developed which take into account pressure effects. A similar diagram that takes into account the effects of heating rates on non-isothermal conditions is the continuous heating time-temperature-transformation (CHT) diagram. Other diagrams include the conversion-temperature property (T_gTP) diagram which identifies drastic changes in mechanical properties as regions dependent on temperature and cure, and the glass transition temperature versus conversion relationship that demonstrates the direct relation between T_g and cure.

In order to satisfactorily develop such diagrams it is necessary to obtain experimental cure information with the use of monitoring techniques. Gillham [34, 35, 78] has provided a method where by the use of TBA solely, one may develop these different

diagrams. Other researchers have worked on these diagrams through many other means. Atarsia and Boukhili [79] presented a study of pultrusion resin where they proposed predicting the degree of cure during non-uniform temperature profiles by use of isoconversion diagrams generated with DSC data, but where no transitions were noted. Mele et al. [80] presented a very interesting approach for developing complete TTT-diagrams by only using a DSC. By using a modulated DSC (MTDSC or MDSC) they were able to monitor both the heat release of the sample and the change in heat capacity (C_p) for both isothermal and non-isothermal reactions. The heat release provides the cure information while with C_p, changes or transitions of the material (e.g. liquid-to-solid) may be observed in order to estimate vitrification. Bilyeu and Brostow [81] did a similar approach but analyzed the gel-point by DMA. Ramis and Salla [82] have developed the diagram using combinations of FTIR, DSC and TMA. Wacker and Ehrenstein [83] and Sbirrazzuoli et al. [84] have combined information from DSC and rheometry in order to generate isoconversion behaviors. As many of the previously mentioned and other researchers have presented [79, 82, 83, 85], these diagrams may be developed in automated ways by use of curing models. Like with any curing model obtaining the appropriate curing parameters experimentally may lead to accurate and reliable results, both for phase diagrams and other types of kinetic information. Some of the common models previously mentioned in section 2.3.1 that are used to understand the kinetics and property dependency of cure are the Kissinger, Ozawa and Kamal-Sourour models. Each are considered mechanistic models, which with the appropriate parameters may well simulate curing conditions. Models provide the added benefit that after developed they may accurately describe a process, but unfortunately, they are very dependent on

stoichiometric ratios of reactive sites. Due to the curing behavior after vitrification, some of these models require modifications in order to account to the slow diffusive reaction period. As it may be observed, basic monitoring techniques become very important and necessary for developing advanced and automated cure monitoring systems and for generating systems to describe the process. The basic problem of thermosets is that due to the variability of the resins compositions, experimental values for each particular resin become necessary for correct estimation of kinetic behavior. Not only might the kinetics change due to composition, but morphology of the material becomes composition and rate dependant and will affect the properties of a final part.

Some morphological studies have been developed to try to describe behaviors occurring during cure and differences within a resin caused by variations in curing conditions and composition [7, 9, 49, 52, 86-88]. These interactions at the molecular level are affected by any changes in the process including temperature and pressure variations. Most morphological studies consist of studying the cure by various methods such as DSC, FTIR, Raman and SEM, and developing mechanisms to describe the network formation during cross-linking. For epoxies, due to the characteristic polyaddition reaction not much has been proposed of morphological changes during cure. The mechanism of a step-growth reaction, as discussed in section 2.1, allows the reaction to proceed at many different locations and propagate throughout. Therefore, the behavior is considered to be comparable to any other step-growth polymerization. Most of the research that has been directed towards the morphology of epoxies has been related to the effects of varying the chemical structure and describing how these morphological changes will affect final

properties. Similar to thermoplastics where the chemistry of the backbone structure will lead to certain mechanical properties, for cross-linked structures, the chemical structure of the segments creating cross-links will also affect physical properties. Lohse and Schmid et al. [88, 89] demonstrated this effect by testing epoxies with different morphologies such as, high and low cross-link densities and long and short basic polymer units. They suggested that for materials that have lower cross-link density, irregular structures may be formed if the reaction begins from centers and propagates as higher cross-linked particles. These irregular structures could have less cross-links between particles which would cause lower properties. For the regular case of composite resins which have high cross-link densities, reactions happen simultaneously throughout all the material and no definite pattern has been determined. For this reason not much has been stipulated of variations within the morphology of the material during cure. In the contrary for free radical *UP* resin reactions some very interesting phenomena have been discovered.

A good publication where a Haake viscometer was used to study the curing of unsaturated polyester resins was written by Yang and Suspene [14]. They studied the initial stages of cure up to gelation of the material looking into changes in gelation and viscosity levels due to variations in MEK-P initiator concentration, cobalt accelerator and temperature. The curing of *UP* resin with MEK-P leads to a slow curing reaction making the use of a Haake rheometer very appropriate. Through the analysis, they proposed a gelation model that would describe the morphological behavior of the material at these lower cure levels. The model divides the pre-gel cure in four stages: induction, microgel

formation, transition and macro-gelation. The model incorporated the idea of the formation of microgels within the *UP* resin during cure due to the variation in inter-cross-linking and intra-cross-linking reactions [86, 87]. As will be described in chapter 4, this morphological cure behavior analysis may be used to describe pressure effects on the material. The microgel formation can be described as a phenomena occurring due to cross-linking within activated areas of the resin. When a free-radical forms it acts as a cross-linking "nucleation site" i.e., an area where the cross-linking may propagate. The result is areas that will grow in cross-linking due to intra-molecular reactions in the "growth region" known as a microgel. Based on their results this pre-gel curing stage mechanism should generally apply to all free-radical cross-linking (co-)polymerizations. Figure 2-16 illustrates the idea of the microgel formations.

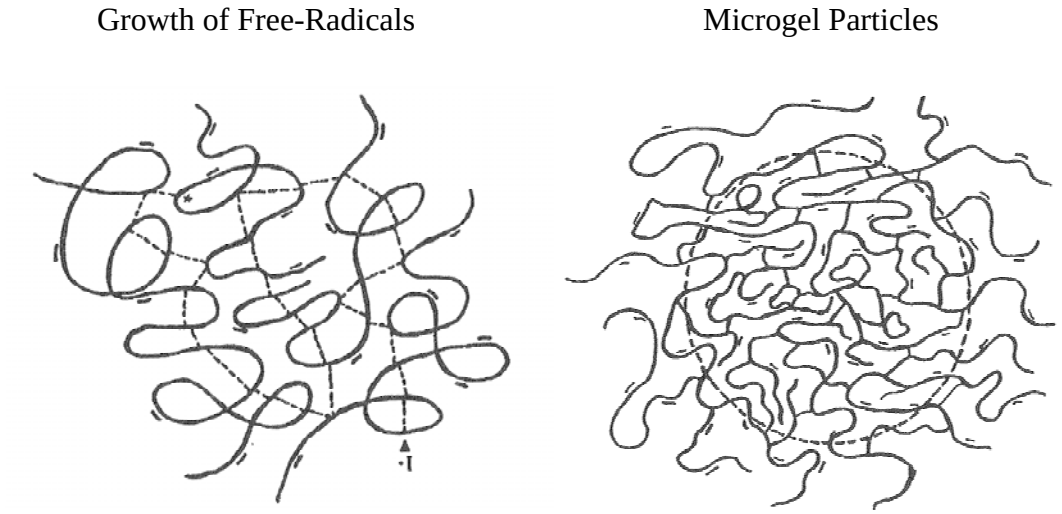

Figure 2-16. Formation of styrene/*UP* microgel. (a) Growth of free-radical through activated initiator: '• I'. Propagating free-radical: '*'. (b) Schematic drawing of microgel [86, 87].

Based on the model, the viscosity rise during the pre-gel state depends on the formation of microgels and the cross-links formed among the microgels. This means that initially the viscosity rise (estimated to occur between 1-7% cure) is due to the intra-microgel reactions and the growth of microgels due to these "intra" reactions. As these microgels grow and get closer together they will start reacting between each other through inter-microgel reactions. The "inter" reaction will continue to happen resulting in time with the formation of a highly cross-linked macro-molecular network structure. Figure 2-17 summarizes the model depicting the four stages of cure.

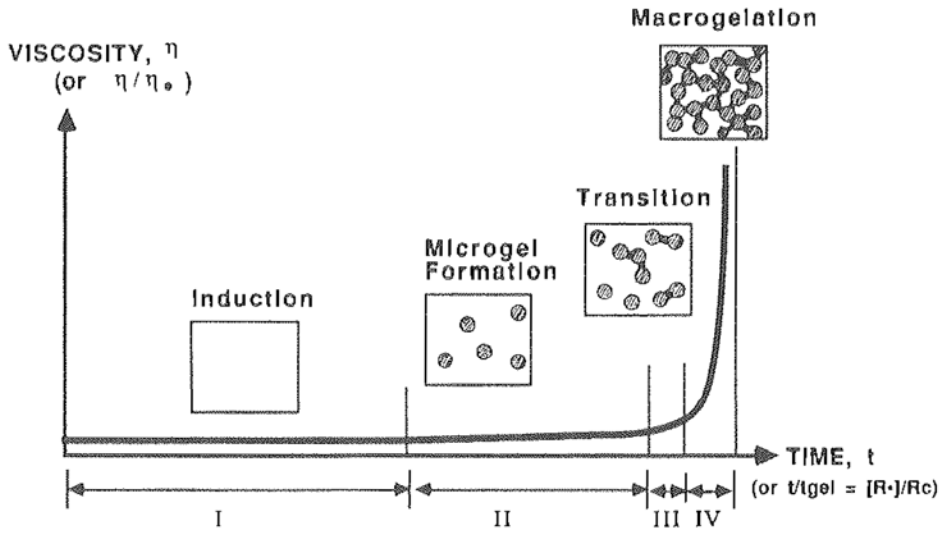

Figure 2-17. Typical viscosity rise during cure of a *UP* resin correlated with the microgel gelation mechanism [14].

Figure 2-17 is representative of a MEK-P slow curing reaction. Induction period for this material, which describes the period of time were the inhibitors are preventing the reaction to proceed, is long due to the slow initiation rates of MEK-P. After the induction

stage, when initiators can continuously break and form free-radicals, the cross-linking initiates. For the case of faster reacting resins the behavior should be similar although less noted due to the high propagation that will result in faster inter-molecular reactions. Huang and Chen [11, 48, 49] introduced the microgel particle mechanism for describing the effects of variations in composition for an unsaturated polyester resin. They were able to relate curing temperatures, accelerator behavior and concentrations to the growth and propagation of microgels.

3 Implementation of a Cure Monitoring System by use of Raman Spectroscopy

3.1 Preliminary DSC Analysis

A Netzsch DSC 200 PC developed by Netzsch-Gerätebau GmbH (Selb/Bayern, Germany) was used for all comparative analysis. The purpose of the analysis was to evaluate the results obtained by the DSC for heat release and temperature of the sample during cure. Pultrusion grade unsaturated polyester resin (refer to section 2.2.1) was used for the analysis. This material is highly reactive and overheating is very common. Recently, co-workers attempted to model the reaction kinetics of the resin and it was noticed, that an error was generated in the kinetics behavior when providing DSC experimental data. It was determined from this analysis that the model could not fit to the experimental data because the assumption of linear heating rates was not sustained. The main concern was the heat delays and conductivity issues between the low conductivity polymer, the pan, and surface (refer to section 2.3.1). When testing highly accelerated reactions commonly seen in unsaturated polyester pultrusion processes, assuming possible overheating is a must, even for small sized samples.

Samples were prepared by mixing the unsaturated polyester resin with styrene-50 PPM Inhibitor to assure a 2:1 ratio of styrene to unsaturated polyester C=C bonds. By obtaining the average number molecular weight of *UP* and average number of C=C bonds per polyester molecule the necessary amount of styrene for a 2:1 ratio was

determined knowing that styrene has a molecular weight of 104g/mol with one C=C bond active site. Approximately 1.46g of styrene per gram of *UP* was to be in solution for the correct ratio, therefore, knowing the initial weight percent of styrene in solution an accurate ratio could easily be obtained. In order to perform a uniform mixing of Perkadox 16 powder, initial dilution in the styrene was performed. Full dilution of such small sample size could be achieved in less than 10 drops of styrene. Perkadox 16 initiator was mixed at 0.2wt%, followed by the addition of the liquid initiators, Trigonox 121-BB75 and Trigonox C, at 0.4wt% and 0.2wt% respectively. A total batch of 27.95g was made with initiators accounting for 0.8wt% of the total batch. Initiators were mixed for 10 minutes then the batch was stored in a closed container at 3˚C to prevent any activation or diffusion of volatiles. DSC sample preparation consisted of using the stored sample batch, mixing for 5 minutes, extracting a small sample with a syringe, and by using a precisely drilled DSC lid, inserting a thin thermocouple directly into the sample inside the DSC dish. A thermocouple wire passed through the internal cavity of the DSC to a temperature data-logger which would accurately record the actual sample temperature. Scanning runs from 25˚C-190˚C were performed for the different samples at rates of 2.5K/min, 5K/min and 10K/min. This would permit us to verify the efficiency of the DSC in capturing or controlling the overheating of these highly accelerated *UP* reactions at various conditions.

Reactions of heat activated thermosetting resins are accelerated with increased heating rates. Therefore, heat generated and sample overheating will be greater with faster heating rates. Due to the low thermal conductivity of the sample it is expected that

samples of greater thickness will overheat much more than thinner samples. With the fixed geometry of the DSC dish we can assume that thickness of the sample although hard to control will be related to the mass.

Results of the temperature profile generated by DSC did not show any sample overheating and showed uniform linear heating rates for the highly accelerated pultrusion resins. When the temperature of the sample was monitored with a thermocouple directly imbedded into the sample, results were very different. Figure 3-1 shows a graph of results for a heating rate of 20K/min. Tests for each heating rate were repeated five times. While small differences were perceived between the tests, mainly attributed to the dependence on the samples' mass, the repeatability between the results was satisfactory. Average overshoots from the programmed temperature profile of above 60°C where obtained for 20K/min heating rates. Table 3-1 shows averages of overshoots obtained between the five samples at the different heating rates tested. One may see how the overshoots are higher for the larger heating rates. Examples of the effect mass has on overheating will be shown later.

Table 3-1. Effect of heating rate on overshoot of the sample temperature (*Ts*) averaged between five samples per rate.

	Heating Rate		
	20 K/min	10 K/min	2.5 K/min
Average Weight	34 ± 4mg	35 ± 3mg	37 ± 4mg
Ts-*Tf* at Overshoot	68 ± 22K	54 ± 17K	6 ± 1.5K

As shown in Figure 3-1, the sample overheats at a similar time to when the exothermic peak generated by the DSC occurs. A delay between the response of the DSC relative to the actual temperature variations in the sample can also be seen.

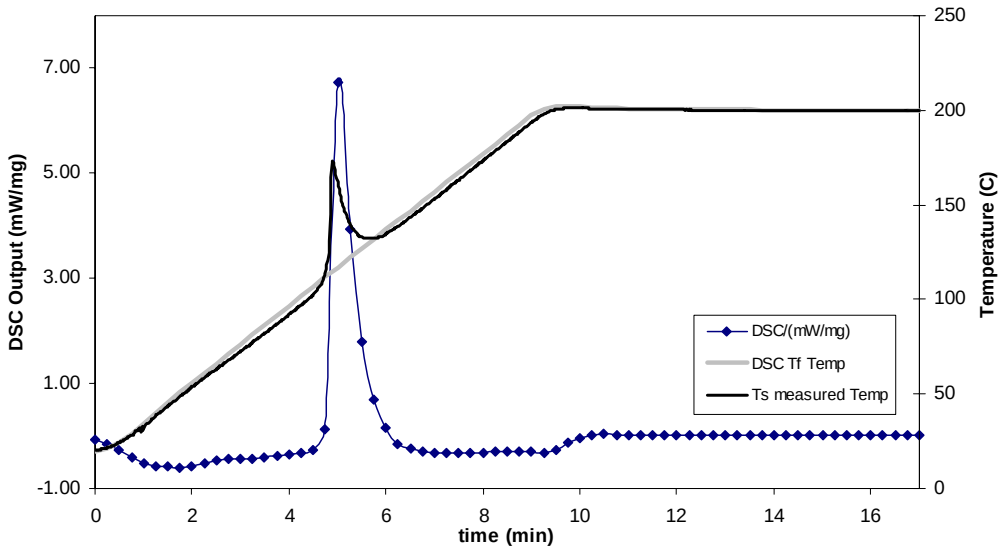

Figure 3-1. DSC exotherm profile and Temperature output (*Tf*) as compared to Data-logger actual sample temperature (*Ts*) for a heating rate of 20K/min and a sample mass of 32.6mg.

As the sample absorbs heat from the furnace of the DSC, heat has to be transferred from the furnace and wall, unto the surface of the pan, then into the low thermally conductive resin. For this reason we can see a continuous delay in time between the DSC temperature (*Tf*) and the actual sample temperature (*Ts*) of approximately 2.5˚C. When the sample is reacting, heat is generated from the sample and must travel out of it and through the pan and surface-to-thermocouple similar to the heat of the furnace, but in opposite direction. Therefore, we can also note a delay between the DSC output of heat

generation and the overheating occurring in the sample. For the case shown in Figure 3-1, there is a difference in time between the maxima of *Ts* and the DSC output peak of approximately eight seconds. At the initial stages of overheating, where the peak growth begins, similar differences may be found. This means that the sample is overheating because of the excessive exothermic heat of reaction, but due to the system and surroundings, there is an eight second offset to when this heat release is detected and reported.

The temperature increase of the sample was found to be very large and may not be neglected. If a sample is not undergoing a constant heating rate any temperature increase will accelerate the reaction and in turn affect the heat release leading to a deviation of results obtained if the sample would have been really maintained at a constant heating rate.

Comparable overshoots and delays were observed for 10K/min samples. For the sample shown in Figure 3-2 there was a difference of approximately 12 seconds in the maxima of the temperature peak *Ts* relative to the DSC heat output peak and a one second average delay between the sample and furnace temperatures during heating. Depending on the weight of the sample maximum temperature rise at overshoot peak ranged between 20˚C for lower mass samples to 80˚C for larger mass samples. Due to the hardships of inserting a thermocouple directly into the sample, the mass of the sample could not be too low in order to assure good thermocouple contact with the resin. Figure 3-3 presents results for a sample with a lower mass of only 17.7mg at a rate of 10K/min. Overheating was still

observed for this sample with 16˚C of overshoot and about 6 seconds difference between the maxima of *Ts* and the DSC output peak. *Ts* peak and the DSC output peak for this case become much blunter and wider because the overheating is lower. Consequently, the reaction rates do not accelerate as much distributing the heat release within a larger period of time.

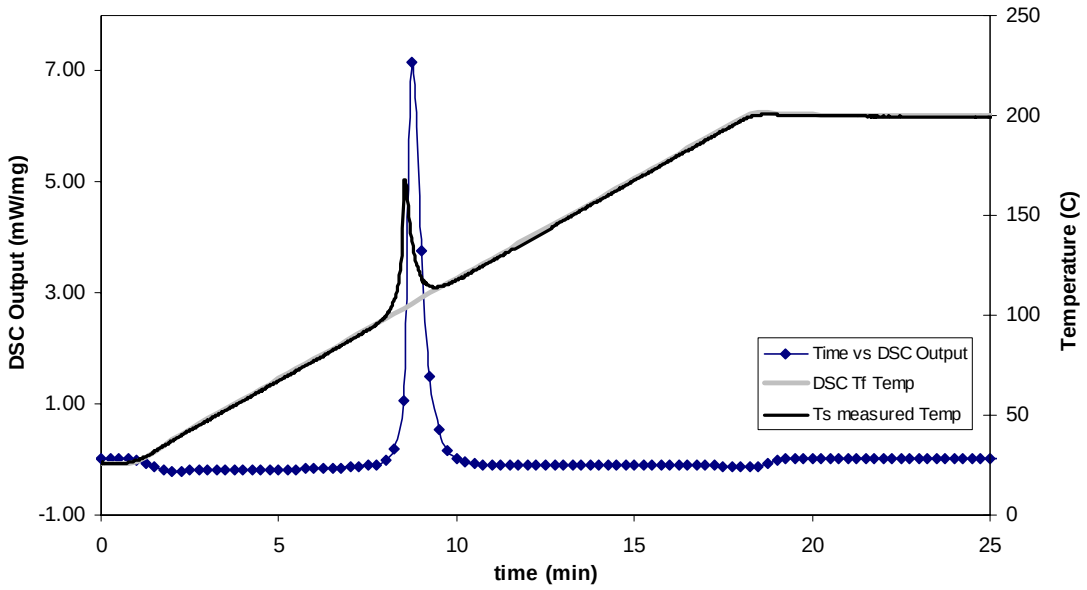

Figure 3-2. DSC exotherm profile and Temperature output (*Tf*) as compared to actual sample temperature (*Ts*) for a heating rate of 10K/min and a sample mass of 28.6mg.

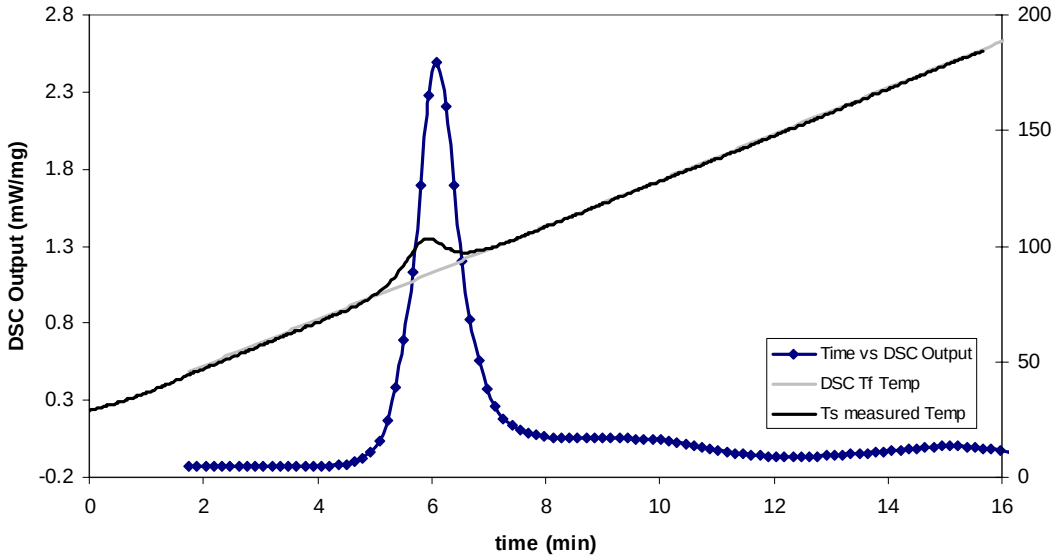

Figure 3-3. DSC exotherm profile and Temperature output (*Tf*) as compared to actual sample temperature (*Ts*) for a heating rate of 10K/min and a sample mass of 17.7mg.

Similarly, Figure 3-4 demonstrates how for heating rates of 2.5K/min delays and overshoots may also be noted on higher weight samples but to a lesser extent due to the slower heating rate.

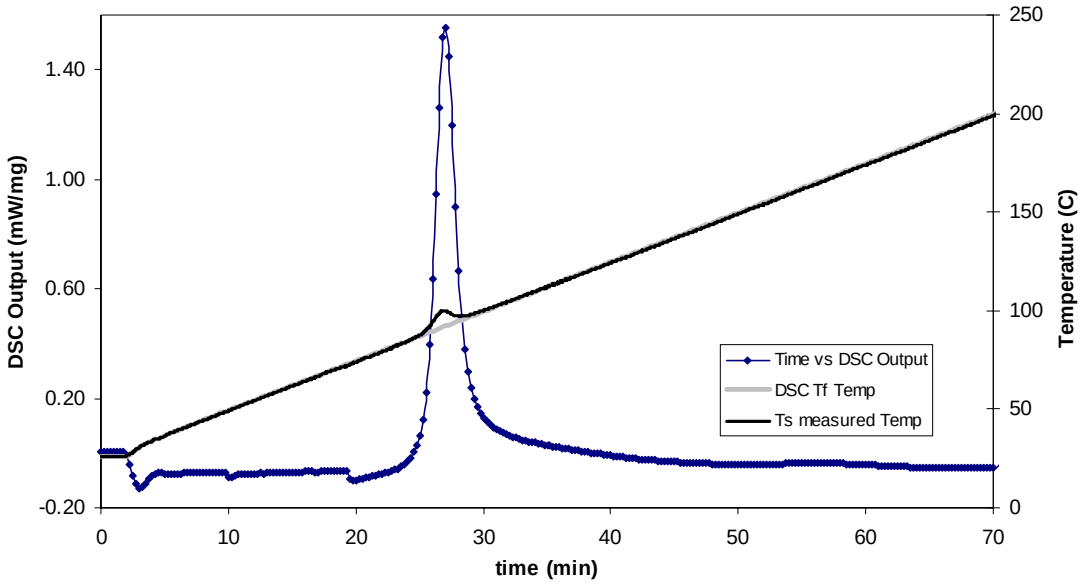

Figure 3-4. DSC exotherm profile and Temperature output (*Tf*) as compared to actual sample temperature (*Ts*) for a heating rate of 2.5K/min and a sample mass of 41.4mg.

Nevertheless, even at such slow heating rates which would in no way simulate real process conditions overshoots of temperature are still present. For 2.5K/min tests, differences between *Tf* and *Ts* during heating time are less than half a degree. The maximum temperature difference at overshoot was 8˚C. As seen on the graph, the temperature overshoot occurs inside the DSC heat output curve indicating that for these slow rates the response time is quite accurate. Only a small misalignment is seen between the maxima of the peaks but do to the curvature of the *Ts* peak, it is difficult to provide an accurate comparison.

Table 3-2 provides examples of results where variations in overheating due to sample mass may be perceived. As observed in the table, if all other variables are maintained

constant, when the sample mass decreases, overheating decreases. Similarly, if the heating rate decreases delays and differences between temperatures *Ts* and *Tf* will decreases because changes are slower and there is more time for equilibrium and heat transfer. It is important to mention that there was not a way to accurately determine the position of the thermocouple inside the sample. Results may vary depending on the location of the thermocouple. Therefore, many runs were performed until accurate and repeatable results were obtained. For samples where the thermocouple might have been slightly closer to the surface of the material, rather than imbedded in the center of the sample, overheating detected may have been smaller.

Table 3-2. Variations in results of heat absorption and release, detected by the DSC and a thermocouple directly imbedded into the sample for various heating rates and sample weights.

Heating Rate (K/min)	Sample Weight (mg)	Average Heating Temp. Difference *Ts-Tf* (˚C)	Max Temperature difference at overshoot *Ts-Tf* (˚C)	Relative Peak Time Difference (sec)
20_{tr6}	38.8	3.1 ± 1	100	16
20_{tr11}	32.6	2.5 ± 2	50	8
10_{tr2}	40.5	2.8 ± 0.5	84	11
10_{tr4}	28.6	1.8 ± 0.2	65	12
10_{tr1}	17.7	1.3 ± 0.15	16	6
2.5_{tr5}	41.4	0.5 ± 0.2	8	0.9
2.5_{tr12}	32.8	0.3 ± 0.1	3	0.11

3.2 Raman Spectroscopy Equipment

A RamanRxn1™ analyzer provided by Kaiser Optical Systems, Inc. (Ann Arbor, MI) was used to monitor the reactions. The benefit of this Raman instrument is that its design has been tailored to be applied for analyzing, monitoring and controlling chemical processes. The system consists of a TE-cooled CCD detector, a high-powered Invictus™ 785-nm NIR laser and Holoplex™ grating technology. The camera, lenses and detector are all confined in a compartment similar to the illustration of Figure 2-13. The Holoplex™ grating permits the collection of the entire Raman spectrum simultaneously by folding scattered Raman photons onto the large-format multichannel CCD. This means all wavelengths are measured at once. A much faster and simultaneous collection of data and analysis is achieved making it especially useful for polymerizations and curing reactions.

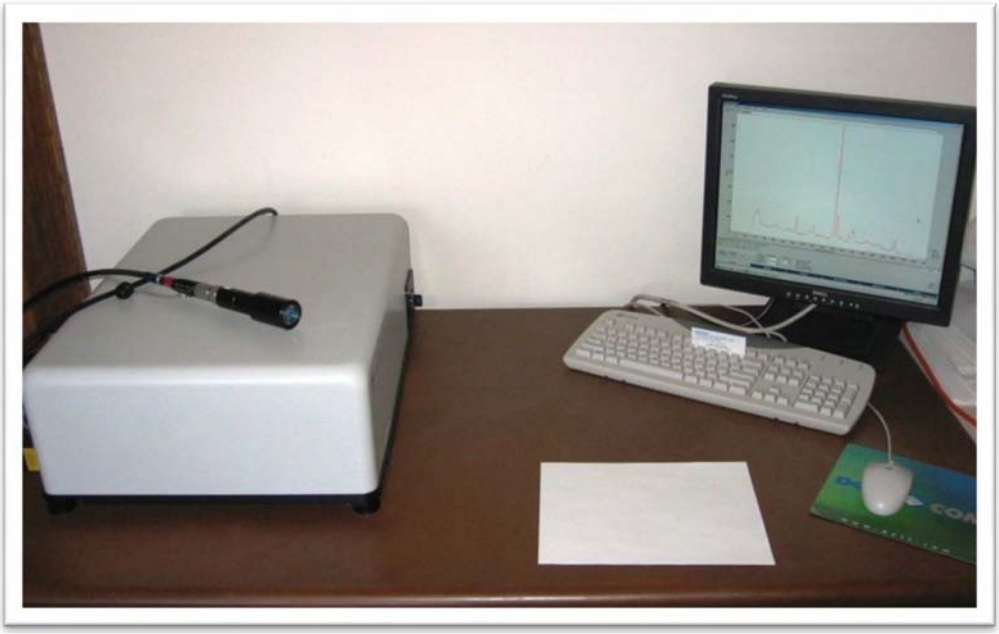

Figure 3-5. RamanRxn1™ analyzer Equipment

As seen on Figure 3-5, the equipment is compact consisting essentially of a computer, the main box and the optical fiber that connects the laser lens to the system. The length of the optical fiber may be extended as needed in order to setup probes at online processes. Two probes may be used: a non-contact optic (shown in Figure 3-5) and an immersion optic. Any of these may allow for non-destructive *in situ* collection of data. Immersion optics are usually used for liquid solutions, but for the case of thermoset resins which harden in time, non-contact optics are preferred and therefore have been selected for this research. Probes of focal distances of up to 17 inches may be obtained. Non-contact probes can be used by focusing the beam through site windows allowing online monitoring or around open tools and conveyer belts for tracing reactions or final residual substances. The laser power used was 300mV, which as will be shown did not induce any local heating effects. Spectra were recorded every 0.3s, 0.6s, and 1-6s depending on the speed of reaction. A

burst mode option is used which provides the ability of recording multiple spectra per second for our fast reactions. Spectra recording time can equal laser exposure time with burst mode. A fiber-optic sampling probe with an optical lens that has a focal distance of 2.5 inches was adapted to a microscope stand for easy focusing. The beam is focused at the depth where maximum intensities are obtained. This depth where the Raman signal will be strongest is assumed to be close to the middle of the thin sample. Equipment is controlled through PC software called Hologram which can be exported to Holoreact™, GRAMS and other managing software. The spectra in time are analyzed based on changes in peaks areas, shapes, positions and heights. For this research, peak intensity was related to conversion and reaction rates evaluated by derivation of the conversion functions.

Prior to any analysis normalization of spectra to a reference peak is required. When a material is being heated it starts in a lower energy level and increases its vibrational energy due to heat absorption. When imposed with an incident radiation the material will already be in a higher energy level increasing the probability for the molecules to release energy (anti-stokes) than to gain energy (stokes). Figure 3-6 demonstrates the variations in intensity of certain low range Raman frequencies due to temperature increases.

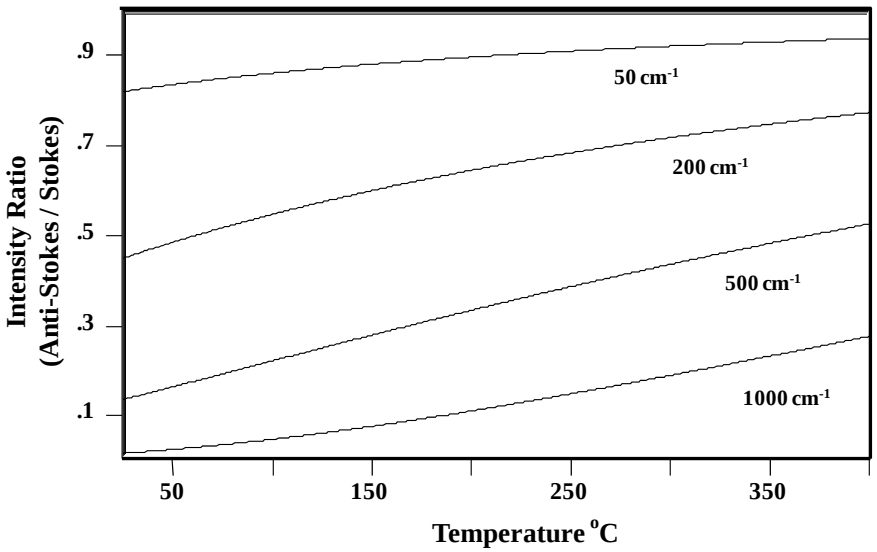

Figure 3-6. Anti-Stokes to Stokes ratio with increasing temperature.

This is the case for most thermosetting resins where some kind of heat is required to drive the reaction. The result will be a reduction of intensity in time for the whole spectrum. In order to compensate for this effect a reference peak for normalization which should be a peak that will not change due to the reaction has to be included in all reaction analyses.

Configuration of the laser to the lowest possible state of energy that would provide strong enough intensities for a reliable peak comparison was done. The reason was to minimize localized sample heating by the laser beam. Exposure time and laser power have to both be considered in the configuration. It was determined that for an adequate analysis the minimum intensity of the peaks being analyzed should be around 1500 counts. Producing at least 1500 counts during the low exposure times required for obtaining multiple spectra to accurately follow the curing behavior limited the laser power to a minimum of 300mV.

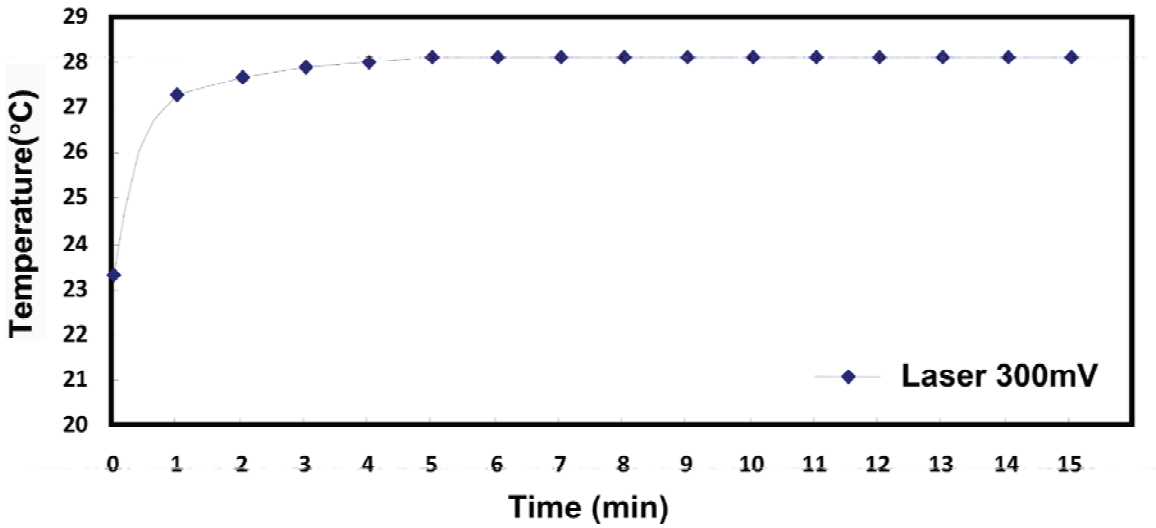

Figure 3-7. Temperature rise at focal point of beam for an unsaturated polyester resin due to laser impact at constant exposure.

Figure 3-7 shows the long term behavior of the material at constant exposure and a laser power of 300mV. As seen, temperature rises significantly for the first minute then levels off at approximately 5°C over the actual sample temperature. This temperature increase is not enough to affect the peak heights, but may significantly affect the reaction. For this reason exposure times have been kept low (0.3s-6s) with enough downtime to equilibrate. Downtime is used with intermittent beams and is the time after exposure and during analysis where laser shutter closes. As an intermittent beam the localized heating of the sample does not even reach 1°C for our longest exposures.

As demonstrated, this Raman reaction monitoring system may be a very valuable tool for monitoring thermosetting reactions. Due to its ease of use and fast spectral response it may be used for online monitoring and control of processes—a field of great interest today within the newer automated systems. In order to expand on this subject matter and

resolve the issues of monitoring highly accelerated *UP* reactions a closed reaction chamber was built. The chamber imitates real process conditions were material is not directly accessible but may be emitted with a laser beam through a window. The combined system would then serve as a new method for testing resins and performing kinetic studies. In order to account for exotherms and variations in heating rates an accurate heating and temperature control system would be adapted to the chamber. With an adequate control system and proper design adequate response for highly accelerated reactions may be obtained.

3.3 Reactor Design

A cylindrical shape reactor (Figure 3-8) with an inner cavity of 0.62in has been designed to specifications. The volume of the inside cavity is about 0.377in^3. The top of the reactor has a half inch fused silica window sealed for pressure by a Viton O-ring and eight screws. There are 2.25in from the top of the reactor to the sample dish which allow enough focusing range for the 2.5in non-contact optic provided with the Raman system. For the complete drawing, view Appendix A. The reaction chamber will offer an alternative method to monitor cure including highly accelerated reactions such as those found to be uncontrollable by DSC. With an accurate control system that reacts to direct temperature changes of the sample temperature overshoots may be directly monitored and controlled.

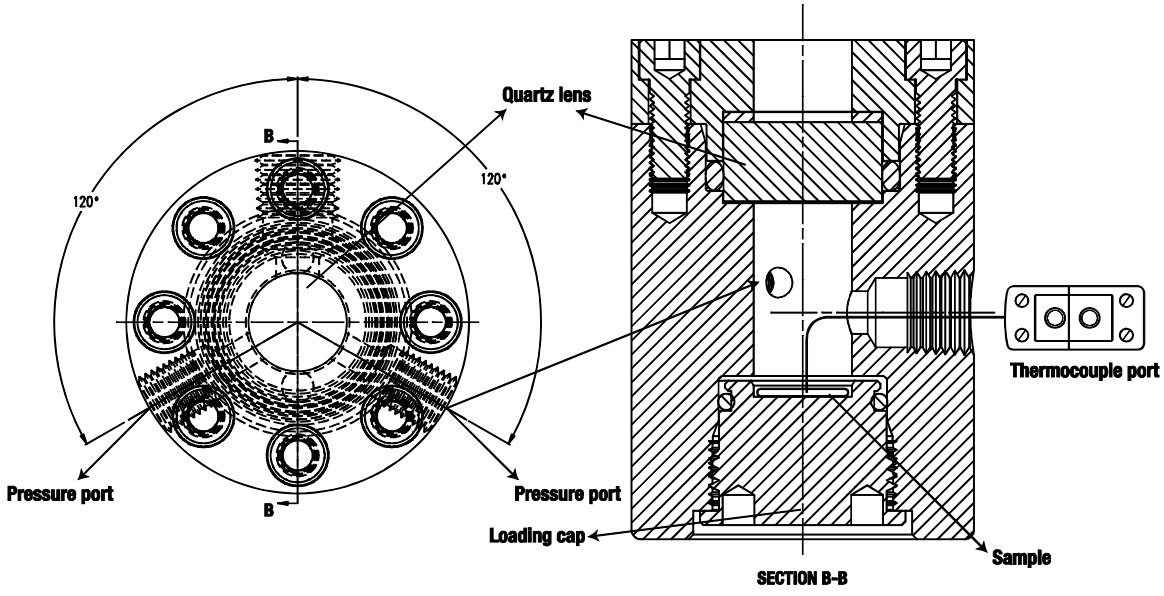

Figure 3-8. Top view of reactor (left). Side view of reactor parallel to direction of thermocouple port (right).

As seen in Figure 3-8, the reactor contains three accessibility ports. One allows the insertion of up to three thermocouples, and the other two are used to nitrogen-purge and pressurize the system. It is of great interest to monitor reactions under pressure to determine the pressure effect, if any, in thermosetting curing reactions, as well as to simulate reaction behaviors in autoclaves and compression molders. One TMQSS-040-6-DUAL grounded thermocouple from omega was used as the process sensor. The grounded thermocouple results in a faster direct response from the tip of the thin sheath. The tip of the thermocouple goes directly into the sample and one output signal is sent directly to the controller. The second output of the dual sensor is connected to a temperature data-logger which records at variable time spans, up to the speed of one measurement every second. All ports are equally spaced at 120 degrees from each other. This permits better nitrogen dispersion in the chamber and prevents the thermocouple from being directly in front of any cold nitrogen shot if cooling is used. The sample is inserted through a screw-in access port at the bottom of the chamber, containing a 0.10in gap for sample placement, and is sealed to pressure with a Viton O-ring and locked into place by using a spanner wrench.

A nitrogen tank is connected directly to the reactor with 1/8 inch OD tubing and compression fittings. At the reactor's exit port, a 2000psi four inch gauge is used to monitor the pressure and a PV 52-1-11 Ideal Needle valve is used to release nitrogen and manually maintain pressure constant during cure. An automated pressure controller may be easily adapted if desired. The reactor is mounted unto a microscope stand for precise focusing of the laser into the reactor chamber.

Heat Requirements

In order to heat the reactor, three 600W flexible electric heaters provided by Watlow Electric were wrapped at full contact around the reactor surface. Power requirements were determined by calculating the required heat energy. Watlow provides a series of equations in order to estimate power requirements by simple heat transfer results. Three methods were used. An approximation method which assumes a solid piece, a short method which includes losses of heat in the part, and a long method which takes into account individual convection, conduction and radiation losses.

Method 1: (Assuming a solid piece of steel of 3.0lbs being heated at 50K/min)

Method does not account for heat losses.

$$W_{required} = \frac{Pounds * 1000 * TemperatureRise(^{\circ}F)}{20{,}000 * Heatup_{time}(hrs)} = \frac{3.0 * 1000 * 356}{20{,}000 * 0.06)} = 890W \qquad (3\text{-}1)$$

Method 2: (determines losses by the use of one equation)

Properties of the material being heated: assuming the sample size is small relative to the reactor size (mostly stainless steel) and that there is insulation around the reactor.

Table 3-3. Properties of the material and calculation parameters. Where κ_{Ins} refers to the thermal conductivity of the insulating material.

Weight = 3.0lb	$Rate_{start-up}$=50K/min	$\Delta Trise_{start-up}$ = 120˚F	Surface A = 0.2ft^2
Cp_{ss} = 0.14 BTU/lb-˚F	$Rate_{operation}$=20K/min	$\Delta Trise_{operation}$ = 3˚F	κ_{Ins} = 84.7 BTU-in/ft^2-˚F-hr

Equations to be calculated:

Start-up watts = A + C + 2/3L + Safety Factor (3-2)

Operating watts = B + D + L + Safety Factor (3-3)

where,

A = Watts to raise temperature to operating point in desired time (for isothermals).

C = Watts to melt or vaporize during start-up (Not present in system)

B = Watts to raise temperature of material during operation.

D = Watts to melt or vaporize during operation (Not present in system)

L = Conduction, convection and radiation losses

For method 2, it is recommended to use a safety factor of at least 10%

No melt or vaporization is occurring at start-up or operation therefore C & D = 0

$$A \text{ or } B = \frac{Weight[lbs] * Spec.Heat * Temp[^\circ F]}{Startup/Cycle-time[hrs] * 3.412[BTU/Watts-hrs]} \quad (3\text{-}4)$$

Substituting gives,

$A = 886.26W$

$B = 22.16W$

$$L = \frac{ThermCondMat/Ins[BTU \cdot in/\ ft^2 \cdot °F \cdot hr] * SurfaceArea[\ ft^2] * (T_p - T_{amb})[°F]}{Ins/MatThickness[in] * 3.412[BTU/Watts - hrs]} \quad (3\text{-}5)$$

Assuming room and max operating temperature to be 68ºF and 428ºF respectively; (T_p-T_{amb}) = 360ºF. Since the thickness of the insulation material is approximately 1.54 inches we obtain,

$L = 1161.16W$

Substituting into equations (3-2) and (3-3),

Start-up = 1826.7W

Operating = 1301.6W

Method 3: (determines individual convection, conduction and radiation losses)

Equation I: (similar to A or B) (applied for each material in reactor)

Start-up ΔT = 360ºF, Operation ΔT = 3ºF

$$AbsorbedEnergy(Q_a or Q_b)[Wh] = \frac{Weight[lb] * Cp[BTU/lb \cdot °F] * \Delta T}{3.412} \quad (3\text{-}6)$$

$Q_a = 44.31Wh$

$Q_b = 0.37Wh$

Equation II: (melt or vaporization) = Not present in system

Qc or *Qd*=0

Equation III: (Conduction losses)

$$Q_{L1}[Wh] = \frac{k_{ins}[BTU \cdot in / ft^2 \cdot {}^\circ F \cdot hr] * SurfaceArea[ft^2] * \Delta T[{}^\circ F] * t_{\exp osure}[hr]}{3.412 * L[in]} \quad (3\text{-}7)$$

where, $t_{exposure}$ is the exposure time and the difference in temperature is obtained by approximating the temperatures between outside(over insulation) and inside wall.

$Q_{L1} = 177.2Wh$

Equation IV: (Convection losses)

$$Q_{L2}[Wh] = SurfaceArea[in^2] * F_{SL(lossfactor)}[W / in^2] * C_{F\{=1vert.\}} \quad (3\text{-}8)$$

$Q_{L2} = 23.13Wh$

Equation V: (Radiation losses)

$$Q_{L3}[Wh] = SurfaceArea[in^2] * F_{SL(lossfactor)}[W / in^2] * Emmisivity_{Almn} \quad (3\text{-}9)$$

$Q_{L3} = 0.83Wh$

Equation VI:

$$Q_L = Q_{L1} + Q_{L2} + Q_{L3} \quad (3\text{-}10)$$

Q_L = 201.16W-hr

For this method it is recommended to use a safety factor of at least 20%.

Start-up power (W)

$$P_s = \left[\frac{Q_A + Q_C}{t_{Start-up}} + \frac{2}{3}(Q_L) \right] * (1 + S.F.) \quad (3\text{-}11)$$

= 1611W

Operation power (W)

$$P_O = \left[\frac{Q_B + Q_D}{t_{Cycle}} + (Q_L) \right] * (1 + S.F.) \quad (3\text{-}12)$$

= 173W

As determined from the power requirements three 125PS38A23A-562 Watlow Flexible Heaters rated for 600W at 240V were installed around the reactor. A ceramic based insulation was applied over the heaters to minimize heat losses. Two convective fans were installed over and under the reactor to provide good heat convection through the non-insulated areas.

Temperature Control

A temperature control system was developed to allow for constant heating of the sample at various rates up to approximately 50K/min with minimal overshoot of temperature upon reaching set-point. Figure 3-9 presents a diagram of the set-up.

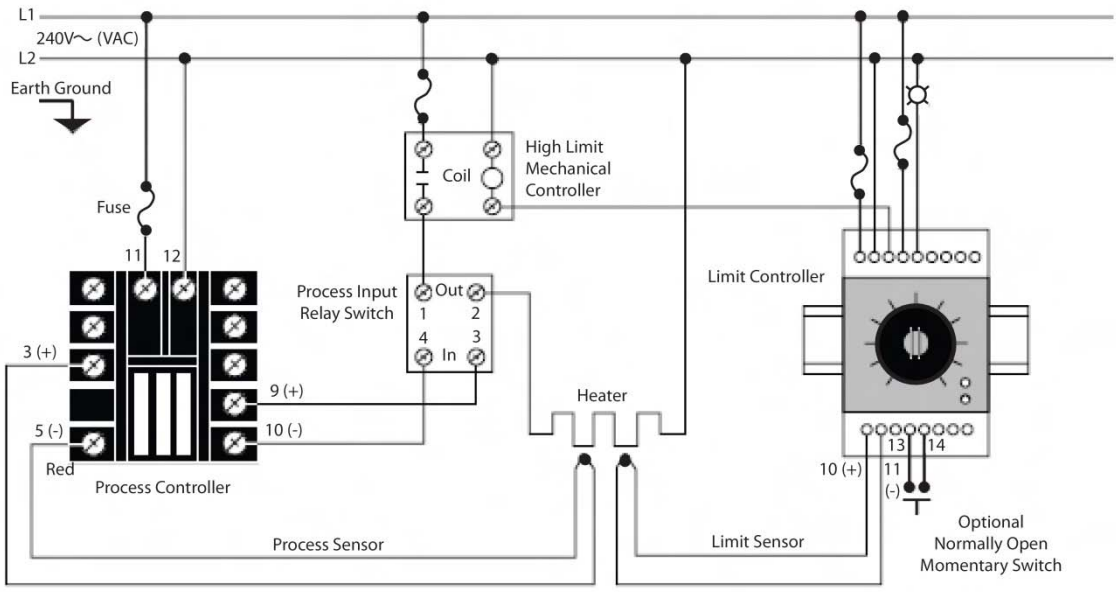

Figure 3-9. Diagram of the wiring setup design for the control system.

As previously mentioned the process thermocouple is directly immersed in the sample and controlled by the process controller. A second thermocouple was attached to the top-side surface of the reactor as a limiting sensor, to assure the reactor would not reach its maximum temperature rating. The limit controller was wired between the heating circuit by a solid state relay to turn off heating if required. All three heaters where connected in parallel to a solid state relay which was activated by the process controller. Based on the heating requirements a 240V input was used for a total of 6 amps throughout the heaters. An additional 10 amp fuse box, heater breaker switch, and main switch were installed as needed.

Figure 3-10 shows the completed set-up. The reactor system allows for automated temperature control at constant and variable heating rates. Pressures of up to 2000psi with or without continuous convective gas flow may be applied with temperatures up to 200°C. Sample insertion is easy with a removable bottom port and purging protects the sample being analyzed. Direct contact of sample with process sensor is a key feature for better reproducibility of experiments and accurate kinetic information.

Figure 3-10. Control box (left). Inner control box wiring set-up (middle). Microscope stand mounted reaction chamber (right).

3.4 Raman Spectral Identification: Unsaturated Polyester and Epoxy Resins

Most spectra contain a great deal of information and many times, valuable information of the molecular structure. From 200cm^{-1} up to 4000cm^{-1} many peaks are seen to be affected by the reaction. As shown in Figure 3-11, one of the areas of the unsaturated polyester spectrum where noticeable peaks of importance reduce during the reaction progress is the range from 700cm^{-1} to 1800cm^{-1}.

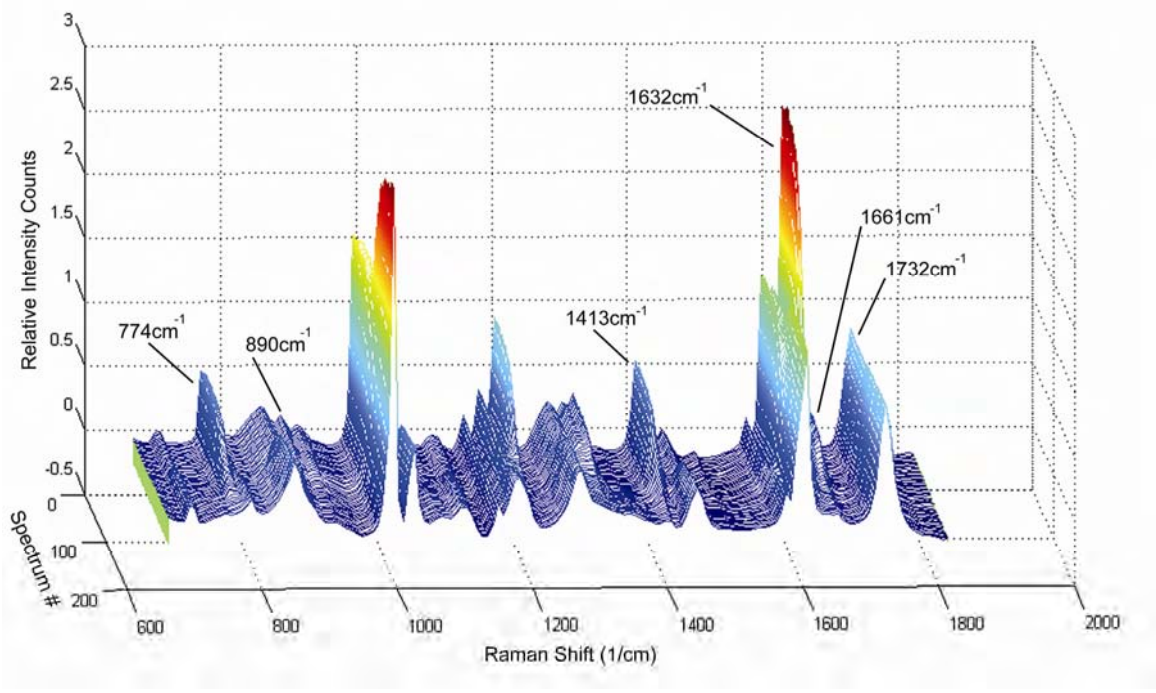

Figure 3-11. Waterfall view of a collection of the unsaturated polyester resin spectra obtained at constant time intervals.

Descriptions of the molecular bond vibration responsible for each peak denoted may be found in Table 3-4. One of the strongest peak vibrations that may be seen is the 1632cm^{-1}

resulting from carbon-carbon double bond (C=C) stretching vibrations in both the backbone of *UP* and branch of styrene. Due to the high concentration of C=C bonds before conversion very high intensities are noted for this peak, but as seen in Figure 3-12, as the reaction progresses spectra taken at later times show the decrease of the peak until ultimately the peak practically disappears.

Table 3-4. Unsaturated polyester peak definitions.

Peak (cm^{-1})	Description
774	Ring or combination mode of styrene
890	*UP* Stretching interactions with $C-\overset{\overset{O}{\|}}{C}-O$
1413	CH_2 deformation (δ) present on styrene
1632*	C=C stretching vibration on styrene and *UP*
1661	C=C stretching vibration particular to *UP*
1732	C=O carbonyl stretching vibration in *UP*

*main peak used for analyses

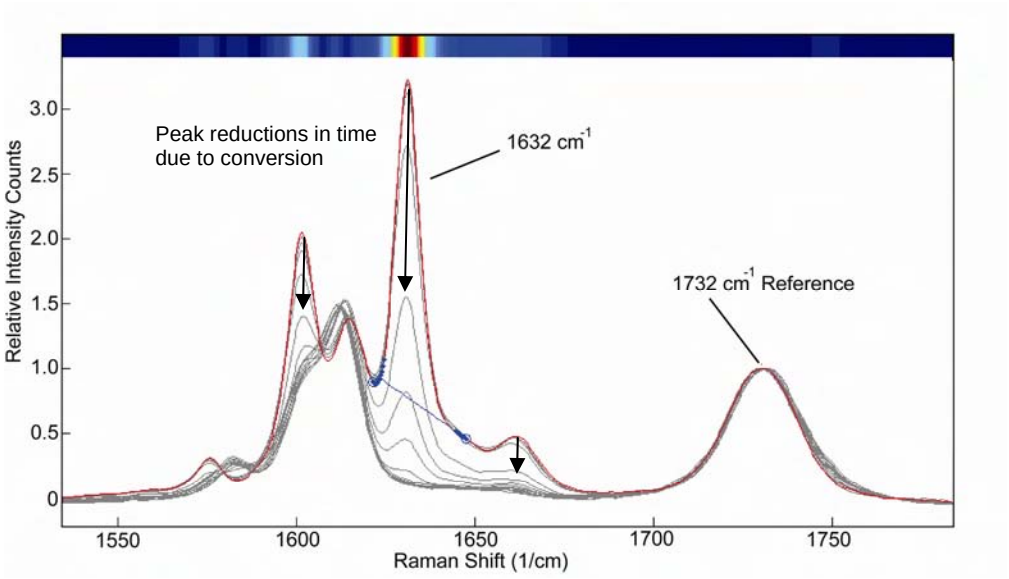

Figure 3-12. Plot of overlapped spectra in time for unsaturated polyester peak 1632cm^{-1}.

A peak height of zero would ideally represent a 100% conversion or consumption of C=C double bonds. In the same way any residual peak refers to incomplete conversion. In reality, peaks never fully disappear, holding true to the idea that reactions never reach 100% conversion due to limitations of molecules to find each other in these solid structures, where final reaction stages are limited to a slow diffusion process. Peak 1732cm^{-1} created by carbonyl (C=O) stretching vibrations in the *UP* molecule does not play a role in the curing reaction and has been identified as a peak that will not change or interact with the reaction vibrational changes. For this reason, it has been used as a basis of normalization.

A similar analysis was performed for epoxy resin, where the peaks consumed during the reaction relative to vibrations occurring before ring-opening of the oxirane are used to

determine conversion. Table 3-5 describes some epoxy spectrum peaks shown to be affected by the reaction conversion in time.

Table 3-5. Epoxy peak definitions

Peak (cm^{-1})	Description
1186	C-H in plane backbone bending vibration
1255	Overlapped Oxirane vibration
1350*	CH_2-O stretch interaction with oxygen in ring
3004	CH_2 stretch vibration in epoxide ring

*main peak used for analyses

As previously discussed in section 2.3.2, most researchers [68, 70, 76] have used the oxirane vibration which for our epoxy molecule results in peak 1255cm^{-1} as the main peak to determine conversion due to the high intensity in Raman spectra. Unfortunately, as shown in Figure 3-13, this peak suffers from an overlap (affected by other interactions) and therefore at this frequency region a residual peak always remains, even after full conversion. To account for this, one must generate a spectrum after a long period of time and designate it as a full conversion spectrum. The problem with this is that realistically there is never 100% bond consumption due to the diffusive reaction stage occurring at infinite viscosities. It has also been shown that for certain resins maximum attainable conversion may vary with external ambient conditions such as atmospheric pressure and humidity levels. It is therefore necessary to make assumptions on unknown systems as to when a maximum conversion has been reached.

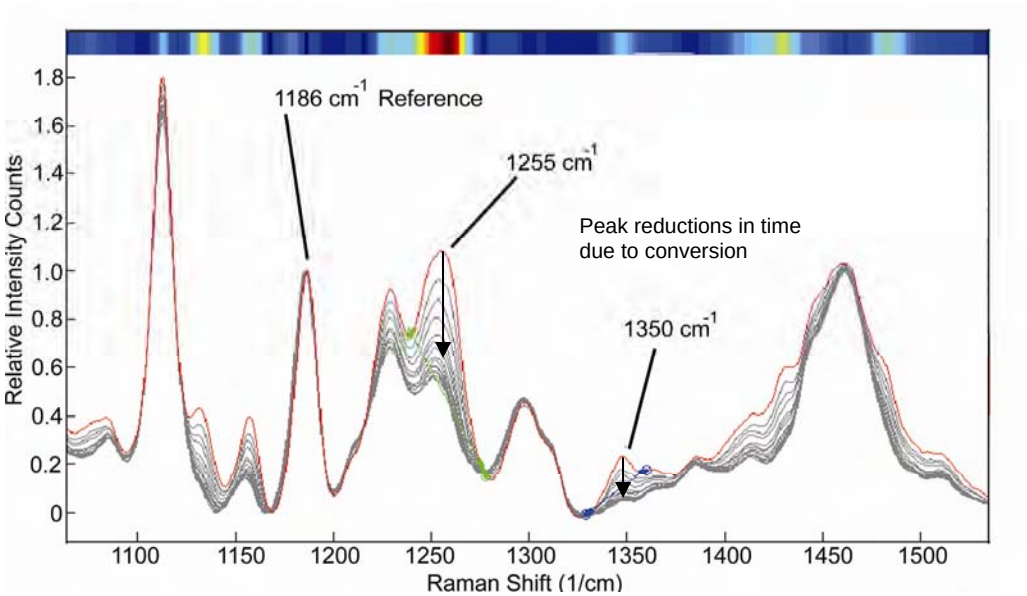

Figure 3-13. Plot of overlapped spectra in time for epoxy denoting peaks of interest.

Peak 1350cm^{-1}, related to the CH_2 stretch interaction with the oxygen within the epoxide before ring opening occurs, will be used for analysis. This peak, although small, fully disappears due to the cross-linking reaction. Peak 1186cm^{-1} (associated with the C-H in-plane bending) [69, 70] was used for basis of normalization, since this peak would not undergo changes in intensity due to the curing reaction.

3.5 Curing Analysis with Raman System

Through the implementation of the reactor design with the Raman system an accurate method for monitoring and studying cure was developed. Unsaturated polyester and epoxy samples were tested with our equipment and excellent results were obtained. A series of different experiments were generated including the cure monitoring of fast and slow *UP* curing reactions, a step process cure, and the comparison of consumption of individual bonds. Since our epoxy resin is a room temperature slow curing material, no particular differences in cure were seen when compared to DSC. Therefore, no plots of epoxy will be presented in this section. Epoxy results will be discussed in Chapter 4 where samples cured under different pressures were compared to each other.

UP Highly Accelerated Reactions

Material used was prepared as described for the DSC analysis (section 3.1) but placed over a thin aluminum shim. The shim was then placed in the reactor cavity on the groove of the loading cap (refer to Figure 3-8). The aluminum works as a low noise background surface for the Raman laser. Thickness is controlled with a surrounding washer of a specific thickness and by use of a glass microscope cover slide placed over the sample which helps uniformly distribute the material. Sample thickness is directly related to mass since the diameter remains constant. The diameter of the sample was 9.9mm, large enough to provide an adequate surface area for heat transfer and to improve thermocouple contact. Thicknesses have been kept low to eliminate sample overheating and not require any liquid nitrogen cooling. Thicknesses were varied between 0.2mm –

1mm with heating rates of 5K/min, 10K/min and 20K/min. Sample size is determinant on how complicated the control of overheating for a sample may be. A thickness of 0.5mm and under was found to be relatively good to ease calibration and optimization of the temperature control system. Figure 3-14 shows a graph of conversion in time for a *UP* reaction at 5K/min and a sample thickness of 0.5mm developed using spectral changes from peak 1632cm^{-1}.

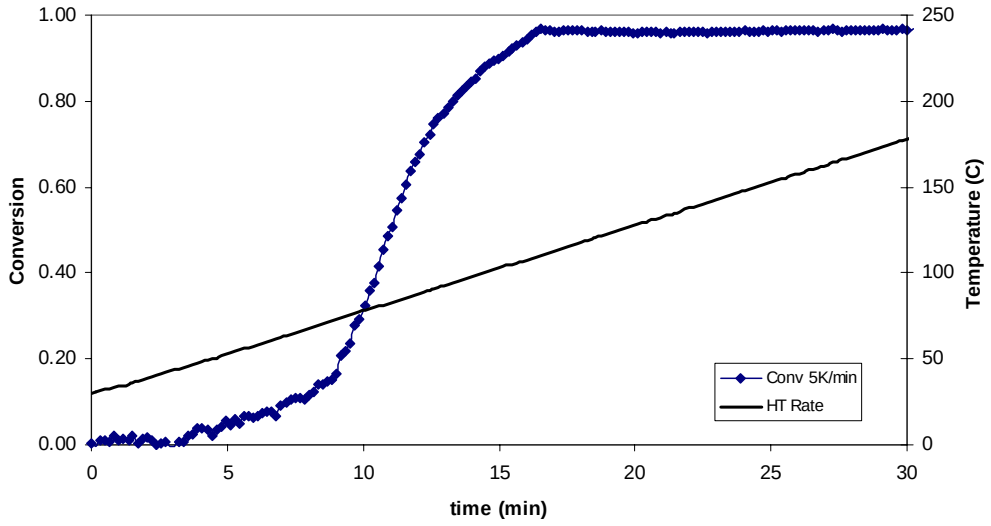

Figure 3-14. Conversion and temperature in time for a 0.5mm sample of *UP* heated at 5K/min from room temperature to 180˚C. Heating rate curve is the actual temperature of the sample recorded in time.

As shown, a very uniform heating rate with no overheating of the sample may be obtained. Smooth heating leads to accurate conversion results that may be directly related to the temperature changes in the sample. Due to the slow rate of heating, slower reaction rates take place as may be seen by the low slope of the conversion curve during the accelerated reaction stage. Figure 3-15 shows results for a reaction occurring at a rate of 10K/min and a sample thickness of 0.5mm.

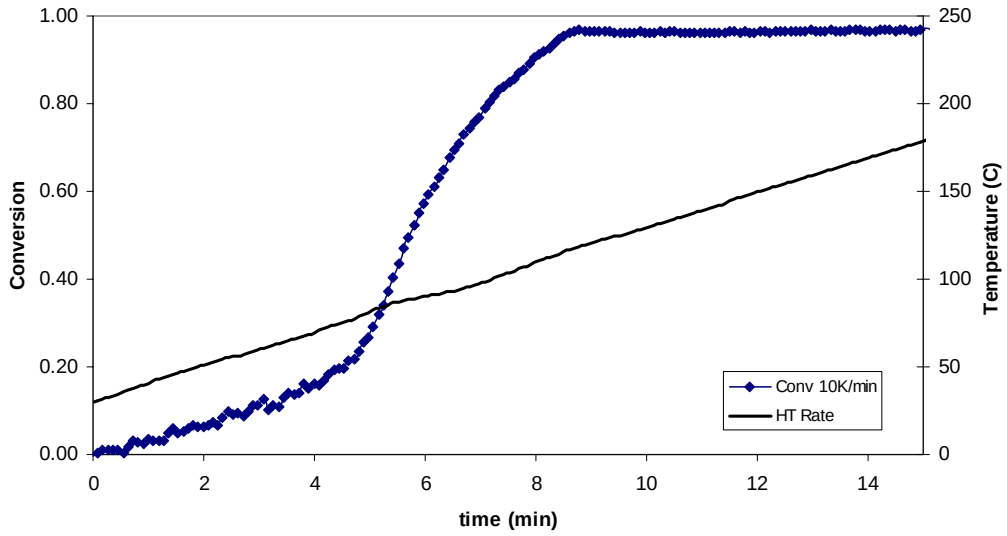

Figure 3-15. Conversion and temperature in time for a 0.5mm sample of *UP* heated at 10K/min from room temperature to 180˚C.

Again, we may notice a very accurate and well controlled heating rate with no sample overheating. Reaction rates are higher for this case with an accelerated reaction period starting around 4.5min into the test and lasting close to 4min, as compared to a period of 7.5min for the 5K/min reaction. At 10K/min overheating is avoided due to the excellent temperature control for these thin sample sizes. It is important to mention that Raman spectroscopy reports a real conversion as a function of time. Here, there is no need to normalize results with respect to a represented “100% conversion” as required with DSC and many other cure monitoring systems. Any molecules that have not reacted are represented by a residual peak in which its height and area are related to the percentage of unreacted bonds.

Results shown with the DSC in section 3.1 demonstrated that big overshoots in temperature occurred for heating rates of 20K/min. The set of graphs in Figure 3-16 show how there is extreme sample overheating for thicker samples with our Raman reactor system as well, and how an accurate heating control with a TC directly imbedded into the sample can control or reduce the overheating greatly. Figure 3-16 (a) presents results for a sample reacted at 20K/min and a thickness of 1mm. Due to the lack of availability of liquid nitrogen for rapid cooling of the thicker sample there is an overshoot in the temperature that could not be eliminated. If purposely, an inaccurate temperature control that assumes no overheating of the sample is used, a large overshoot will result, as seen in Figure 3-16 (b). When comparing the heating curve on Figure 3-16 (b) to a DSC sample temperature (T_s) curve (Figure 3-16 (c)), it is clearly seen that a similar temperature overshoot is present at such high reaction rates. Key differences are seen when comparing the conversion curves. Since the Raman spectroscopy equipment is monitoring the actual molecular reaction, the overshoot of the temperature results in an increase in reaction rate that leads to a sharp rise in the curve up to maximum conversion. Figure 3-16 (a) shows a similar behavior but to a lower extent due to lower overheating. On the other hand, the DSC does not report such a behavior but shows a smooth curved transition to full conversion as if the reaction had lowered its rate after about 80% cure. This shows that for these highly accelerated reactions the heat release in time detected by the DSC is not directly related to the real conversion of the resin, due to heat transfer delays present and the overheating of the sample.

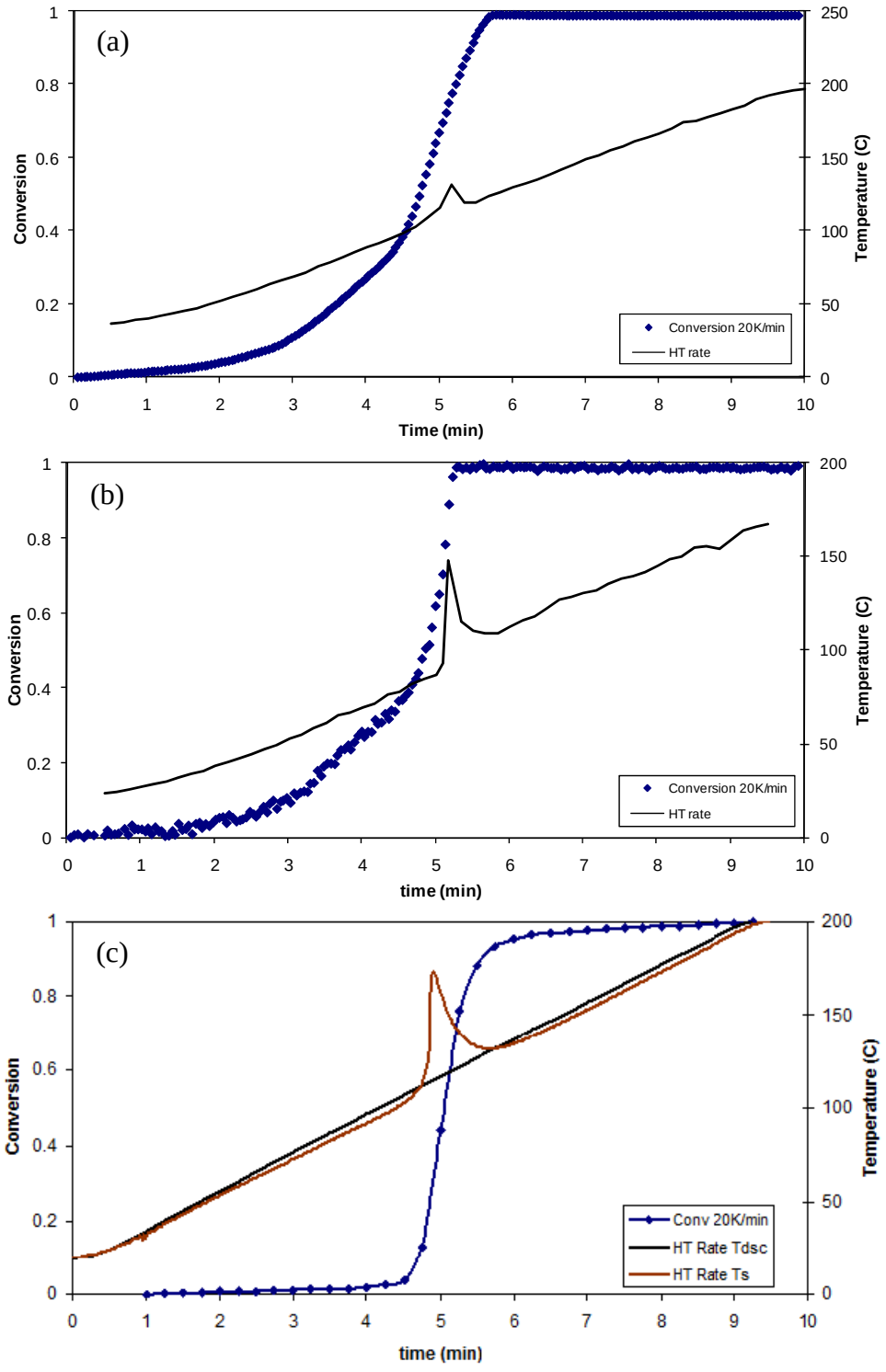

Figure 3-16. Conversion and temperature in time for 1mm sample of *UP* at 20K/min. (a) Controlled sample temperature. (b) Uncontrolled. (c) Conversion and temperature in time for *UP* sample of 32.2mg analyzed by DSC at 20K/min.

In order to be able to control the heating rate at 20K/min without the need of liquid nitrogen or other advanced cooling systems, the thickness of the sample had to be reduced. Figure 3-17 shows a result for a sample thickness of 0.5mm.

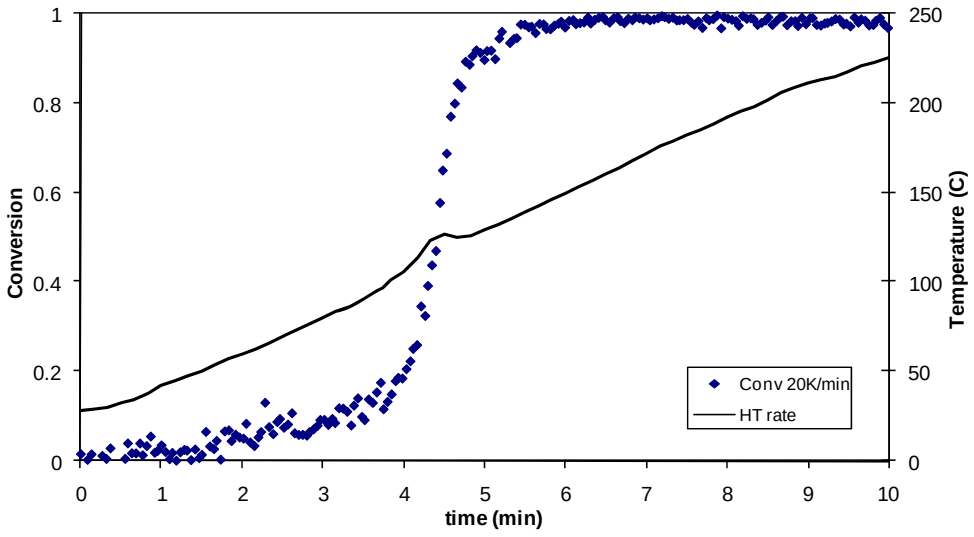

Figure 3-17. Conversion and temperature in time for a 0.5mm sample of *UP* heated at 20K/min from room temperature to 180˚C.

Overheating of the sample was greatly controlled by the control system but not fully eliminated. A hump on the heating rate curve may be seen right over the steepest part of the conversion curve, demonstrating how the sample overheated and simultaneously the reaction rate increased. For this case due to the better control of sample overheating a decrease in the reaction rate is seen after 85% conversion. By reducing the sample size

again, this time to 0.2mm as shown in Figure 3-18, the sample overheating was eliminated.

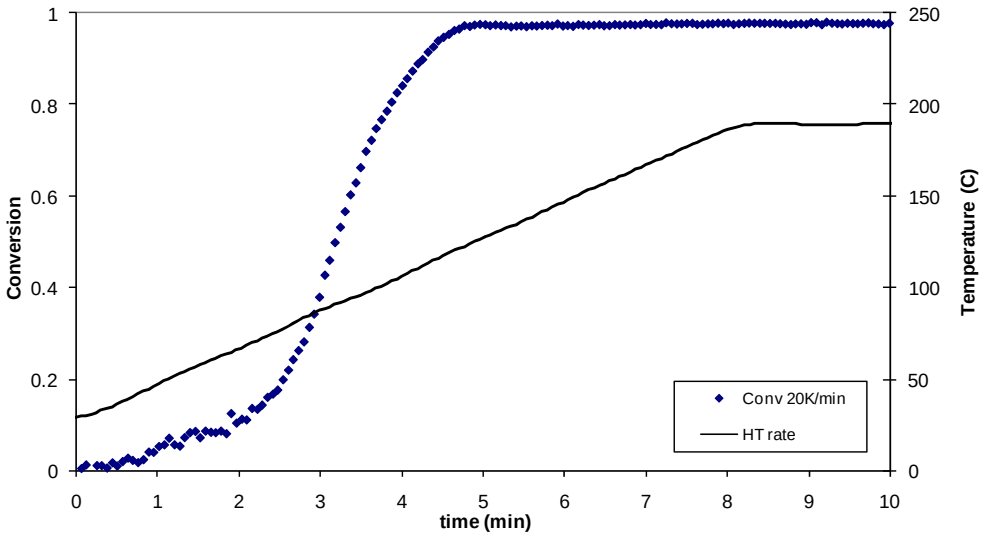

Figure 3-18. Conversion and temperature in time for a 0.2mm sample of *UP* heated at 20K/min from room temperature to 180˚C.

The advanced temperature control proved efficient at the reduced sample size and cooling systems were not required. A lower overall reaction rate may be observed, seen by the lower slope of the conversion curve. Smoother changes were obtained during the initial and final stages of the reaction with a period of 2.5min where the reaction was accelerated, and accomplished at a very uniform heating rate.

UP Slow Curing Reactions

A set of experiments were performed with MEK-P as an initiator. Peak analysis is completed in the same manner since the material being monitored is distinctively the styrene and *UP*, not the initiator. Studying the vibrations of peroxides is possible if there is an interest in evaluating the rates of initiation. The cure behavior results were similar to results reported by Skrifvars [90] for slow reaction rates. Figure 3-19 presents an example of *UP* resin reacted using MEK-P through a series of step heatings. The purpose is to demonstrate the application in a variable unstable process. As shown, precise curing results are obtained throughout all stages of cure.

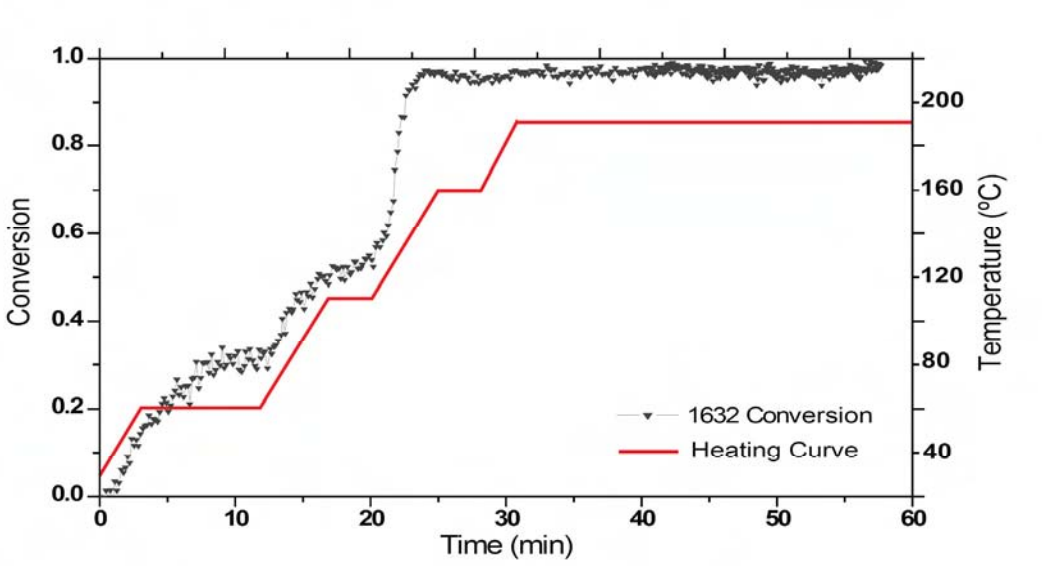

Figure 3-19. *UP* resin reacted using MEK-P as initiator. Reaction performed in a series of heating steps. The heating rates were maintained low at 10K/min.

During the first step of the reaction, a heating rate of 10K/min was applied until the sample reached around 60°C. After 10min, a heating of 10K/min was applied up to 110°C. A shorter hold, then again, a heating rate of 10K/min was applied until 160°C. Finally, the sample was superheated from 160ºC-190ºC and sustained at 190ºC to obtain the highest possible cure. This last heating step increased the percent conversion from 97% to 99.5%; a minimal amount achieved in a diffusive process. The final peak reduction was not due to styrene evaporation, but a small percent increase in conversion was observed for the 1661cm^{-1} peak which was used to report the final conversion results. As may be noticed, all the steps of the reaction are clearly defined as changes in slope during different heating rates. Reaction rates vary depending on the changing T_g of the material, active sites and energy provided for cure. As noted, the temperature range and activation properties of the initiator control the stages of cure and dictate when the cure accelerates.

Comparative Peak Analysis

As described in section 3.4 many peaks may be used to monitor the reaction. The peak selected for analysis is dependent on the kinetic or chemical information of interest. For curing reactions, peaks directly related to functional groups are the ones mainly considered. By analyzing individual peaks one may determine if stoichiometric ratios have been maintained. For an unsaturated polyester resin, depending on the ratio of monomer to polymer (styrene to *UP*) used, active sites may be hindered and for certain reactive groups, incomplete reaction could occur. For an amine hardened epoxy it is even

more critical since one amine is needed for each epoxide group. *UP* resin reacted in an excess of styrene will lead to a brittle part. If the ratio is too low, *UP* active sites will not have a chance to react with styrene monomers and although some might react amongst each other, due to the reduced mobility of a polymer network, many sites will remain unreacted. Figure 3-20 illustrates this effect. For this example, a lower styrene content of 1:1 rather than the recommended 2:1 ratio was used.

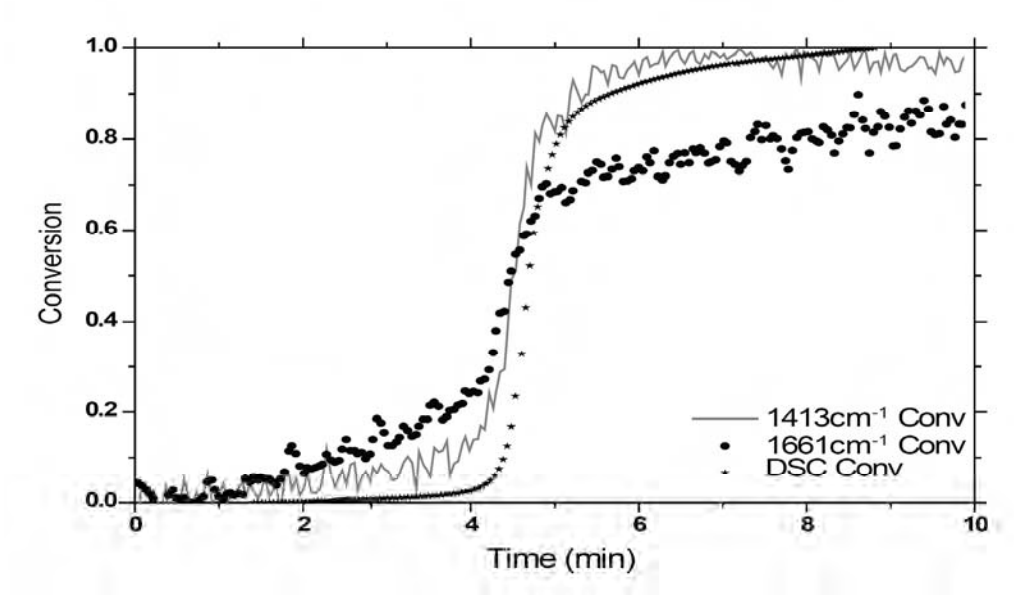

Figure 3-20. Conversion as a function of time for individual *UP* and styrene bonds of a sample reacted at 20K/min with a 1:1 *UP* to styrene ratio.

Each curve is representative to respective peak reductions. A DSC analysis for the same system was included for comparison. As discussed in section 3.4, there are certain peaks that directly relate to molecular transformation and can individually describe how styrene and *UP* C=C bonds are consumed in time. Peak 1413cm^{-1} relates to the reaction of

styrene and may also account for any evaporation of styrene in the system. Similarly, peak 1661cm^{-1} relates to only *UP* C=C bonds. As observed in the figure, styrene reached a much higher conversion than *UP*. Final average bond consumption after 10 minutes was estimated to be 97% for styrene and 85% for *UP*. When comparing the Raman results to DSC we may see how the 1413cm^{-1} curve and the DSC curve are most similar with very comparable rates of reaction. It is also important to note the two main differences between the DSC and Raman results. During the initial period of the reaction there is a difference in the conversion values because Raman is monitoring the real conversion process. At approximately 3 minutes average conversion estimated by the Raman system is 10% whereas the DSC reports 1%. The other difference is the shifted DSC curve to later times due to the delay of heat transfer. For this case, approximately a 12 second difference is seen between the DSC curve and styrene curve during the highest conversion rate. A similar behavior was observed throughout every run performed. Other experiments were generated with different initiator combinations and the curing behavior correlated well to the activation temperatures and ranges of the initiators.

3.6 Applications

As demonstrated throughout the chapter, Raman spectroscopy cure monitoring systems are very powerful tools that allows for a precise, reproducible and real cure analysis. Through the design of an accurate control system kinetic parameters may be obtained with minimal errors. This may lead to better and more accurate results for models used to describe thermoset reactions. Our reactor design may be expanded into many different areas of research. It is capable of being used for studying thermoplastics and many other thermosets. For thermoset resins the key to monitoring cure is identifying the chemical changes occurring during a reaction. The reaction chamber may be used as a laboratory device for material characterization including; identifying proper stoichiometric ratios, studying changes in cure with different initiators and catalysts, relating cure to temperature and pressure, obtaining kinetic parameters and developing phase diagrams.

The Raman system itself has been tested with our reacting chamber and reactions have been monitored through a 0.5 inch window. This provides another realm of applications for online monitoring of cure. Many industrial processes may be monitored online by the use of non-contact optics. A window may be installed in an autoclave or RTM system to monitor cure. For pultrusion and extrusion, optics may be installed throughout different sections of the die to obtain cure level at these points. Completed parts may be tested after curing to determine the amount of unreacted substances remaining within the part. This finds extensive use within medical devices, dental resins and for some prosthesis that will be in direct contact with the body.

4 Pressure effects on Reaction and Mechanical Properties of Unsaturated Polyester and Epoxy Resins

4.1 Pressure Cure and Morphology

The complicated reaction mechanisms taking place during cure are highly dependent on processing conditions such as time, temperature, pressure, and concentrations. Not only processing conditions but geometry of the part plays a significant role in cure. For example, variations in thicknesses cause changes in the heat transfer and release affecting the reaction rates and curing times. Final mechanical properties, chemical resistance and long-term behavior of thermosets are dependent on the degree of cure. Therefore, a thorough understanding of the variables which affect cure has to be met to obtain the highest quality parts. Many thermoset processes require the use of pressure. Pressure ranges for these processes vary but in many instances pressures may be well over 1000psig.

As discussed in section 2.4 reports have been published that describe the curing behavior of thermosets at the molecular level [7, 9, 49, 86, 87]. These interactions at the molecular level are affected by any changes in the process including temperature and pressure variations. Relations between the curing of the material, temperature and viscosity have been well described and based on the cross-linking behavior, researchers have suggested how pressure might affect the cure [9, 91-93]. These relations vary based on the polymerization process and the rates or exotherms suffered by the system. Highly

accelerated pultrusion resins, modified resins and many epoxies such as those used for infiltration and coating are yet to be studied. Huang et al. [9] studied the effects of pressure for an unsaturated polyester resin reacted isothermally at 110°C from 0 to 900psig initiated with tert-butyl perbenzoate (TBPB). They performed the study through a combined approach of kinetics using a pressure DSC and IR, rheology with a Haake rheometer and morphology by use of SEM. Variations in reaction kinetics for these slower reactions which lasted approximately 50 minutes were seen with increased pressures. The morphological study based on micro-gelation reaction mechanisms was used to describe the kinetic changes.

When looking at a conversion curve three main steps may be noticed. Figure 4-1 depicts the three stages.

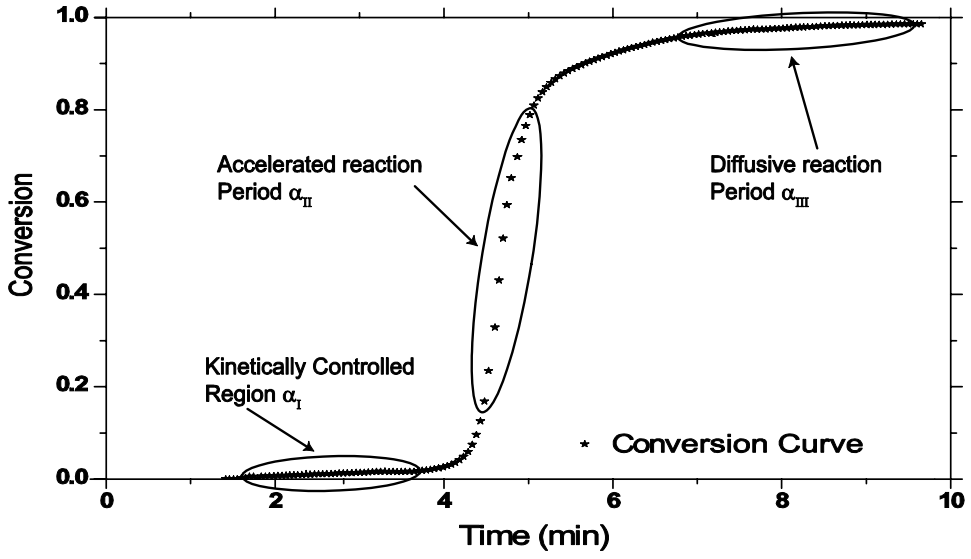

Figure 4-1. General conversion curve depicting the main kinetically and morphologically varying regions during cure.

The kinetically controlled region (α_I) is a region representative of the activation behavior of the initiator at the respective activation temperatures and any cure inhibitor that might have been added to the resin. Reaction is slow and initiates growth of microgels (section 2.4). Pressure will affect the growth of these microgels by affecting the reaction rate constants, distance between neighboring molecules and molecular mobility. As the pressure increases microgel structure becomes more compact and less porous and this leads to the idea that a possible enhancement in mechanical properties may be observed. The pressure effect will hold true for $\alpha_{II.}$ During the final stages of the reaction microgels have overlapped each other forming a rigid flake-like structure. This structure limits molecular mobility and pressure effect with be minimal in this solid structure.

Huang et al. noticed an important pressure variation occurring within their pressure range studied during the initial stages of the reaction and an overall behavior when pressures reached over 500psig. Increasing pressure will delay the gel effect and "flatten" out α_I thus increasing the cure in α_I through mostly intra-microgel reactions. Increasing pressure decreases molecular mobility in the liquid state but accelerates the reaction rate constants. It will be demonstrated how this behavior may be different (less noticeable) for highly accelerated reactions due to the short period of liquid state conversion. For pressures between 0-500psig they noticed that the effect of pressure on the following regions (α_{II} and α_{III}) was minimal and concluded that a molecular mobility reduction which would slow the reaction rate was being counterbalanced by the acceleration of the reaction rate constants due to pressure. On the contrary, over 500psig the reaction rates lowered which they described to be occurring due to the overwhelming effect of pressure on the free

volume. Overall conversion increased below 500psig, then decreased, and they found the highest final conversion value around 500psig. Increasing pressure was also proven to increase the styrene conversion over *UP* C=C conversion affecting the overall final resin ratio with about a 5% difference. This effect might have a result in the final mechanical properties of the resin. It was also noted that the final flake-like structure appeared to be more regularly oriented at certain pressures.

Pressure effects on a high cure temperature epoxy have been reported by Lee and Pae [92, 93]. A DGEBA-DDS epoxy system was cured isothermally at 150°C in a predesigned high-pressure torsion pendulum that allowed for extreme pressures of up to 18,000psi. They also generated some isobaric experiments at 10,000psi at temperature of 135°, 150°, and 165°C. The equipment permits monitoring gelation and vitrification points for the resin. Resin was also tested with FTIR at certain points in the reaction to determine conversion values. It was determined that vitrification and gelation happen faster with pressure which translates to an acceleration of the reaction. The effect of pressure in shortening the time for vitrification was 3 times more notable than for gelation. The high pressure greatly influences the molecular mobility and transition to solid which would reverse if pressure were removed. Gelation, on the contrary, has greater dependence on the cure degree. It was determined that since vitrification would happen faster at approximately 23,000psi (based on extrapolation) gelation and vitrification would happen at the same time.

A set of results was presented which described the effect of pressure on conversion values at gelation and vitrification. It was shown that the conversion at gelation always increased for the pressure range studied (0-10,000psi). Conversion at vitrification was found to decrease approximately 8% up to 13,000psi and increase about 3% between 13,000-18,000psi. It is important to remember that conversion results reported for vitrification and gelation are relative to the time when they respectively happened. In this case, since vitrification happens in less time with increasing pressures there might be an overall conversion rate increase and still the vitrification point could show a lower conversion. There is also the possibility that the excessively large pressures described compact the material too such an extent that molecular mobility is greatly hindered and reaching high conversions will take longer. Unfortunately, only the conversion at gelation and vitrification are shown. Also, since the pressure range selected is extremely large the values are widely scattered and an overall effect of cure rate change in time may not be sensed. After 0psig the next pressure reported for conversion was 5000psig. Despite this, it may be concluded that with epoxy, as well as *UP* resin, pressure increases the kinetic rate constants which will in turn affect the reaction rate.

It is known that for many chemical reactions of organic and inorganic liquids, the rates of the reactions are influenced by hydrostatic pressure [93]. A common way to describe the pressure effect on reactions is through the concept of volume change. Based on the transition theory [94]

$$\left.\frac{d\ln k}{dp}\right|_T = -\frac{\Delta V^*}{RT} \tag{4-1}$$

where ΔV^* is the activation volume, R is the gas constant, and T is absolute temperature; a pressure (p) dependence of the rate constants (k') is seen for any individual reaction stage such as initiation, propagation and termination. In general, pressure increases the propagation constant while it decreases the initiation and termination constants. Since initiation and termination constants are approximately canceled out an overall activation volume may be expressed and said to be mostly negative [9]. If ΔV^* is negative, then the rate constant increases with pressure. For similar reasons it is hypothesized that polymers synthesized under hydrostatic pressure may have greater molecular weights and various structural modifications than those synthesized and atmospheric pressure. As for final material properties encountered with pressure variations, not much has been proposed. Knowing that the curing reaction i.e. the reaction rate constants is what ultimately controls the final properties of the part it is important to recognize if pressure effect could be strong enough to create a significant change on the final mechanical properties of resin; not by affecting the macro-structure (void reduction, density control, etc.) but through actual molecular or microscopic changes among others.

4.2 Development and Procedures

The effects of pressure on reaction rates and final mechanical properties were studied for unsaturated polyester and epoxy resin. Raman spectroscopy has been used to study and monitor reactions with the chamber previously described in chapter 3 although other spectroscopic techniques that incorporate fiber-optic lasers may also be used. The designed chamber allows for pressures up to 2000psi at 200°C. A precise control system guarantees repeatable and accurate results. Samples for studying the mechanical properties of the resins were developed in the same reaction chamber by the installation of a slide-in mold piece that would generate DMA samples of consistent geometry.

A pultrusion grade *UP* resin and coating grade *EP* were used for all analyses. For specific material information refer to the end of sections 2.2.1 and 2.2.2. *UP* resin tested is activated through a combination of three different initiators that cover the entire temperature range of the process. For pressurized experiments the percent weight of initiators was the following:

Table 4-1. *UP* initiator combination for accelerated reaction.

Initiator	Active Temperature °C	Weight %
Perkadox 16	45-95	0.2
Trigonox 121-BB75	85-125	0.1
Trigonox C	135-170	0.1

This resin combination is common for high throughput processes. Reaction rates are very fast leading to a very distinctive molecular curing behavior that is also uniquely affected by pressure. As shown in chapter 3 these fast reactions have to be well controlled to prevent overheating. Control is possible with the developed reaction chamber. The epoxy resin is a two-part system mixed in a 5:1 weight ratio of resin to hardener with a cure temperature range between 0°C-32°C when fully mixed.

Two different system set-ups were used; one for Raman cure analysis and another for DMA/hardness tests sample creation. Raman analysis details and specific equipment information may be found in sections 2.3.2, 3.2 and 3.4. For Raman curing analysis, the sample is placed at the bottom of the reactor, providing a 2.25” focusing distance and a sample loading screw-in bottom port allows for easy sample insertion. Sample material thickness is kept low (0.5mm-1mm,~0.1g) in order to prevent exothermic overheating, permitting a constant temperature assumption. With epoxy samples that undergo slow reaction rates at low reaction temperatures thicker samples may be used. Samples are placed on a pre-cut natural finish aluminum piece which allows for easy control of the sample thickness. The aluminum surface will also provide a low noise background for the Raman measurements. *UP* reactions were monitored at 5 and 10K/min up to 190°C and epoxy reactions at isothermal 30°C. In order to create consistent samples that could be tested by DMA and micro-hardness a second set-up which consisted of an insert mold was designed to fit perfectly inside the inner cavity of the reactor. Figure 4-2 shows reactor design including the adapted cylindrical mold piece.

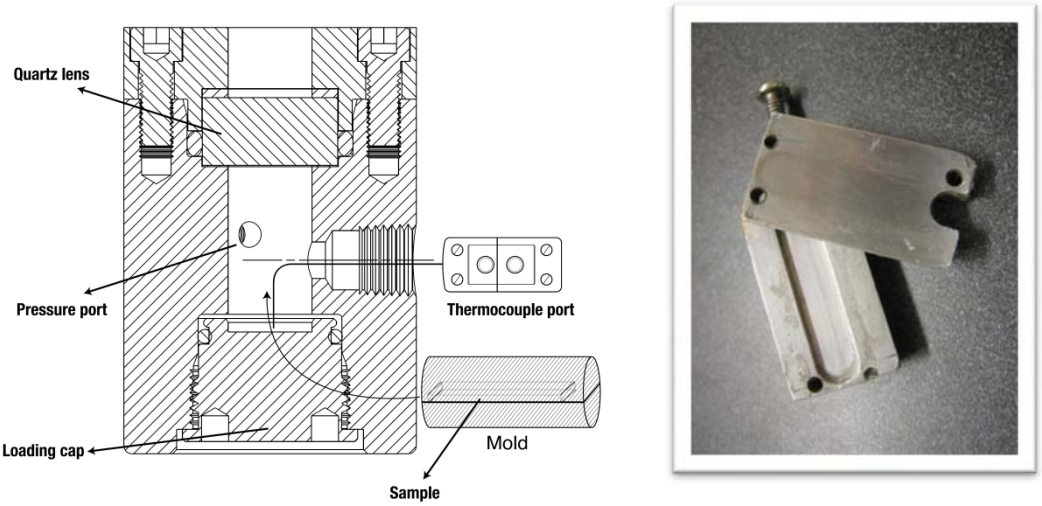

Figure 4-2. Drawing of reactor illustrating entrance for mold piece (left). Mold piece image (right)

The custom machined aluminum mold consisted of two pieces, a polished bottom half with 1mm x 6mm x 22mm cavity and a polished flat top. The mold covered the full radial inner dimensions of the reactor cavity and included an open end space for monitoring the actual sample temperature with the inner thermocouple. High-conductivity grease assured good heat transfer between the mold and reactor. A screw in the backside of the mold piece provided a support for installation and removal. For proper mold insertion with liquid resin the chamber was modified and placed in a horizontal position. This prevented resin loss through the thermocouple gap and eased thermocouple insertion. Sample geometry was predefined so that the sample end where the thermocouple had been placed could be removed. For *UP*, dynamic scans from 30°C to 180°C were performed on the samples followed by an isothermal at 180°C for 5min. This optimal full curing time was determined prior by Raman spectroscopy analysis. The final chamber setup is shown on Figure 4-3.

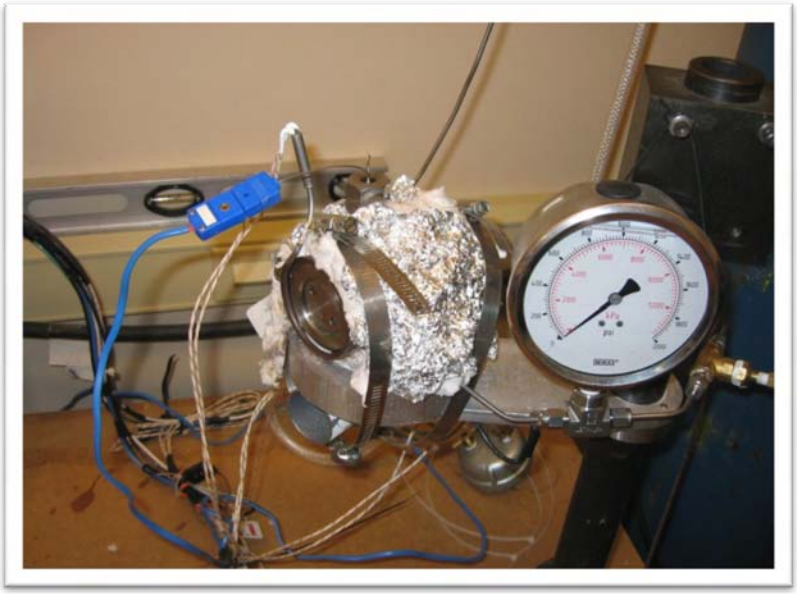

Figure 4-3. Horizontal reactor setup for creation of DMA and hardness testing samples.

DMA experiments were generated on an RSA III Rheometrics System Analyzer from TA Instruments. Due to the limit of sample size within the pre-designed reaction vessel, 3-point bending tests were selected as the primary tests for determining modulus. The system set-up consisted of a lower support of 10mm and an upper V-fulcrum. Sample temperature was maintained isothermal at 30°C and a pre-load of 10g normal force was performed prior to testing to prevent sample contact separation at the low end of the frequency sweep. Dynamic strain sweep tests at a frequency of 5 rad/s with strain varying linearly from 0.0001 to 0.01% were performed on all samples. In order to guarantee well controlled sample batches with minimal microscopic and macroscopic variations, a very rigorous sample preparation and pre-testing process was followed. Additionally, the mold surfaces were tested for surface quality and thickness control before every sample was

made. Due to the small geometry of samples minimal variations will greatly affect the results. An initial predetermined mechanical mixing process was performed to improve homogeneity. After mixing, a full vacuum was done to remove bubbles and reduce volatiles in order to minimize final voids within the samples. Additional variables taken into account during the making of the parts for DMA/hardness testing were: pressure between the mold halves (related to final thickness), volume of material, shape due to permanent shrinkage deformations, voids and flash within the mold. Due to the manual sample insertion onto the mold cavity there is possibility of the creation of bubbles and so, prior to testing, a microscopic examination was performed on cured samples to guarantee no voids were present within the tested samples. Microscopic examination was also used to reveal other sample defects. Finished samples were monitored for variations in geometry, weight, and external (surface) or internal defects. All samples with variations over 3% and significant defects were discarded. A minimum of 10 samples were DMA tested for each of the different pressures and statistical analysis performed to guarantee no outliers would affect results.

Indentations on the cured samples were performed on a Buehler Micromet® 2003 digital Hv micro-hardness device. A Vickers head was selected rather than any other testing head based on previous publications of hardness testing on thermoplastics and thermosets [95-100]. It has been determined that higher loads would provide better correlations to the actual hardness of the resin. Also, due to the elastic behavior of a polymer, the higher load allowed for better estimation of the diagonals. Figure 4-4 presents an image of an indentation used for estimation of the hardness. Hv was determined by diagonal length

($H_{V,L}$) rather than indentation depth ($H_{V,d}$) due to equipment limitations. Nevertheless, it has been shown that for increased loads the difference between the results for the two methods is greatly reduced [97].

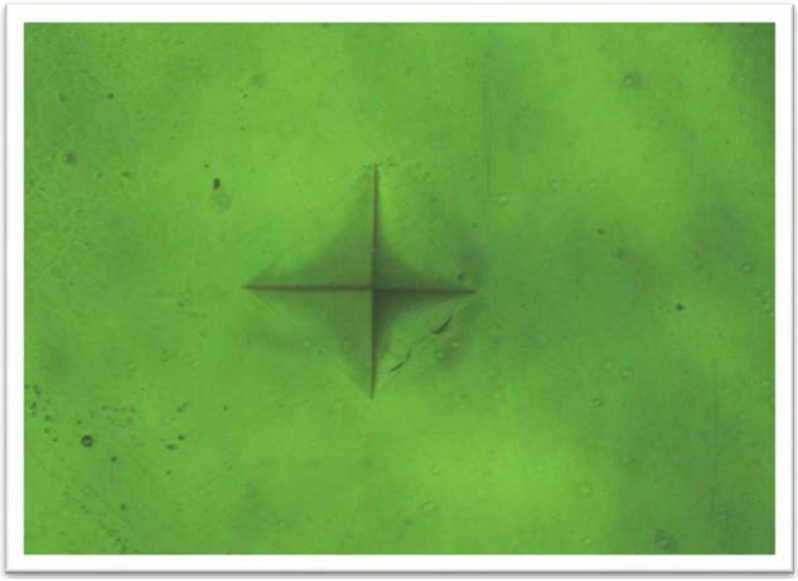

Figure 4-4. Micro-hardness indentation. The elastic behavior of the material may be seen in the shape of the deformation.

Samples were placed over a flat plate and subjected to a sustained load of 1000g for a period of 10 seconds. Samples were tested over their surface area at ten different points throughout their length and two different areas throughout their width. A minimum of 10 samples of each pressure were tested and after all data had been collected statistical analyses were performed to account for any variations within the results.

4.3 Pressure effects on the Curing Reaction

The pressure exerted on a reacting resin like any other dependant process variable, will affect the behavior of the material as it cures. Pressure is known to have an inverse effect to temperature on molecular mobility. For high viscosity liquids rather than compressible gases the effect of pressure will be much smaller and harder to quantify; although in some circumstances, such as polymerizations reactions, pressure will have a significant effect on the molecular behavior. The cross-linking process in most thermoset reactions consists of certain functional groups finding each other and bonding by going from a higher to a lower state of energy which leads to a heat release and is the basis of what is known as a net negative activation volume. If molecular mobility is affected by increasing pressure this will consequentially influence the reaction rates. On the other hand, as previously described, pressure affects the rate constants which may in turn accelerate the reaction.

Figures 4-5 (a) and (b) show conversion in time for isobaric *UP* resin reactions cured at a heating rate of 10K/min and 5K/min respectively. Actual sample heating rate curves have also been included in the figures to demonstrate the high efficiency and reproducibility of the reacting chamber heating control. Comparable linear heating rates may be seen for all samples with no exothermic overheating of the material.

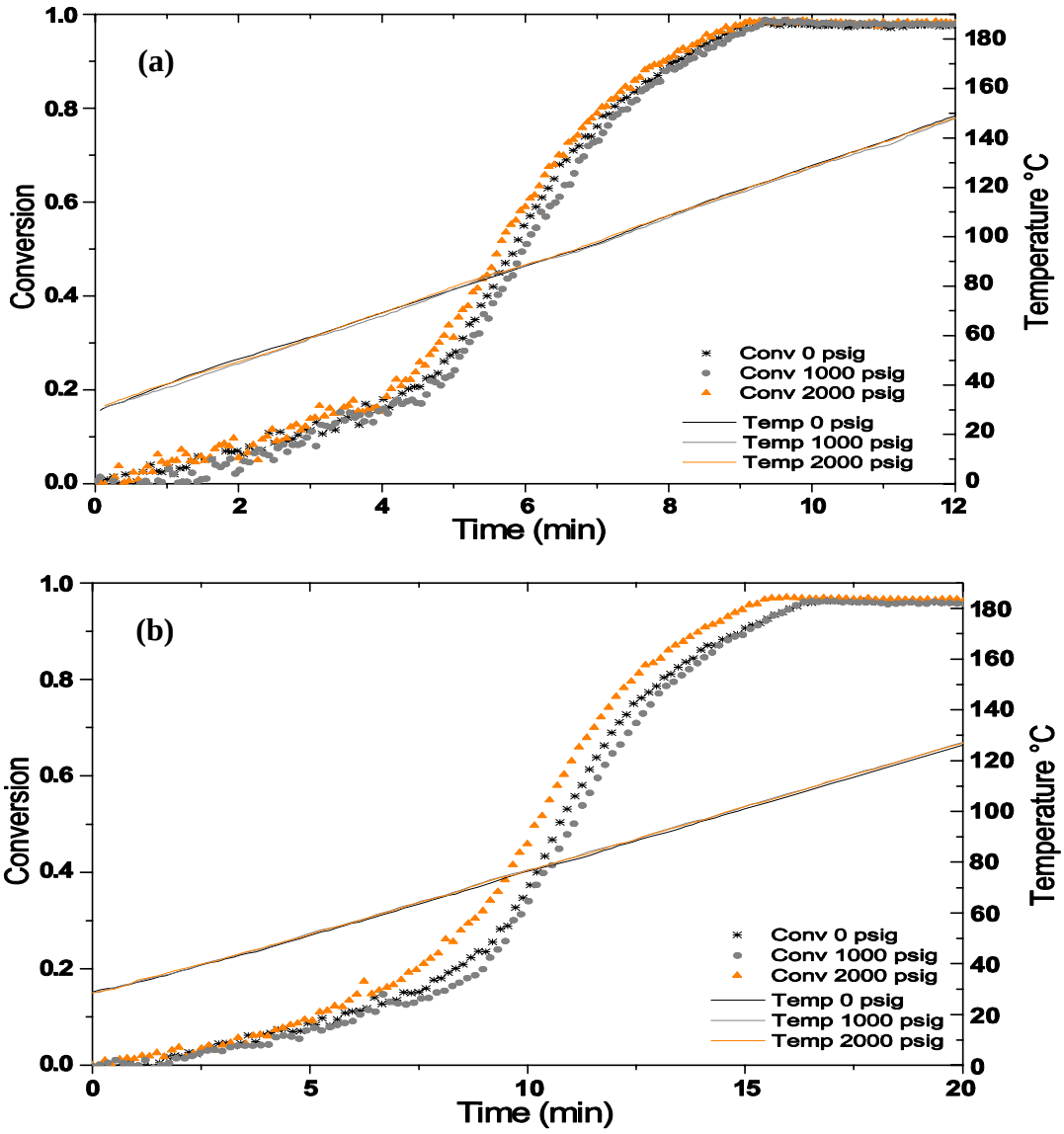

Figure 4-5. Conversion analysis for *UP* resin cured at isobaric pressures of 0, 1000 and 2000psig and heating rates of (a) 10K/min and (b) 5K/min.

Optimization of heating rates was possible with the temperature control sensor directly inserted in the sample. It is important to mention that due to the high sensitivity of the reaction rate with temperature for these highly accelerated reactions, multiple runs had to be generated until consistent invariable heating rates were obtained between a particular

set of isobaric runs. Heating rates were verified by generating plots from the data obtained with our external data-logger. As mentioned in section 3.3 the process thermocouple was a dual thermocouple sending signals to a data-logger and the controller. In order to minimize any variations due to heating rates among the different curves down to an extent that the pressure effect would be well accounted for, certain guidelines were followed. Heating rates between the samples should be within ±0.005K/min, fitted linear trend lines should have an R^2 value over 0.9995 and at any single point in time the variation between individual heating curves should not be greater than 1°C. For example, for the runs shown in Figure 4-5 (a), the heating rates were 9.8800, 9.8788 and 9.8762K/min for 0psig, 1000psig, and 2000psig respectively with a minimum R^2 of 0.9996.

Curing results show that within the pressure range tested reaction rate of *UP* resin is indeed affected. A similar trend was observed for all heating rates evaluated. During the initial stages of the reaction, when only the first initiator has activated, a similar trend is observed for all the curves with no variation noted due to pressure. As the reaction continues one may observe an acceleration of the reaction for the 2000psig samples and a decrease in reaction rate for the 1000psig samples as compared to the 0psig results. The 0psig curve lies between the other isobaric conversion curves within all the accelerated reaction period (α_{II}). For both the 10K/min and 5K/min samples α_{II} begins close to when the 2nd initiator starts its activation. A decline of α_{II} starts to be noticeable around 100°C. These highly accelerated reactions sustain relatively fast rates until most of the reaction has been completed and it is not until conversion levels are extremely high that we see a

significant reduction in reaction rate. The result is a high overall conversion when transitioning into α_{III} which in turn results in excellent final conversion at any pressure. Consequently, since all final conversion differences were so small no definite conclusions could be obtained. Even so, for all unsaturated polyester results final conversion values exhibited a trend of being slightly higher for the materials reacted under pressure. Table 4-2 shows final conversion results for the samples shown in Figure 4-5. As for differences in cure with pressure among 5K/min and 10K/min heating rates it was observed that for lower heating rates slightly greater shifts of the conversion curves with pressure may be seen; more noticeable for the 2000psig curves than for any other.

Table 4-2. Table 3: Final conversion for samples of unsaturated polyester resin reacted at different pressures.

Heating Rate	0 psig	1000psig	2000psig
10 K/min	0.980	0.982	0.986
5 K/min	0.967	0.968	0.977

The conversion though does not always dictate the optimal properties but high conversions with incorrect ratios such as excessive styrene may lead to a brittle part. As previously described in section 4.1 there have been certain publications that have described the pressure effects on *UP* resin. Although the material is slightly different and processing conditions are also different both undergo a free radical cross-linking reaction. *UP* resin suffers from a very particular effect which may be described with micro-gelation theory such as that shown by Huang and Chen [9, 48] for a slower reacting *UP*. Two factors influence the curing rate; molecular mobility which is usually achieved by increasing molecular excitation (i.e. temperature increase) and distance between reactive

molecules, which affects the reaction rate constants. Depending on the reactive species and pressure applied, either of the two effects may dominate. Huang and Chen found that for their resin studied no noticeable pressure effect was noted below 500psig due to counterbalance and over 500psig up to 900psig the rates lowered. Our system on the other hand allows monitoring the reaction up to much higher pressures. When considering the transition state theory (equation 4-1; section 4.1) it may be deduced that if the pressure is raised high enough (being the rate constant of exponential behavior) there should be a region where the pressure is enough to induce an acceleration of the reaction rate constants. For our highly accelerated *UP* reactions the concentration of initiators is very high and the rate of reaction even at lower heating rates is much faster than normal causing the evaluation of pressure effect to be more difficult since the scale of change with pressure will be much smaller as compared to the other key parameters of the process. Even so, a noticeable effect has been observed that is in close correlation to the transition theory. Initially pressure increase leads to a reduction of the rates of reaction due to the effect of molecular mobility but the reaction rate constants are not high enough at this value to overcome free volume effect. At 2000psig, on the contrary, the rate constants have exponentially increased overcoming the effect of free volume and increasing the reaction rate substantially.

As presented on section 2.2.2 the epoxy analyzed, opposed to the *UP* resin, is a much slower reacting material with a different kinetic reaction mechanism. Figure 4-6 shows the changes exhibited by the epoxy resin with pressure for a period of five hours.

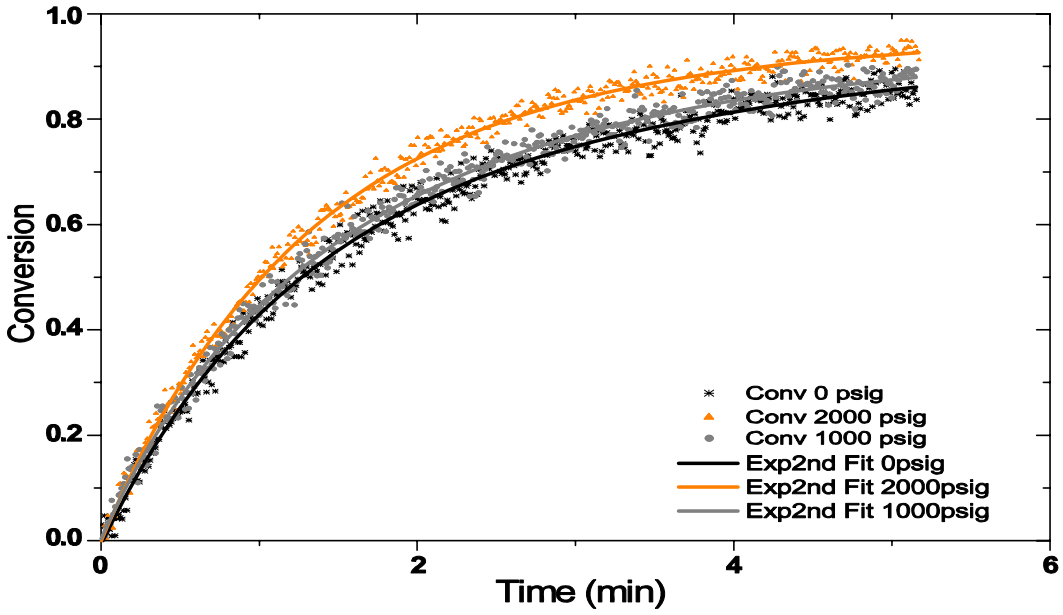

Figure 4-6. Conversion analysis for Epoxy Resin resin cured isothermally at 30°C while varying pressure.

Like with *UP*, during the initial stages of the reaction (10% conversion and less) the conversion values are very similar with pressure. Since the reactions are all performed at 30°C, this low isothermal temperature may be controlled very accurately allowing the generation of fittings curves based on multiple runs to accurately estimate the curing behavior. Therefore, when evaluating initial trends a slope difference that separates the reaction curves from each other is observed. It may be concluded that throughout all the reaction stages pressure increases the reaction rates and becomes more evident at higher pressures. This again relates to the transition state theory and reaction mechanisms for an addition polymerization reaction. For such a reaction, pressure brings molecules closer together and the issue of finding radicals is not present, but reactive functional groups are all throughout the system. It is important to mention that with epoxy although the temperature was maintained constant other important processing parameters could affect

the results leading to the variability seen within the data points. Unlike *UP*, where one batch was used for all experiments, epoxy required preparations of different batches for every run due to the lower curing temperature. Even so, differences between the trends are large enough to conclude a positive effect with pressure. By looking closely at the final section of the trend lines in Figure 4-6 it may be observed that with extended periods of time the curves will eventually converge. This was proven when curing the material for a 24hr period and verifying the final conversion values for the different pressures. After the 24hr period all the samples reached about 99% conversion with no definite pattern between conversion values. For this reason we may conclude that under the pressure ranges tested the reaction rates are accelerated but conversion is not hindered only offset to reduced times at higher pressures. This correlates well with the idea that at higher conversion (past vitrification) where the material is not a liquid or gel anymore and has turned into a glassy structure the effect of pressure will be reduced.

4.4 Pressure effects on Final Mechanical Properties

For thermoset parts curing is what ultimately controls the final properties of the part. With this in mind, it could be hypothesized that pressure might also affect the final mechanical properties. Huang et al. [9] hypothesized a similar idea when they mentioned that with pressure increases, microgel structures are more compact and less porous, thus an enhancement in mechanical properties may be observed. Similarly for epoxies, Lee and Pae [92] suggested that with the high pressure effect on cure, which reduces distance between molecules, there is believed to be an increase in crosslink density of the gel phase which could also affect the final mechanical properties of cured parts. We have addressed this hypothesis by modifying the reactor with a mold piece where samples for mechanical testing could be prepared.

Evaluating samples for pressure effects, a phenomenon generally recognized as being much smaller than effects of temperature or composition, requires a very controlled sample preparation methodology so other variables do not affect the results. Voids or any variations in the material preparation and process had to be avoided. It was also a requirement for samples to have a perfectly polished flat surface finish so that consistent results could be obtained. As seen in Figure 4-7, extremely thin layers of mold release achieved by a drying step after application are essential to maintain a perfectly smooth surface. Roughness or imperfections within the surface, such as those seen in Figure 4-7 (a), would alter the results.

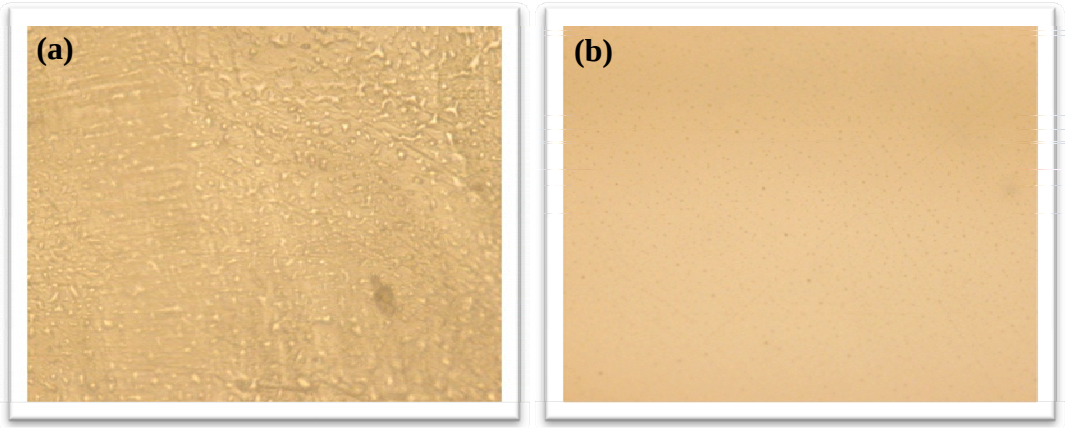

Figure 4-7. Microscopic image of the surface quality of an epoxy sample at magnified at 200X. (a) Surface with imperfections due to improper mold release application (b) Proper mold release application

Figures 4-8 and 4-9 show results for Young's modulus of unsaturated polyester and epoxy pressure cured samples. Figures 4-10 and 4-11 present hardness testing results.

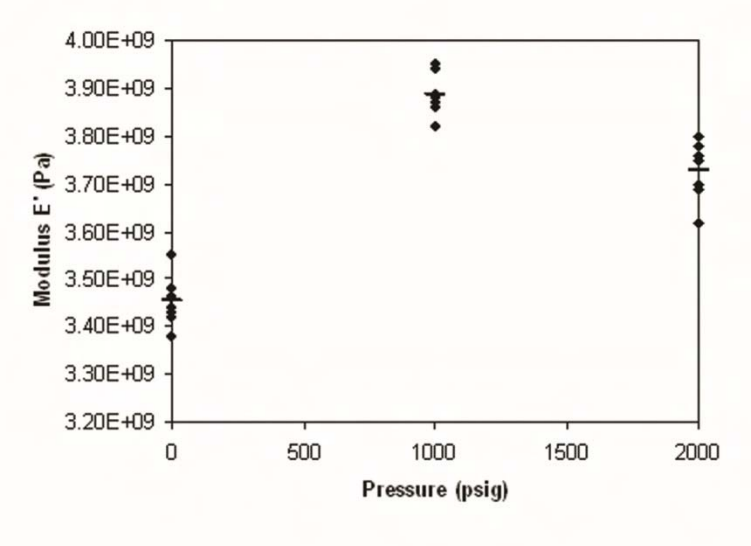

Figure 4-8. Modulus (E') results for unsaturated polyester resin cured at different pressures.

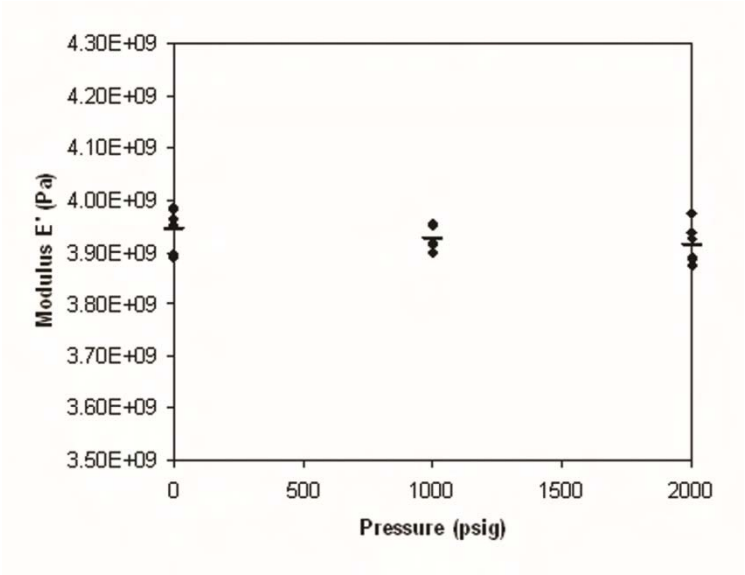

Figure 4-9. Modulus (E') results for epoxy resin cured at different pressures.

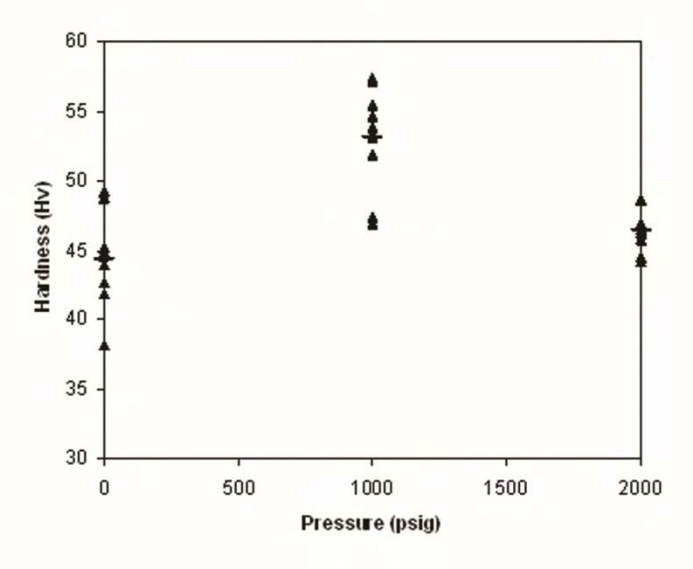

Figure 4-10. Micro-hardness (Hv) results for unsaturated polyester resin cured at different pressures.

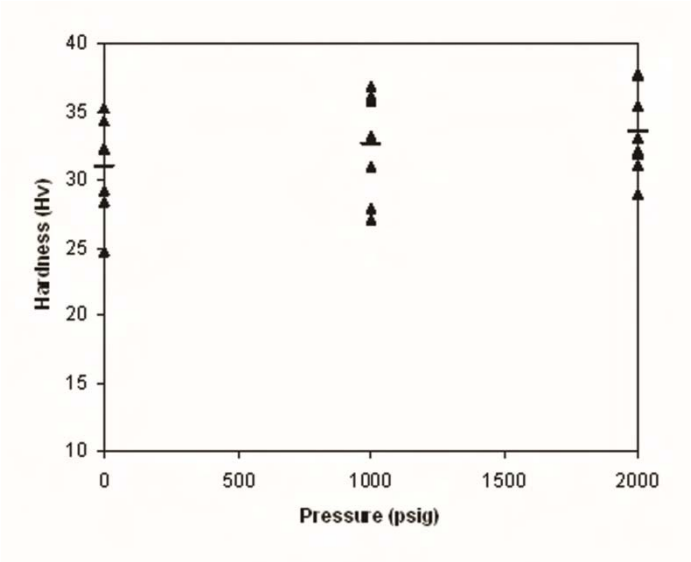

Figure 4-11. Micro-hardness (Hv) results for epoxy resin cured at different pressures.

Table 4-3 summarizes the graphed results. Each sample average shown on the table is illustrated in the graphs by a short horizontal line. The mean dispersion (%) column simply describes how dispersed the experimental points are from the mean in a normalized way obtained by dividing the standard deviation by the mean. This gives us a more reasonable value which is not dependant on the scale of the results.

Table 4-3. Average results for Modulus and Hardness of *UP* and epoxy.

	Pressure	Average	Mean Dispersion (%)
UP E'	0	3.453E+09	1.45
	1000	3.886E+09	1.17
	2000	3.729E+09	1.67
Epoxy E'	0	3.944E+09	1.06
	1000	3.925E+09	0.57
	2000	3.915E+09	0.97
UP Hv	0	44.37	7.15
	1000	53.07	6.74
	2000	46.42	3.36
Epoxy Hv	0	30.91	11.97
	1000	32.55	12.31
	2000	33.50	9.45

By observing the mean dispersions it is seen that the values for micro-hardness testing, a method very sensitive and dependant on many parameters is higher than modulus results, especially for epoxy. Unsaturated polyester modulus increased at a pressure of 1000psig then decreased for samples cured at 2000psig. A similar trend was observed for the hardness. For epoxy, no distinctive changes were observed for the different curing pressures tested, although hardness exhibited a slight increase with increasing pressure. The increase was determined to be inconclusive by the generation of a T-test. Results from the T-test are shown on Table 4-4. The pressure effect observed for *UP* was considered to be significant, with an average modulus increase of 12.5% and 8% to that of atmospheric pressure for samples reacted at 1000 and 2000psig respectively. Similarly, the *UP* hardness results show a similar trend with an average increase in hardness (Hv) of 19% for 1000psig and 4.6% for 2000psig as compared to the value at atmospheric pressure. This behavior shows a similarity to the curing changes with pressure shown in

Figure 4-5. Curing rate initially slows down with pressure but eventually reaches a minimum where the reaction constants take over and the reaction may again accelerate.

Table 4-4. Statistical T-test percentages for results of modulus and hardness for *UP* and epoxy samples.

%T-test	0-1000	0-2000	1000-2000
UP E'	2.05E-08	3.22E-05	0.02
Epoxy E'	34.80	23.96	59.93
UP Hv	1.87E-03	9.85	0.01
Epoxy Hv	44.14	16.76	61.74

This *UP* behavior, where certain pressure values positively affect the mechanical properties while others negatively affect it, may possibly be described through morphology and kinetic effects. It has been described for *UP* sheet molding compounds, which initially are reacted at very slow rates to achieve the desired sheet viscosity, that this slow cure actually increases the hardness of the fully cured material [101]. We have determined that at 1000psi we actually obtain the slowest initial curing rates within the material. At pre-gel stage microgels are forming and high intra-molecular reactions should occur. By providing longer time for free radicals to migrate while decreasing distance between molecules, tighter cross-linked structures may possibly be formed. At a pressure of 2000psig, the effects of lowering molecular mobility are greater preventing the needed molecular arrangement. In addition, faster initial rates are seen due to kinetic effect on the reaction constants, which also impedes proper intra-molecular reactions. Another proposed effect is the increase of styrene cross-linking due to the inhibition of volatiles which may happen throughout all the reaction. An effect similar to the one seen by Huang et al. [9] on the final reaction stages by use of IR. Cross-linking ratio of styrene

will affect the mechanical properties with an excessive amount leading to a brittle part due to formation of polystyrene crystals within the structure. At high conversion values and temperatures, certain pressures can inhibit volatile formation but if the pressure is too high it will prevent adequate diffusion (mobility) within the rigid structure.

As previously mentioned, no variations with pressure could be determined for the final mechanical properties of epoxy. Figures 4-9 shows very close averages slightly dropping but with the percent mean dispersion being much larger than the changes between pressures tested. Similarly, Figure 4-11 has small changes compared to the standard deviation and although it seems that the hardness could slightly increase within the pressure range studied, the T-test proved the assumption to be inconclusive. The T-test (Table 4-4) allowed for a better interpretation of the results by statistically assuring that the confidence level of the assumptions for variations between data was high. The T-test results are essentially a statistical percentage of the probability that a data set could have come from an identical population. By simply glancing at Table 4-4 one may see that the %T-test probability of all epoxy samples is excessively high confirming that no accurate comparison may be made between the data-sets. Conversely, *UP* samples have much lower percentages with only one value close to but below 10%, which is still considered a low statistical probability.

4.5 Future Work

The equipment developed in this research has provided a new way for monitoring cure of thermosets. Resins with high exotherms may be well controlled and studied. By use of Raman spectroscopy and the reaction monitoring chamber the dependence of temperature, pressure and composition on the curing behavior may be well described. Through the modification of the chamber with the insert mold samples for testing mechanical properties may be created. This may open research areas for many other materials. Since the dependence on processing parameters varies with resin composition further studies on pressure effects may be done with many other resins. Whether for epoxies and unsaturated polyesters, their many blends, or almost any other thermoset, the system developed provides an accurate way to determine kinetic parameters to be used for cure modeling. Now that the dependence between pressure, temperature, reaction kinetics and compositions may be experimentally evaluated further studies may be directed towards developing models and cure diagrams which incorporate the pressure effect on the material. Similar to TTT and CHT diagrams, isoconversion diagrams with pressure may be developed.

For our current resin systems further evaluation may also be performed. Mechanical property studies may be done while varying composition in order to determine the optimal resin to initiator, catalyst, monomer or hardener ratios. It may also be possible to establish for the particular *UP* resin system at what temperature and pressure combination the material has the best mechanical properties by making isothermal and isobaric runs at

pressures close to where our highest modulus was determined. By use of Raman, the kinetic behavior may be studied further and the transition pressure when the kinetic effect dominates over the molecular mobility effect may be determined. For epoxy, the system allows the user to determine optimal curing time at different pressures. It was determined for the pressure ranges tested that the higher the pressure the lower the curing time. This could generate some possibilities for LIM or other high throughput processes.

As previously described, the effects of pressure are related to changes in molecular behavior and may be described through morphological changes. SEM experiments may be performed in conjunction with the kinetic analysis to study microgel growth and pressure dependence for these highly accelerated reactions (a similar study to the one presented by Huang et al. [9] for slower *UP* reactions). SEM may also be used to study final mechanical properties and correlate them with our results. For unsaturated polyesters it is known that increased pressure may lead to an increase of styrene conversion in the material. Raman spectroscopic analysis may be performed to determine exact styrene increases. These results may be compared to mechanical property variations with pressure. SEM fracture analysis can be done in conjunction to determine how the styrene level might have an effect in the fracture mechanics of the material. Optimal fracture behavior should correlate to an optimal monomer ratio. Similarly, epoxy may be studied by SEM in order to see if any change in fracture behavior is noted with pressure. Figures 4-12 and 4-13 present SEM images obtained from the epoxy samples analyzed in section 4.4. It is difficult to determine any specific changes for these samples. The only noticeable difference is that at 0psig, as compared to 1000 and 2000psig, the material

seems to have broken into smaller pieces leaving greater number of cracks and humps throughout the fractures surface, but this effect may be dependent on many other factors like the loading and rate when generating the fracture.

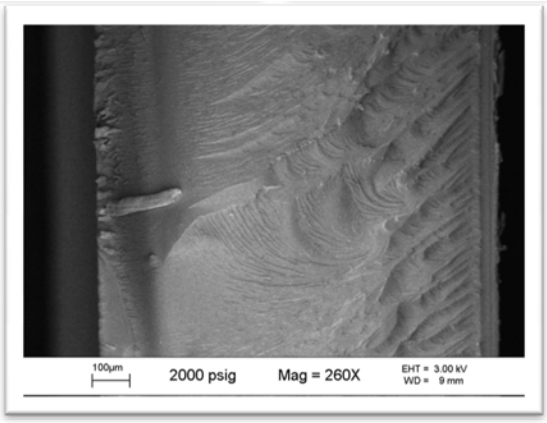

Figure 4-12. SEM images at 260-270X magnification of fracture surfaces for epoxy samples reacted at different pressures.

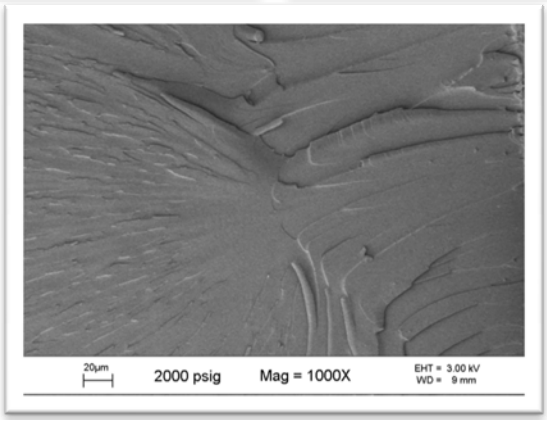

Figure 4-13. SEM images at 1000X magnification of fracture surfaces for epoxy samples reacted at different pressures.

Figure 4-14 and 4-15 show fracture surfaces for *UP* samples reacted at different pressures. As seen in the images there are slight differences between the fracture patterns among the *UP* resin samples. Larger fracture patterns are seen for 2000psig samples than 0psig ones. 1000psig samples lie in between showing patterns from both but also showing smoother areas of the fracture. From these images, it seems that 0psig samples undergo a fairly brittle fracture with small micro-cracks creating “delaminated” (undercut) layers. 1000psig samples don’t show much of this and micro-cracks are smaller, lower in quantity and more distributed. It also seems that cracks are more patterned.

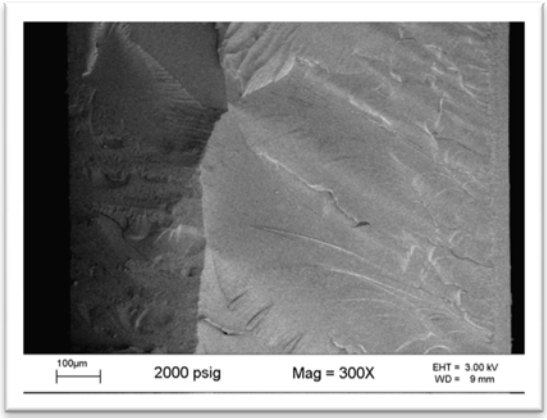

Figure 4-14. SEM images at 300X magnification of fracture surfaces for unsaturated polyester samples reacted at different pressures.

A very interesting image is the 1000psig scan shown on Figure 4-15 (center left) that shows what seems like a behavior of material resistance to the stresses of fracture shown by rips with a fibrous pattern. For 2000psig samples cracks are much larger suggesting a more brittle fracture than any other. Large cracks with undercut layers are seen and the fracture does not show an obvious pattern as with the other pressures. This may be due to a greater concentration of reacted styrene. Since there may be great variations between fractures in a same sample due to the way the material is stressed when being fractured, more research and greater number of tests have to be done for this material in order to draw any conclusions. Nonetheless, the possibility of different fracture behaviors is

present and could result as another interesting approach to relate cure behavior to mechanical properties.

Figure 4-15. SEM images at 1000X magnification of fracture surfaces for unsaturated polyester samples reacted at different pressures.

5 Development and Evaluation of an Impregnation Process of Epoxy Resin on Wood

5.1 Background and Motivation

Thermoset processes tend to be very complex because they involve a chemical reaction in combination with the making of a part. For this reason, an efficient process is most likely obtained by thoroughly understanding the overall system and the dependencies of the variables within the system. In addition, since most thermoset resins are not used alone but as supporting material in a composite structure, the reinforcing material's chemical and physical interactions with the matrix must be understood. One of the most complicated processes when working with resins is impregnation and it is the basis for making strong non-defective composite parts.

Impregnation is a process which requires great knowledge of the resins properties including curing rates and viscosity. Whether it be during the actual processing stage (e.g. RTM, vacuum-bagging) or before, as a material preparation step (e.g. SMC, BMC), most processes for creating a composite structure require some kind or wetting or impregnation of the fibers with the matrix material. We have selected the impregnation of wood with a low viscosity resin. Due to the anisotropy of wood and the many different kinds of woods available developing a systematic method or model to relate parameters and properties is not an easy task.

Much research has gone into the development of wood-plastic composites with most of the work focusing on impregnating wood fibers [102] rather than the solid wood itself. Wood impregnation has been tried in the past with many different thermoset resins and thermoplastics. A recent development currently on the market has been the impregnation of wood with MMA monomer followed by an *in situ* polymerization [103-105]. The benefit of this process is that the MMA monomer will have a much lower viscosity than PMMA which will ease the impregnation. Most of the thermoset impregnations being done have been with formaldehyde resins [106-119] including phenol formaldehyde, melamine formaldehyde, and urea formaldehyde resins. The benefit of most formaldehyde resin combinations is that they chemically interact with the wood allowing for different modifications rather than solely mechanical property increases. Properties evaluated for many of these resins on wood include dimensional stability, surface hardness, moisture excluding efficiency, chemical and weathering resistance, fire retardancy, modulus of rupture, modulus of elasticity, and even termite resistance.

An important consideration when developing wood-resin systems is the possibility of generating an all renewable based composite. An epoxy resin made from linseed oil extract will be used for the application. This BORR (based-on-renewable-resource) resin has been found to be a promising candidate for impregnation of solid wood parts with resin. Standard epoxy has not been very popular for impregnation of solid wood due to its high viscosity which makes it difficult to enter into the small lumens of the wood. A 1983 publication by Moore et al. [120] demonstrated how, by use of high temperature and slow curing hardeners, a vacuum-pressure-soak procedure may be used to impregnate wood

with a high viscosity epoxy. Unfortunately, the process is limited to small wood pieces. Epoxies have excellent mechanical properties. They are also resistant to many chemicals and provide great protection against humidity. For these reasons, they have always been used on wood, but mostly, as a coating. The BORR resin presented in this research not only has the advantage of being made from a renewable resource but also, has a lower viscosity as compared to most standard epoxies. By optimizing vacuum-pressure levels and temperature before cure, and by using a high temperature curing agent, impregnation with resin at very low viscosities is possible which could permit the full impregnation of thick sections. This could open new opportunities for wood decking and flooring materials. It was hypothesized that with proper impregnation techniques reasonable improvements in mechanical properties of the infiltrated wood compared to that of pure wood would be obtained. The purpose of the research was then to modify a lower cost wood, such as southern pine, and improve its properties up to the level of an expensive hardwood. Due to the chemistry of the resin it is also possible for a chemical wood-resin interaction to occur which would lead to an even stronger composite.

The impregnation process usually consists of vacuum and pressure combinations in order to drive the material into the wood. Figure 5-1 shows the interior view of a treating cylinder where vacuum and pressure may be applied. The impregnation process is generally used to chemically treat the wood for purposes of preservation. When wood is left untreated, especially in outdoors applications, it is subject to a variety of natural degradation processes including the attack of decay fungi, harmful insects, or marine borers. By applying chemical preservatives the decay resistance may be greatly increased

but its long-term efficiency is dependent on adequate penetration and retention of the treatment chemical [121].

Figure 5-1. Interior view of a treating cylinder at a wood-preserving plant [121].

Similarly, when impregnating with resins properties of the material will vary depending on the impregnation depth. Penetration varies widely among the different wood types depending on their densities, thickness of earlywood and latewood layers, and many other variables including where in the trunk the wood piece was cut. Wood of the same species can vary widely based on the length of the seasons and climate changes. The anisotropy

also affects the ability to impregnate in the different wood directions, through and between lumens. Figure 5-2 is an SEM image of structure of wood. This image illustrates well the complexity of penetrating a 2×4 inch wood piece where the lumens are parallel to the wood length requiring the transport of liquid to happen through the small bordered pits and junctions between lumens.

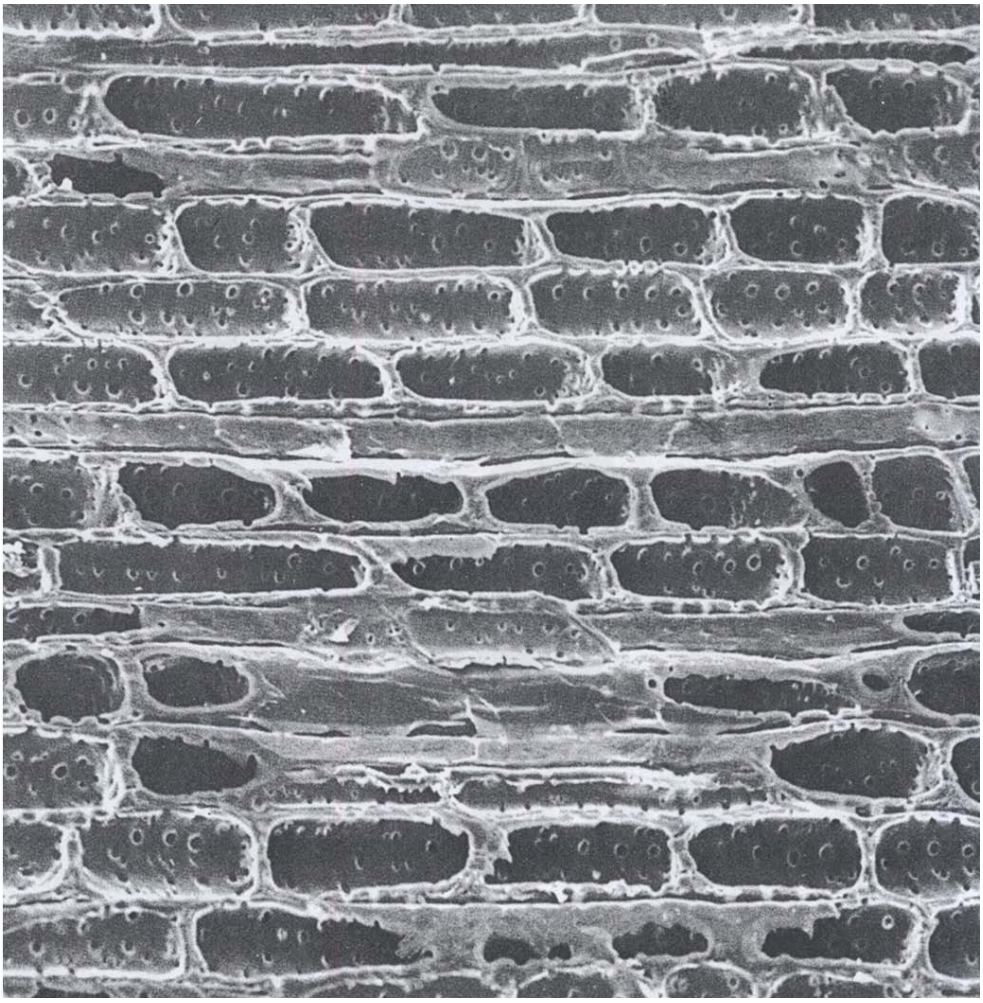

Figure 5-2. SEM image of a cross-section of wood cut in the tangential plane (plane perpendicular to the vessels or tracheids and tangential to the tree rings) clearly illustrating many small bordered pits [122].

For more information on the basics of wood and a better understanding of the wood structure a review of comprehensive references [103, 122, 123] is recommended. Knowing that wood structure is very complex, methods following specific parameters have been developed to guarantee effective (deep) wood treatments. Some of the pressure processes developed for treatment of wood are full-cell, modified full-cell and empty-cell. They all consist of the use of pressure to drive the fluid into the wood. The greater impregnation depths are usually obtained with the full-cell method. The method consists of applying vacuum for over half an hour, inserting the liquid treatment into the chamber while maintaining the vacuum and after the wood is immersed in the liquid, applying pressure. A final vacuum may be used to remove excess chemical and prevent dripping. Non-pressure processes include surface application, brushing or dipcoating, and soaking but none of these generate impregnation depths as deep as with pressure processes.

5.2 Linseed Epoxy Resin

Numerous epoxy resins are available. Each with very different chemistries and designed for specific applications. The basic structures of epoxies and general information on the material may be found on section 2.2.2. The key element that identifies an epoxy resin is the epoxide functional groups within the short polymeric molecules. In general, these functional groups are found as end-groups in the chemical structure although, this is not always the case. Linseed epoxy resin is one example where the epoxide groups are found as internal groups in the backbone structure.

Linseed also known as flaxseed is many times crushed or milled to extract oil. The oil appears as a hard transparent varnish, which itself, has been used in the past on wood surfaces. When used as a wood finish, linseed oil does not cover the surface as varnish does, but soaks into the pores of the wood surface leaving a shiny and natural non-glossy surface that shows off the grain. As will be shown, a similar surface finish was obtained with linseed epoxy samples. Wood treated with linseed oil is somewhat resistant to denting and scratches, but not to the extent as with a modern varnish, and it slowly absorbs moisture if allowed to stay wet.

Linseed contains 30-40% fixed oil, 6% mucilage, 25% protein, and small amounts of linamarin (a cyanogenic glycoside). The important element for the making of epoxies is the oil which is entirely composed of fatty acids. Although linseed oil is quite expensive it is the most highly molecularly unsaturated of all plant oils, which gives it a high

potential to synthesize rigid polymers with high stiffness [124]. Linseed oil contains approximately 58% linolenic acid (omega-3 fatty acid), 14% linoleic acid (omega-6 fatty acid), and 20% oleic acid (mono-saturated). These acids are typically found combined with a glycerol to form triglycerides. The general chemical structures of each are shown on Figure 5-3. The brackets on the triglyceride molecule demonstrate the different positions where the fatty acids may be located. A triglyceride may be composed of many different groups, but for linseed oil, it will mainly be any of the three shown. As seen in the figure, these omega fatty acids are unsaturated, which allows for the process of epoxidization on the unsaturation points.

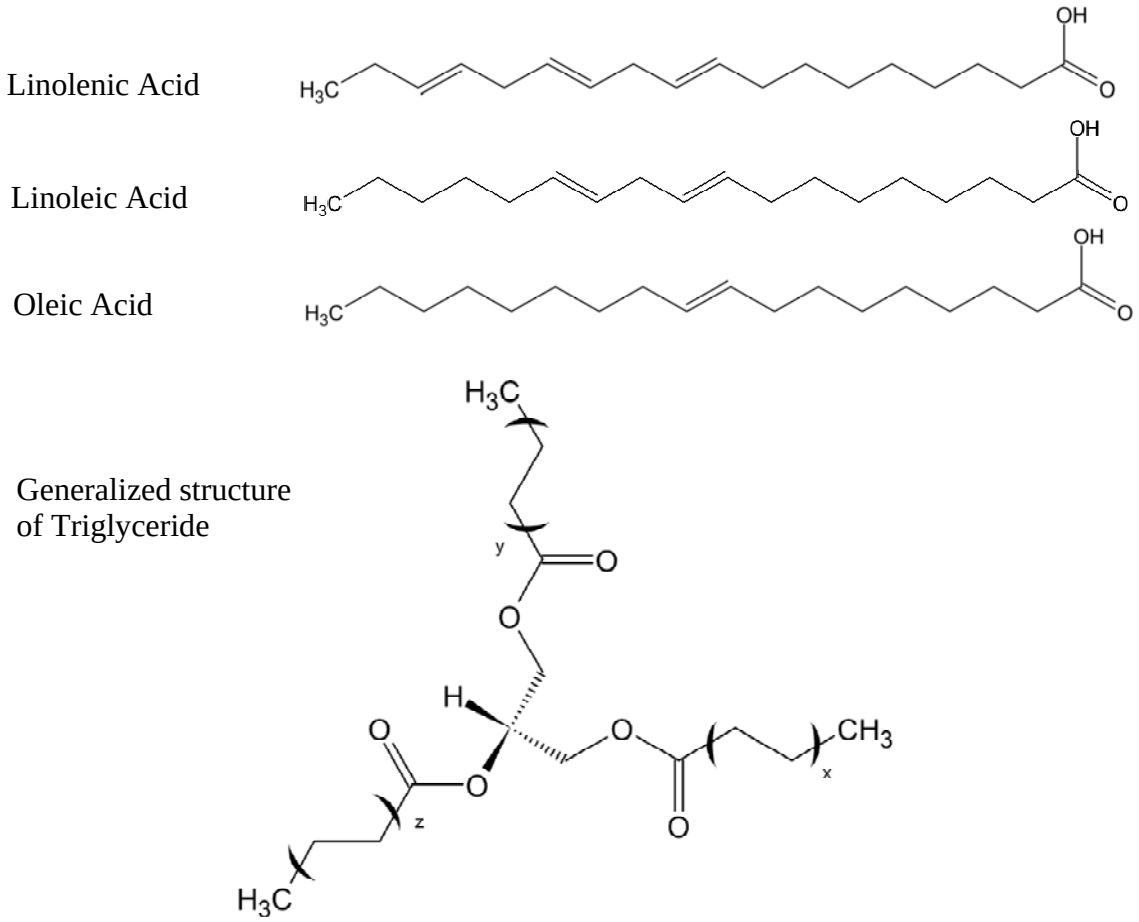

Figure 5-3. Molecular structure of basic fatty acids in linseed oil and the triglyceride molecule general form on which these fatty acids may be found.

Figure 5-4 illustrates the preparation stages undergone to make the linseed epoxy resin. Researchers have used similar methods to prepare linseed polyesters for SMC applications and have found favorable results [124]. Since C=C bonds on triglycerides are not free-radical polymerizable, unsaturation is introduced by opening the double bonds with an epoxidization step and creating new C=C bonds using maleic anhydride [124]. Other methods that do not require epoxidization have also been used, such as functionalizing the oil triglyceride molecules in two basic steps: glycerolysis to produce a monoglyceride and then reaction with maleic anhydride to produce a maleinated

monoglyceride [125-127]. The linseed resin used in this research has been epoxidized, and used in an epoxidized form by reacting it with polycarbonic anhydrides to induce the cross-linking reaction. For this reason, the resin has been termed PTP®; for polymer from triglycerides and polycarbonic anhydrides.

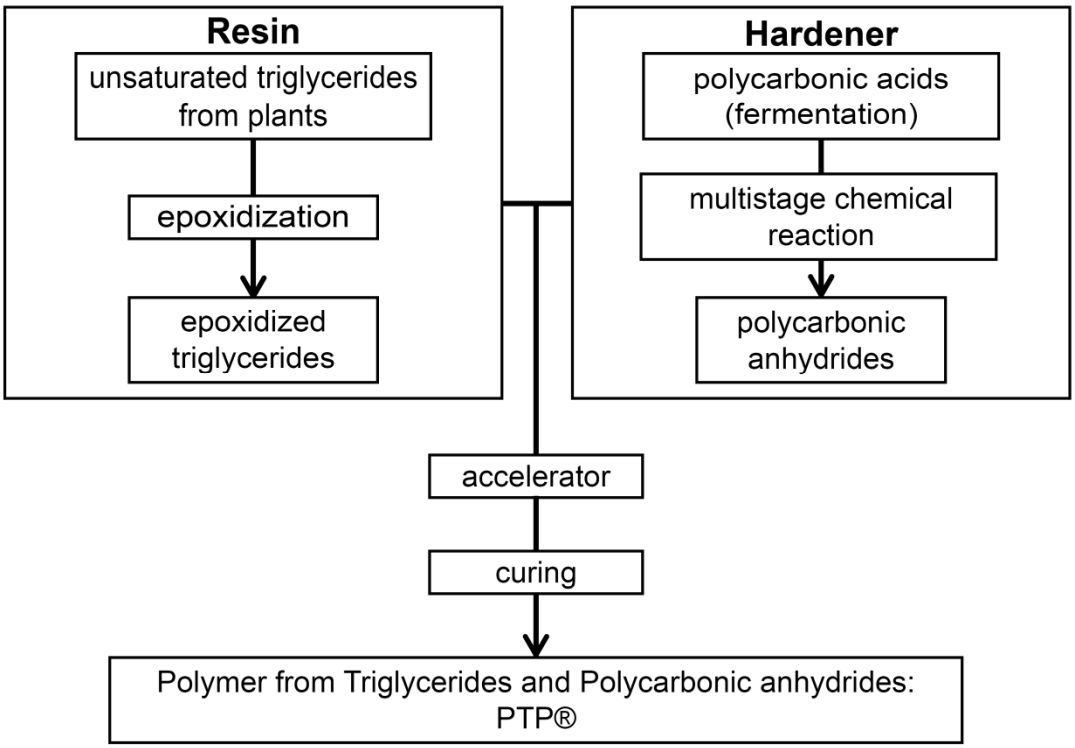

Figure 5-4. Schematic of the preparation steps required for the preparation of PTP® linseed based epoxy resin.

Table 5-1 presents some basic properties of the resin. The processing conditions suggested by the manufacturer for PTP® resin are estimated for a variety of applications and are only used as a reference in order to obtain optimal processing conditions for the impregnation process. The concentration of accelerator recommended is between 3 to 5 % wt. Resin may become separated during long shelf times and requires mixing prior to

and after adding the accelerator. Optimal reacting temperatures are between 130° to 180°C. Prior to cure, resin is very unstable with water and high humidity levels, but after cure, it is more hydrophobic than hydrophilic.

Table 5-1. Typical properties for PTP® resin.

Property	Value
Density (20°C)	1.05-1.1 g/cm^3
Viscosity (20°C)	450 mPa-s
Cure Temperature	100-190 °C
Tensile Strength	60-70 N/mm^2
Tensile Modulus	1600-1800 N/mm^2
Water Resistance	Stable

5.3 Development of the Impregnation Process

In this study, impregnation depths of the PTP® BORR resin were studied under vacuum only and vacuum-pressure conditions. Hardness and modulus tests were used to determine the benefits of impregnating with the resin and to find a relation between impregnation depth and mechanical properties of the material. Due to the high viscosity of our material and the short processing time a combination of processes which will drive the impregnation in the least amount of time is necessary. Processing parameters have to be optimized based on their dependence on material properties. In conjunction with the preliminary experiments for characterizing the resin a dimensional analysis of the impregnation process was done to better understand the complex system. The dimensional analysis results may be found in Appendix B.

5.3.1 Vacuum/Pressure Chambers

The preliminary study to determine the ability of the linseed resin as an impregnation material for wood required the construction of chambers that would allow a full vacuum to be applied on the resin. A variety of different chambers were designed for the impregnation process. A set of chambers, such as the ones shown on Figure 5-5 were the first design. These chambers were built out of PVC pipe of different sizes depending on the size and quantity of the wood pieces being impregnated.

Figure 5-5. Images of two vacuum chambers built for the impregnation of wood.

In order to seal the chambers but be able to see into it, ¾ inch acrylic lids were used. Sealing was done with custom liquid silicone rubber seals which provide a good seal between the PVC and the acrylic. Two top ports were installed: one as a release valve and another to pull vacuum. In the bottom of the chamber another port was installed that permitted the insertion of resin under full vacuum conditions. By looking closely at the right image of Figure 5-5, a metallic mesh may be seen inside the chamber which was used to prevent the wood from floating out of the resin during impregnation and eliminate any wood contact with air. Similar meshes were used between every wood piece to prevent contact between them and allow for proper resin distribution. The chambers were covered with a heating blanket controlled with a Variac autotransformer. The PVC chambers provided an economic way of performing impregnations. Unfortunately, they would take very long to heat and small temperature changes in the resin were hard to

control due to the low conductivity of the plastic pipe. Time and temperature are critical to a good impregnation—not to mention the vacuum level which is the driving force for the resin. Sometimes, the heating blanket had to be heated very close to the temperature limit of the PVC to make a significant change in the temperature of the resin. When this was necessary and high vacuums were applied, pipes would occasionally deform. To account for this, a new chamber was built that would have high heat conductivity and would maintain the temperature of the resin as stable as possible. Figure 5-6 (a) shows a picture of the new chamber.

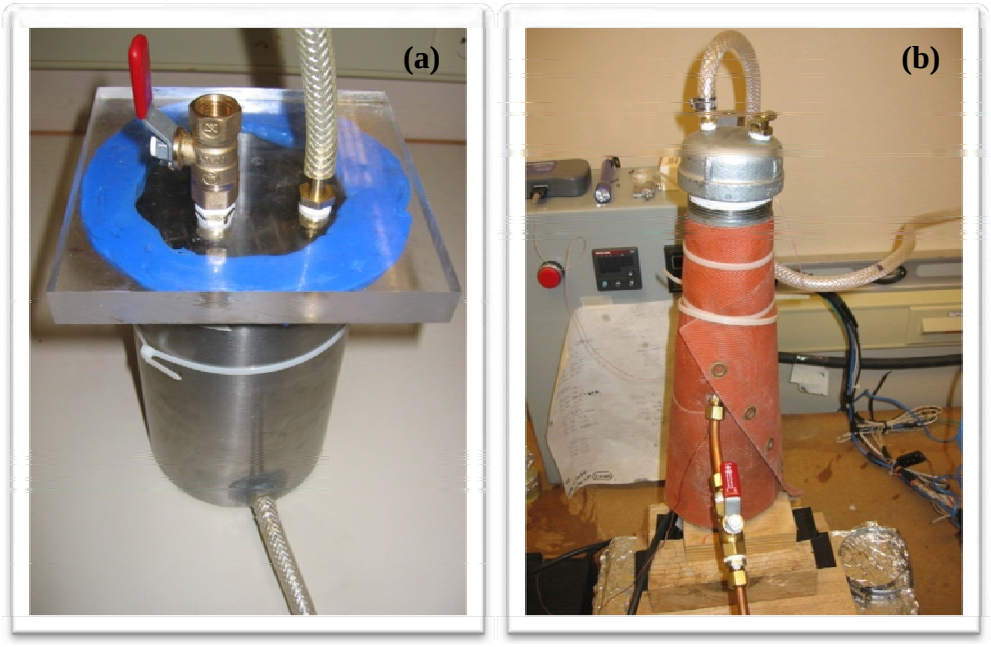

Figure 5-6. (a) Vacuum chamber with better heat transport. (b) Vacuum/Pressure chamber

The new chamber, made from oil-filled double layer aluminum, provided much better heat transport. The initial temperature could be attained faster and resin temperature was sustained more accurately. Connection ports and an acrylic lid were adapted in the same

manner. Finally, for a last set of experiments a chamber that could be sealed for pressures up to 250psi was built. The chamber was smaller and only allowed the insertion of one wood piece at a time rather than four to six as in the other chambers. The vessel consisted of galvanized piping, sealed with end-caps, and ported as with the other systems. Pressure was applied with a nitrogen tank. The purpose of the pressure vessel was to obtain the highest impregnation depths and to determine a relation between impregnation depths with time at different isobaric conditions.

5.3.2 DSC and Viscosity Analysis

The process of impregnation can be optimized by applying the material under the lowest possible viscosities. Unfortunately, as viscosity is reduced by increasing temperature the reaction is accelerated. As the reaction is accelerated the time at which the material will remain at the low viscosity will shorten because the cross-linking chemical reaction will rapidly increase the viscosity until a hard rigid structure is formed. To evaluate the curing reaction at different conditions several DSC experiments were performed. For information on the DSC system refer to section 2.3.1. A NETZSCH DSC 200 PC developed by NETZSCH-Gerätebau GmbH (Selb/Bayern, Germany) was used for all analyses. Figures 5-7 and 5-8 show a set of different isothermal runs at 150°, 130°, 90° and 80°C. Dynamic runs such as the one shown on Figure 5-9 were also generated to estimate total heat of reaction.

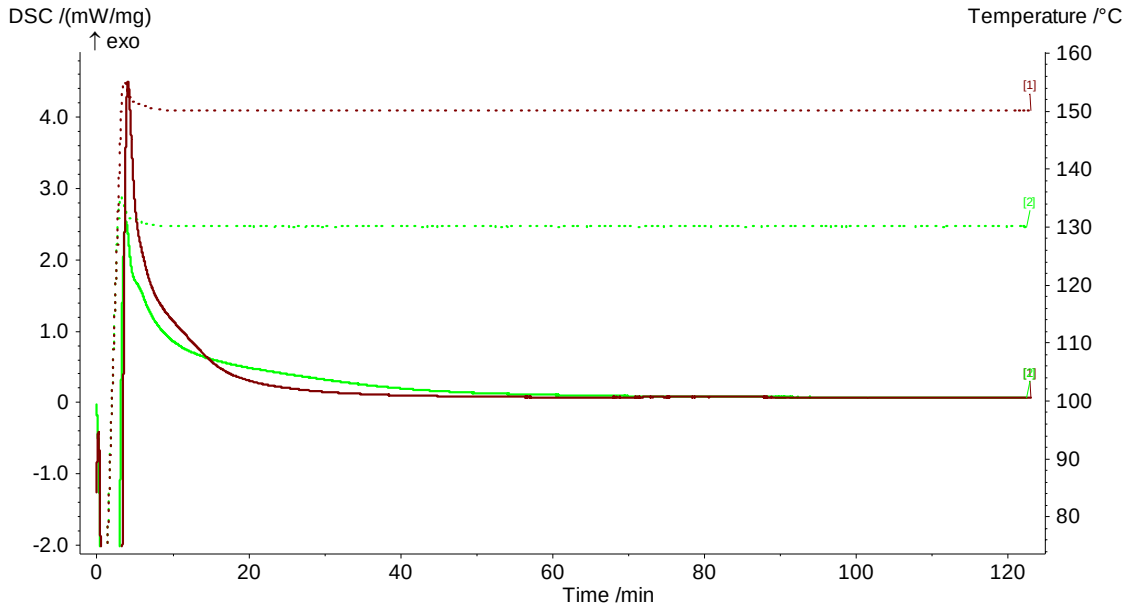

Figure 5-7. Isothermal DSC runs at 150° and 130°C. Note high exotherms.

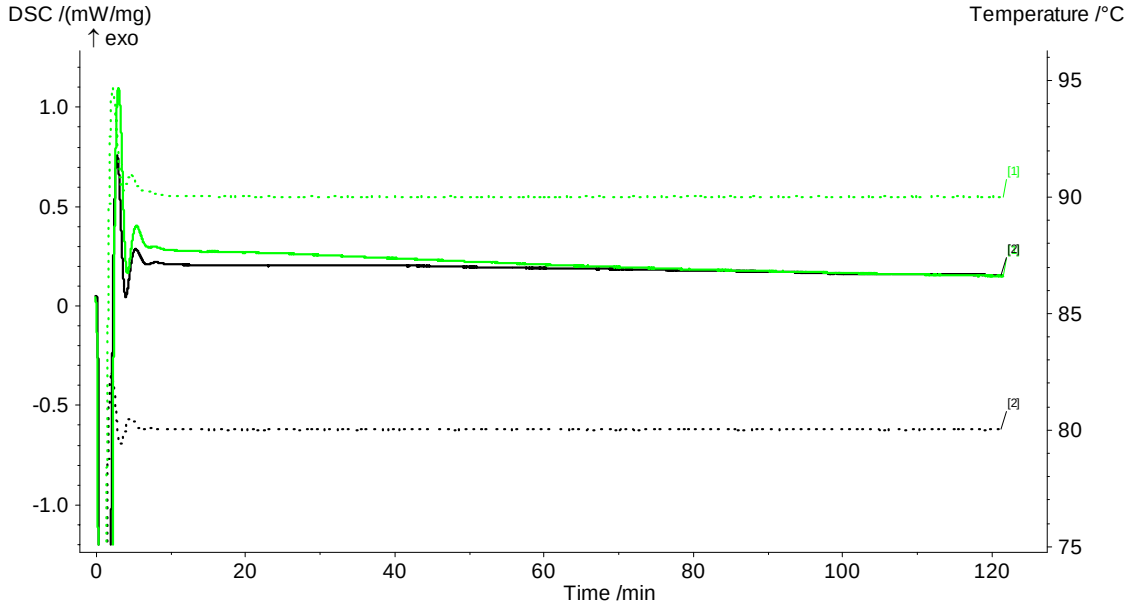

Figure 5-8. Isothermal DSC runs at 90° and 80°C. Exotherms are greatly reduced and almost unnoticeable below 80°C.

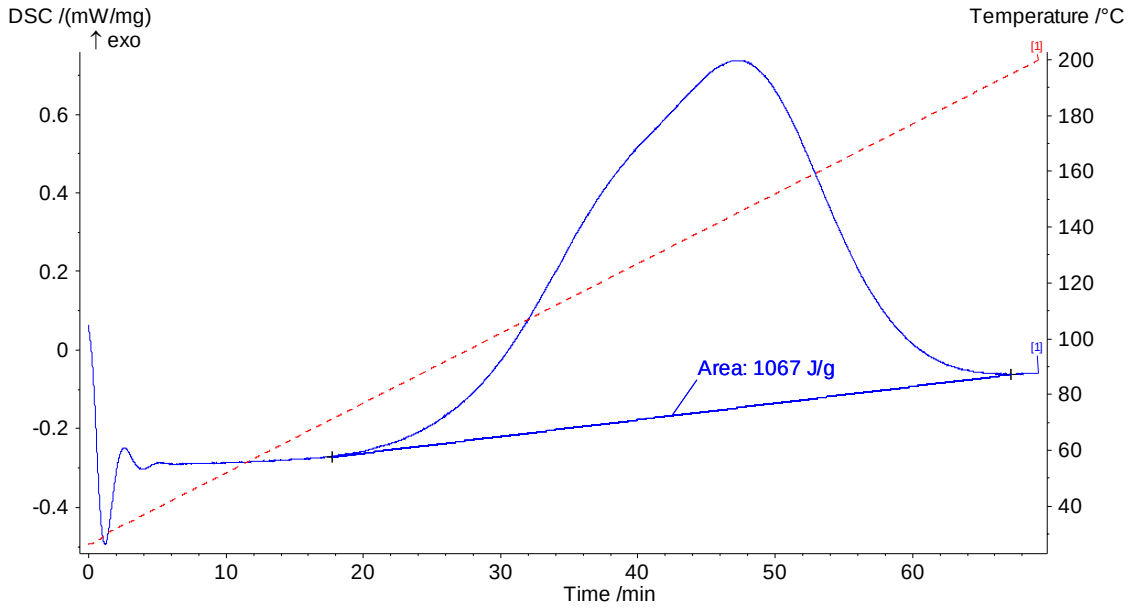

Figure 5-9. Dynamic DSC test at 2.5K/min up to 200°C.

Figure 5-7 shows large exotherms and high degrees of cure obtained at 130° and 150°C. Much slower curing rates are obtained for temperatures of 80° and 90°C (Figure 5-8), and below 70°C, exotherms are hardly noticeable. Unfortunately, the curing information does not provide an idea of the extent of viscosity rise with cure, therefore, rheometry experiments were generated as well. Direct viscosity measurements would confirm the DSC results and provide an idea of the lowest viscosity at which the material would be able to be impregnated. Viscosity measurements were done on a TA Instruments Advanced Cone-and-Plate Rheometer 1000 with a 40mm, 1° cone. It was determined that optimal results may be obtained with a 2.8Hz frequency and 1.7% strain by generating various frequency and strain sweeps for the resin. The established values were held constant for all the experiments. Figure 5-10 presents dynamic cure results for a 5K/min heating rate up to 130°C.

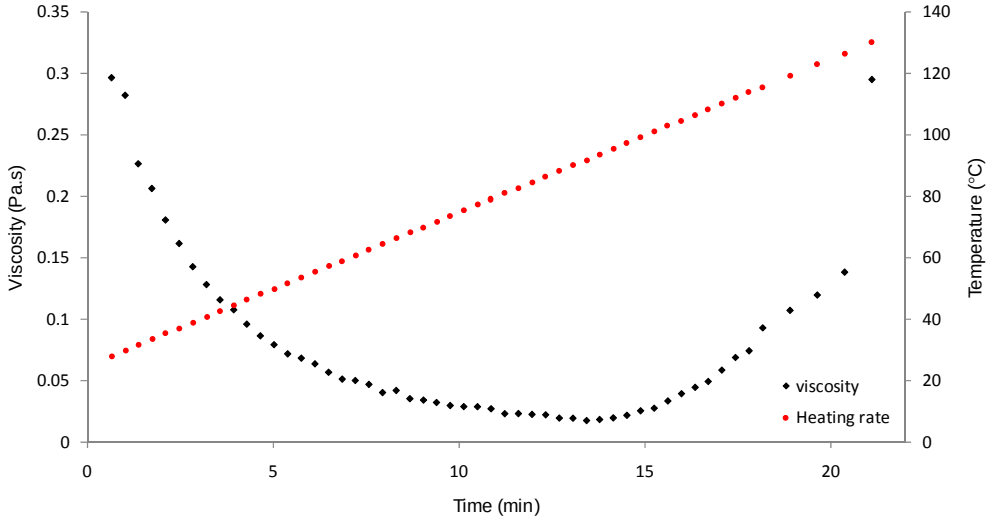

Figure 5-10. Viscosity in time for a sample of PTP® resin cured dynamically at 5K/min up to 130°C.

During the dynamic sweep the lowest viscosity attainable was 18mPa-s at approximately 13.5 minutes and a temperature of 92°C. The low viscosity rapidly increased as the temperature was raised further. Figure 5-11 shows viscosity results for isothermal runs.

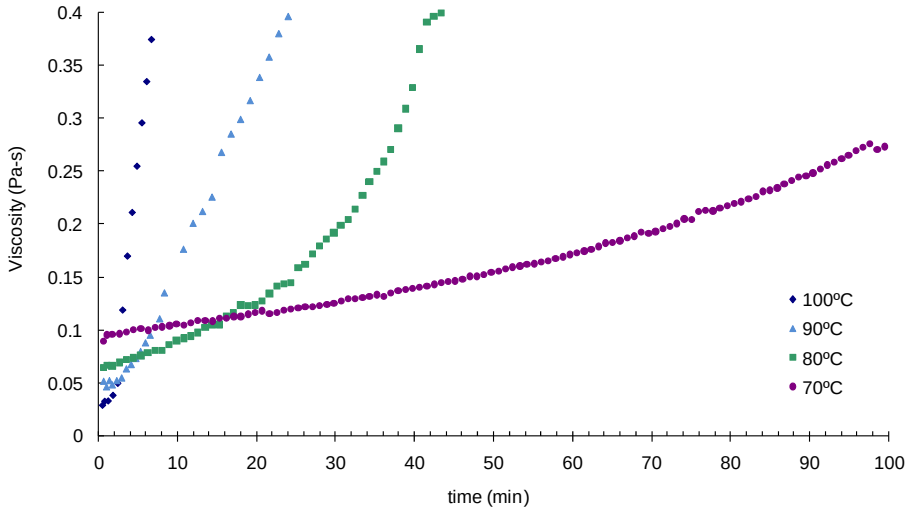

Figure 5-11. Viscosity in time for PTP® resin cured isothermally at 70°, 80°, 90°, and 100°C.

Isothermal runs provide very interesting results about the curing behavior of the resin. As shown, as the temperature is raised the initial viscosity decreases but the time it remains low shortens.

Knowing that the minimum viscosity of the resin was around 18mPa-s, which is similar to the viscosity of olive oil at 25°C, impregnation experiments were performed with olive oil and very favorable results were obtained. Unfortunately, the impregnation process was an all manual process and as will be discussed in section 5.3.3, it requires a certain amount of time to prepare the resin, pull the vacuum, fill the chamber, and begin the impregnation. It was estimated that preparation time after the resin had been mixed with the accelerator to the point of impregnation would be approximately 8 min. Therefore, based on this assumption the value of 18mPa-s would not be possible. Table 5-2 shows the rheometry values of the first 8 minutes. As seen in Figure 5-11 and Table 5-2, for our particular process the optimal temperature should be close to 80°C. This temperature is the point where the material maintains the lowest viscosity during enough time to perform the impregnation. Soaking time for the impregnation is approximately 20 minutes which was also taken into account to determine the optimal temperature.

Table 5-2. Viscosity (mPa-s) values at specific times for isothermal cure of the PTP® resin.

Time (min)	70°C	80°C	90°C	100°C
0	93	65	51	27
4	99	73	66	205
8	103	81	130	520

The other important consideration for our process is the period of cure after impregnation has been completed. Since the curing of the material will be done within the wood, the resin cannot be heated higher than the wood can withstand. 105°C is considered the first temperature where some disruption of the wood may be seen during extended periods of time. Even so, at this temperature the wood is not significantly affected to reduce the mechanical properties of the part. The wood should not be exposed to temperatures higher than 150°C for extended periods of time or significant disruption may happen. As seen on the DSC results, 105°C is too low to obtain a high cure degree. With the high activation temperature accelerator used, the temperature may be increased in order to lower the viscosity without significant curing, but unfortunately, a higher temperature will also be needed to reach a full cure. Various curing curves were generated with the DSC to simulate the process and determine if high levels of cure would be obtained. Figure 5-12 shows a group of results simulating the process. As previously determined, an initial impregnation temperature of 80°C would be done followed by a temperature rise after impregnation to complete the cure.

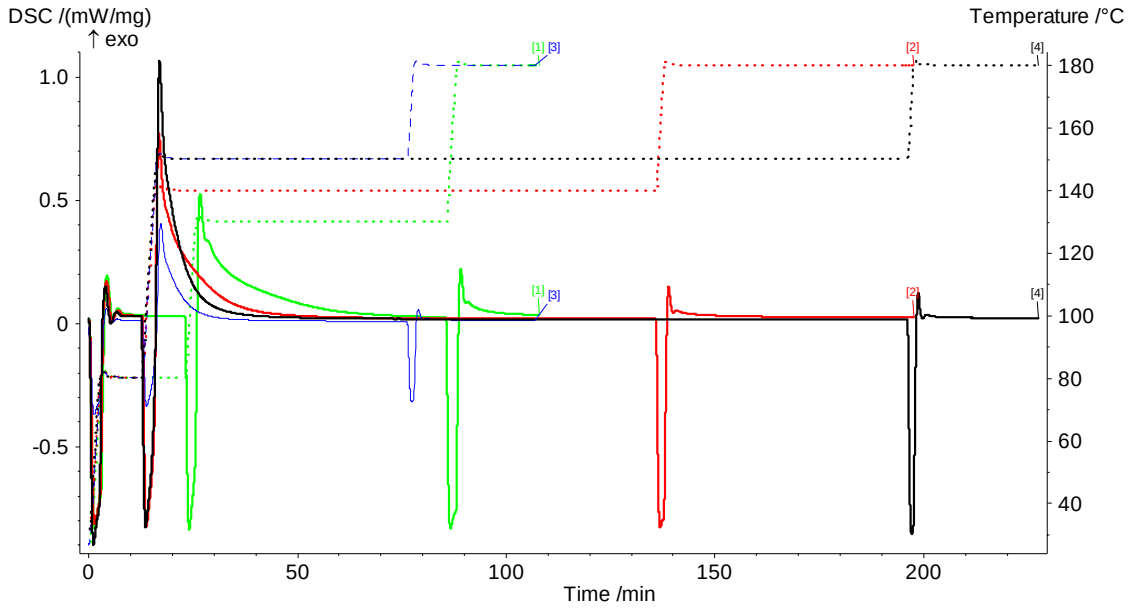

Figure 5-12. Impregnation process simulation of heating steps by DSC.

For all runs temperature was raised to 80°C and maintained for 10-20 minutes. Subsequently, the temperature was raised to a high curing temperature and finally the material was tested for any residual cure. Initially, temperatures of 130°C and 140°C were tested but a significant residual cure was found. This residual cure may be noticed by the residual exotherm during the final heating at 180°C. In order to obtain high cures the temperature was raised to 150°C and excellent results were obtained after curing for one hour. The curing temperature selected for the process was then 150°C but due to the size of the wood blocks longer time was required for proper heat transfer. With three hours at 150°C the resin would fully cure, the wood would not suffer any significant degradation and enough time would be allotted to heat the inner core of the thick wood sections.

5.3.3 Impregnation Procedure

Southern yellow pine (SYP) wood sections were selected as the material to be infiltrated based on end-applications, cost, structural properties and availability. SYP is a low cost, fast growing wood mainly used for structural applications. It is one of the most common woods used in the United States. Properties are low when compared to many other hardwoods. For that reason, they are a good candidate for impregnation. Two different wood sizes corresponding to two different SYP types were tested for impregnation depths and hardness: 3×1.5×3/4 inch and 4×2×1 inch sections. The larger blocks are longleaf SYP and the smaller blocks are shortleaf SYP. Longleaf is known to be somewhat stronger that shortleaf. Only samples with relatively well patterned growth rings were used. The transverse and radial directions are cut the same as an industrial 2×4 inch section—as these are scale-downs of a 6×4×2 inch geometry. For DMA testing, samples of 1.5×1/4×1/8 inch were cut. In order to obtain information on the softest component when doing tension and compression tests, the samples were cut with the longest dimension perpendicular to the growth rings. The wood selected for DMA experiments was green-house grown in a well controlled environment leading to a very symmetric growth ring pattern with large earlywood rings and very small latewood rings. Figure 5-13 shows an image of the wood samples. For impregnation depth analyses, sample ends were coated with a room temperature cure epoxy to prevent impregnation through the large capillaries in the end of the wood pieces and reduce the system to a two-dimensional impregnation. One-dimensional impregnations were also done by coating everything but the top and bottom walls.

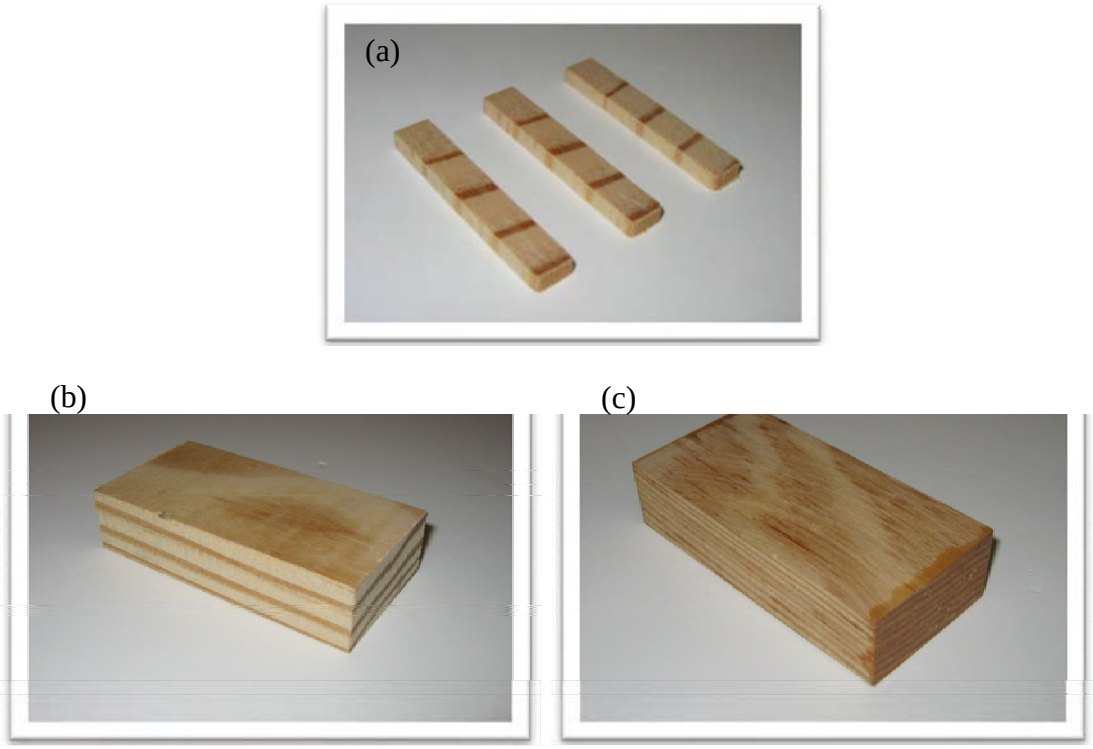

Figure 5-13. Wood samples used for the mechanical tests. (a) DMA sample. Note the cut-direction of the DMA samples. (b) 3×1.5×3/4 inch and (c) 4×2×1 inch for impregnation depth and hardness testing evaluation.

The wood was dried for 16 hours at 105°C. After drying the samples were stored in Ziploc bags until used. The uncatalyzed resin was vacuum preheated to 80°C. The initial vacuum would reduce volatiles during the process. Simultaneously, the wood was preheated to 90°C. The preheating of the wood was key to assure the resin would maintain its temperature when inserted into the vacuum chamber. Preheated wood samples were placed in the vacuum chamber and secured in place using metal mesh. A full vacuum was pulled on the system. After the preheating temperature of the resin had been attained and immediately after full vacuum (close to 30inHg) in the chamber had

been reached the resin was removed from the vacuum oven and placed on a hot plate to maintain its temperature constant for impregnation. 3% accelerator was added while a magnetic stirrer mixed the resin and helped maintain the temperature of the resin homogeneous. A suction tube was placed in the resin, and immediately, the input valve was opened to allow resin to slowly fill the chamber until the wood was fully covered. After resin had filled the chamber vacuum was stopped and the release valve was slowly opened. Negative pressure on the liquid would drive the resin into the wood. The wood was allowed to soak for 20 minutes before samples were removed. The inner temperature of the system was monitored with an Omega OMPL-TC temperature datalogger. The heating blanket around the chamber was manually controlled with a Variac autotransformer to maintain the temperature constant. The temperature of the resin prior to being inserted in the chamber was monitored with a Fluke 2170A digital thermometer. If the pressure chamber was used, a pressure of 150psi was applied throughout all the soak period. After impregnation was completed samples were removed and cured in a convection oven at 150°C for three hours. Cured samples were sanded down to the wood surface to remove any coating layer of resin. Initial weight of the wood was measured and compared to final weight. Humidity levels of the room were recorded and compared to color change of the resin. The air pressure sustained and any temperature changes in the system when resin was inserted into chamber were monitored and recorded.

5.4 Material Testing and Impregnation Results

DMA was the first method used to obtain some preliminary results on the mechanical improvements of impregnating southern yellow pine with the linseed based epoxy. The benefit of DMA is the small sample size which could be easily impregnated with the resin. As described in the previous section, the selected geometry of the DMA samples provide a specific result for the increase in modulus of the softest component on the wood—the thick early wood sections. An RSA III Rheometrics System Analyzer from TA Instruments was used for all DMA experiments. Tension and compression tests were done with a clamped tool geometry. Tests were done isothermally at 25°C and a humidity controlled environment at 30% RH. A constant frequency of 10Hz and percent strain of 0.6 were determined to be appropriate by running frequency and strain sweeps. Samples were tested prior to impregnation and after full impregnation under vacuum-only conditions and results were compared. Figure 5-14 shows images illustrating difference in sample color after impregnation.

Figure 5-14. Unimpregnated DMA sample (left). Fully impregnated sample (right).

When lightly sanding samples to remove any coating layer, it was noticed that slight shrinking of the early wood occurred. Tension results are reported on Figure 5-15. As seen on the figure, the increase in tensile Young's modulus (E') for impregnated samples is significant and very consistent with all values tested reporting a modulus over three times higher. Very similar results were observed for compression (Figure 5-16). Each result consists of an individual sample. Reported value consists of an average taken between three trials. Highest error between trials for all samples (both in tension and compression) was 0.8% with an average overall error of 0.23% and errors as low as 0.02%. Table 5-3 summarizes the results and provides an average modulus increase.

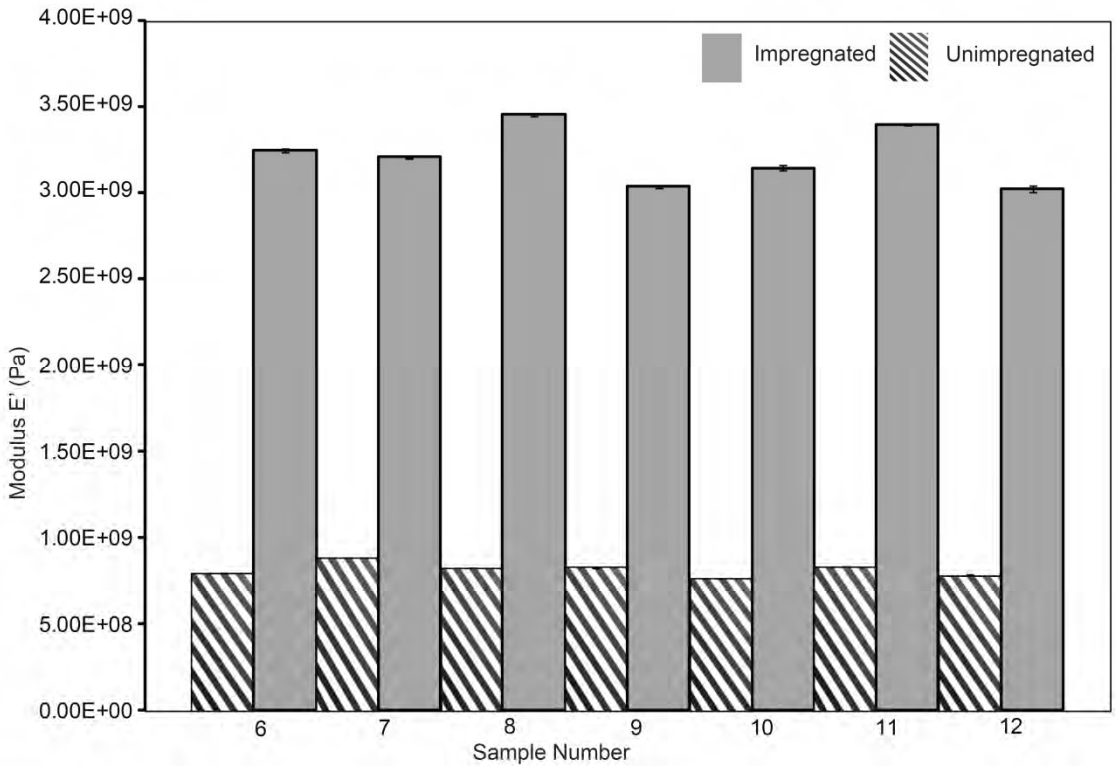

Figure 5-15. DMA tension test results for unimpregnated specimens compared to results for the same samples after impregnation.

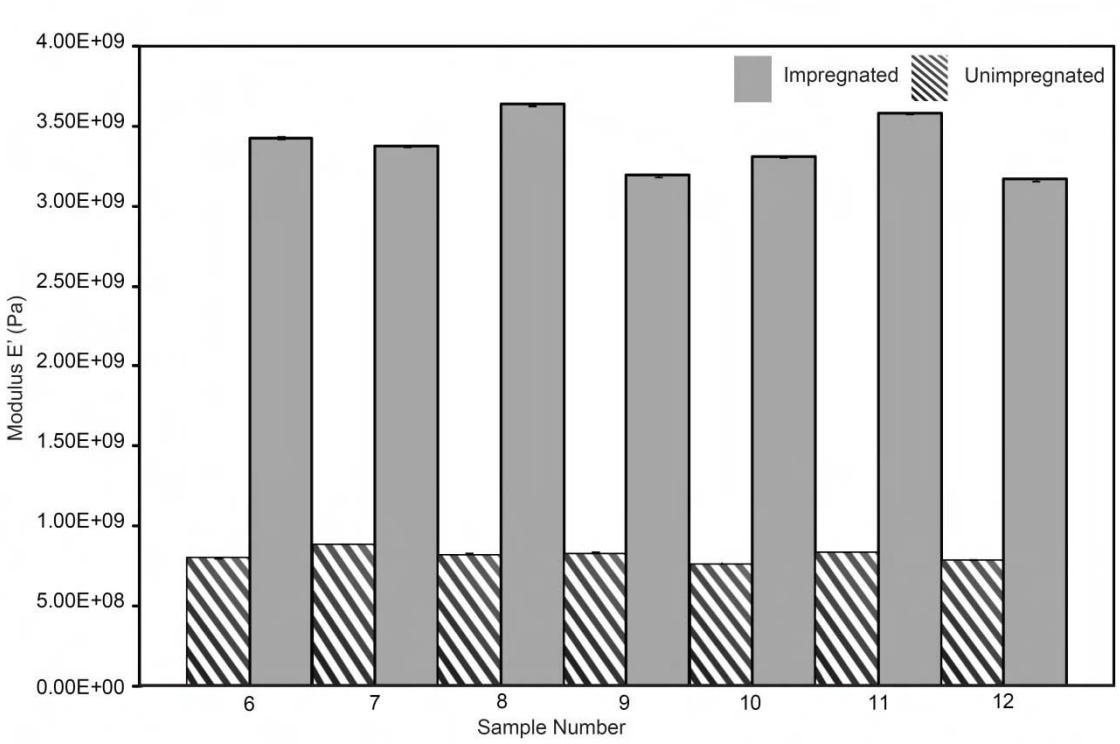

Figure 5-16. DMA compression test results for unimpregnated specimens compared to results for the same samples after impregnation.

Table 5-3. Summary of DMA Modulus (E') results

Tension

Sample #	6	7	8	9	10	11	12	
Unimpregnated	7.99E+08	8.84E+08	8.25E+08	8.32E+08	7.68E+08	8.37E+08	7.86E+08	
Impregnated	3.25E+09	3.21E+09	3.45E+09	3.04E+09	3.15E+09	3.40E+09	3.02E+09	AVG%
% Increase	306.89	262.63	318.42	265.61	309.54	306.00	284.59	293.38

Compression

Sample #	6	7	8	9	10	11	12	
Unimpregnated	8.08E+08	8.93E+08	8.31E+08	8.39E+08	7.73E+08	8.42E+08	7.95E+08	
Impregnated	3.42E+09	3.38E+09	3.64E+09	3.20E+09	3.31E+09	3.58E+09	3.17E+09	AVG%
% Increase	323.83	278.56	337.83	281.24	328.24	325.24	298.69	310.52

As seen in the results presented on Table 5-3, experiments are very repeatable. This condition was secured by using samples cut from a wood piece grown in a controlled

environment. Moreover, differences in results between samples tested were not higher than 13%. In general, standard wood variations may be well over 25%.

Following the excellent results obtained with DMA testing, a series of experiments were performed to optimize the process for obtaining thick impregnated sections. The procedure for impregnation was very complex, considering it was mainly a manual procedure. Two or more people were required to perform a complete setup in the appropriate time. For this reason, a number of experiments had to be generated until the desired results were obtained. The most common problem was impregnating at a temperature that was too low. Table 5-4 presents a summary of experiments and may be used as a reference for further results.

Table 5-4. Summary of results for impregnated samples.

				Weight(g)			
Sample #	% Area impreg.	Temp °C	Temp range °C	Initial	Final	Resin wt.	Comments
Large 2D 1	15.27	60.0	55.0-65.0	76.8	81.8	5.0	Air exposed
Large 2D 2	16.10	60.0	55.0-65.0	75.8	86.8	11.0	Air exposed
Large 2D 3	60.09	74.2	79.0-72.4	66.1	101.2	35.1	
Large 2D 4	73.51	74.6	73.5-77.5	68.1	107.9	39.8	
Small 2D 1	30.99	75.7	70.5-77.5				no wood Pre-Heat
Small 2D 2	27.56	60.0	80.0-60.0				no wood Pre-Heat
Small 2D 3	48.56	83.3	84.8-81.6				
Small 2D 4	63.77	74.2	79.0-72.3	26.6	45.5	18.9	
Small 2D 5	59.04	75.2	79.0-72.5	25.6	42.5	16.9	
Small 2D 6	74.72	74.6	73.5-77.5	26.0	47.4	21.4	
Small 2D 7	72.52	74.6	73.5-77.5	*27.3*	*47.8*	20.5	
Small 3D 8	27.46	60.0	80.0-60.0				Long end-impreg.
Small 2D 9	87.98	75.0	74.0-76.3				Long end-impreg.
Step 2	19.56	76.0		28.4	34.8	6.4	2min Impreg.
Step 5	31.88	74.0		26.1	34.9	8.8	5min Impreg.
Step 10	36.89	73.0		29.2	39.0	9.8	10min Impreg.
Step 15	39.43	73.0		28.3	39.6	11.3	15min Impreg.
Step 20	42.30	62.5		28.5	40.2	11.7	20min Impreg.
Pressure1	50.86	75.0	67.0-75.0	60.8	84.0	23.2	Uneven
Pressure2	89.13	76.0	67.0-76.0	58.4	115.1	56.7	

The small and large samples refer to the sample geometries shown on Figure 5-13 (b) and (c) respectively. The two-dimensional geometries are samples which have had their ends coated and may only absorb resin in the radial and tangential faces. The second column of Table 5-4 reports results for an estimation of the area impregnated to that of the total cross-sectional area of a sample cut perpendicular to the longitudinal direction of the wood. Figure 5-17 provides a better description of the concept. The "% area impregnated" value is an average of two cuts for the small blocks and three cuts for the large blocks. The temperature reported is the actual resin temperature when soaking time starts and the temperature range describes the variation in temperature during the process. The resin weight provides an idea of the amount of resin absorbed by the wood and correlates well to the value of % area impregnated.

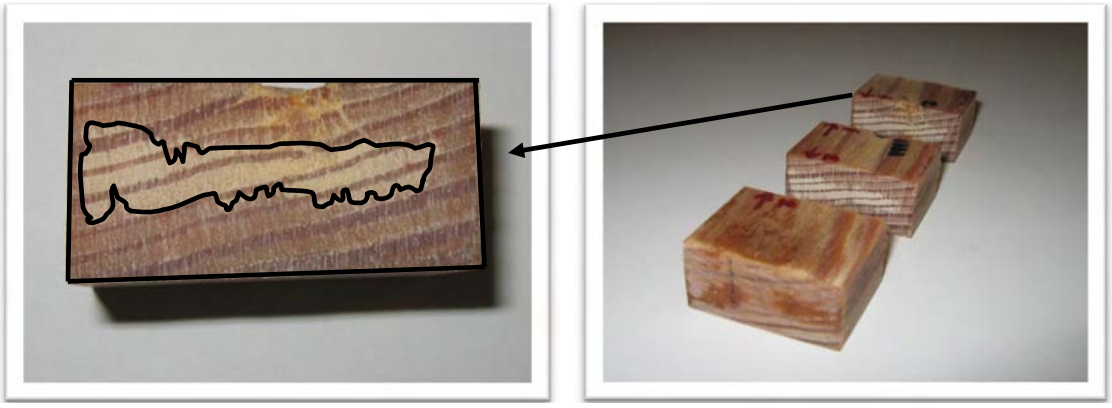

Figure 5-17. Sample "Small 2D 6" cut perpendicular to the longitudinal direction of the wood where inconsistencies in impregnation depth may be observed. An illustration of the impregnation area has been included.

Relevant information that may be obtained from Table 5-4 is the large inconsistencies which are currently obtained during the impregnation process. The main reason for these

inconsistencies other than the natural variations in the wood is the unavailability of an automated system control. Even with these great variations, it will be shown that very valuable information may be obtained about the improvements in mechanical properties of the wood through resin impregnation.

A step-impregnation was performed by doing a run with five small-sized wood samples and removing them from the resin at different times. Since the resin is inserted into the chamber under vacuum, when the vacuum is released a net pressure results that drives the material into the wood as long as the wood is fully immersed in the resin. Due to the high viscosity of the resin this may take several minutes. Figure 5-18 shows the results obtained for the step-impregnation. These results are also shown in the summarized data on Table 5-4.

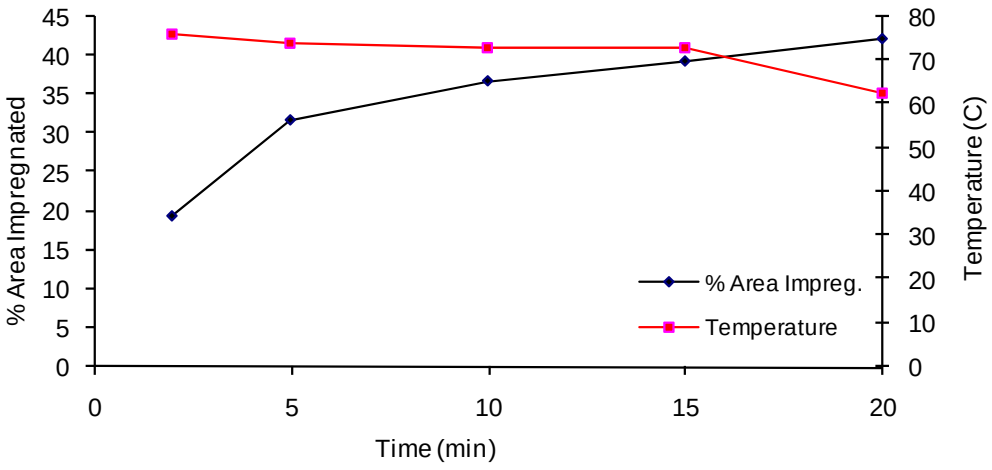

Figure 5-18. Step-impregnation results obtained by removing samples from the resin at different times.

Unfortunately, a good temperature control was not possible. Even so, it is clearly seen that after 20 minutes the wood is still absorbing resin. With an optimal temperature control that may allow for lower viscosities and possibly the use of external pressure, this process time may be reduced. Figure 5-19 is an image taken of the cross-sections of the blocks removed at the respective plotted times.

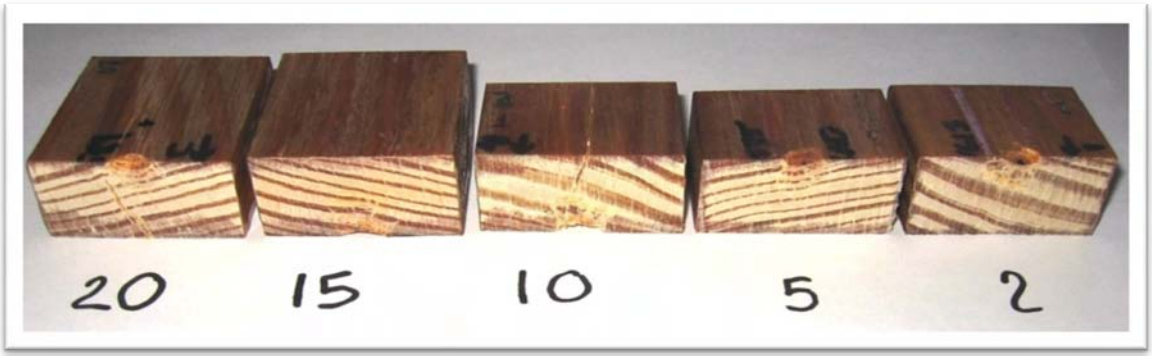

Figure 5-19. Image of samples used on the step-impregnation analysis. Larger impregnation depths may be seen for the longer times.

An important aspect of the process of resin impregnation is the ability to harden the wood's surface. In many applications where wood is used, a major factor in wood selection is the hardness of the wood. A material that is easily scratched may not be used for flooring or similar applications where aesthetics are critical. As the resin impregnates the wood surface it fills holes and gaps increasing the density and hardening the material. The deeper the resin reaches into the wood the denser the structure and the smaller the unimpregnated core becomes. The properties of the resin and interaction between the wood and resin will affect the final hardness of the material. Due to the synergistic effect between the materials it is possible to end with a product harder than both the resin and

wood themselves. By performing hardness tests on the impregnated wood samples and recording the impregnation depth at the testing area, a relation between impregnation depth and hardness was determined.

Janka hardness is the standard method for determining hardness of wood. The method is a derivation of the Brinell hardness test. A Janka test consists of measuring the force required to push a steel ball with a diameter of 0.44" (11.28mm) into the wood to a depth of half the ball's diameter. The resulting area produced in the indentation will be of 100mm^2. Results are generally stated in the force units (lbf). The standard wood size is a 2×2×6 inch specimen. Green et al. [128] demonstrated that similar results may be obtained when other wood sizes and ball sizes are used; a relation for the projected ball area to the force required to indent the surface holds. Also, as the indentation is performed at the standard constant rate of 0.25in/min a linear increase in force with time is observed that may be represented as a hardness modulus. A relation also holds for the hardness modulus and the hardness value obtained at the indentation depth of half the ball's diameter. Based on these conditions a set of experiments were performed with a smaller ball size of approximately 11/32". The indentation depth based on the exact ball's radius was 0.1717". The two determining reasons for using the smaller ball size were the limits of our testing equipment and the geometry of our samples which are smaller than the standard. The standard requires a larger wood piece to prevent obtaining wrong information from the supporting surface and wood compression. Our testing equipment was an MTS tensile/compression tester modified for these experiments. The limit of the loading cell of the system is 1000lbf. It was found that this limit was easily reached with

the standard ball size of 0.44in with natural wood specimens. With the 11/32 inch ball, only highly infiltrated samples would reach the limit of the system. As shown on Figure 5-20, hardness setup was custom made by use of a screw head and ball bearing.

Figure 5-20. Modified MTS tensile/compression tester used for Janka hardness testing of impregnated and unimpregnated wood specimens.

Through the use of MTS software, loading and extension are automatically controlled and recorded in time. Hardness and modulus data are obtained simultaneously. Therefore, the standard hardness rate of 0.25in/min is used for both. In order to obtain hardness infiltration from modulus data, fittings are done to relate unimpregnated modulus and hardness which is later used for determining hardness of impregnated samples. Hardness of impregnated samples has to be determined by estimating the Janka hardness through measures of the modulus. The reason is that the material is only hardened up to a certain

distance, the depth to the core. When the ball reaches the core or gets close enough to be influenced by the core's compression the linear increase in load drastically drops as shown on Figure 5-21. Another reason why it is necessary to estimate hardness with modulus is because highly infiltrated samples reach the 1000lbf limit of the testing machine before the ball reaches half its diameter which is the proper extension for determining a hardness value.

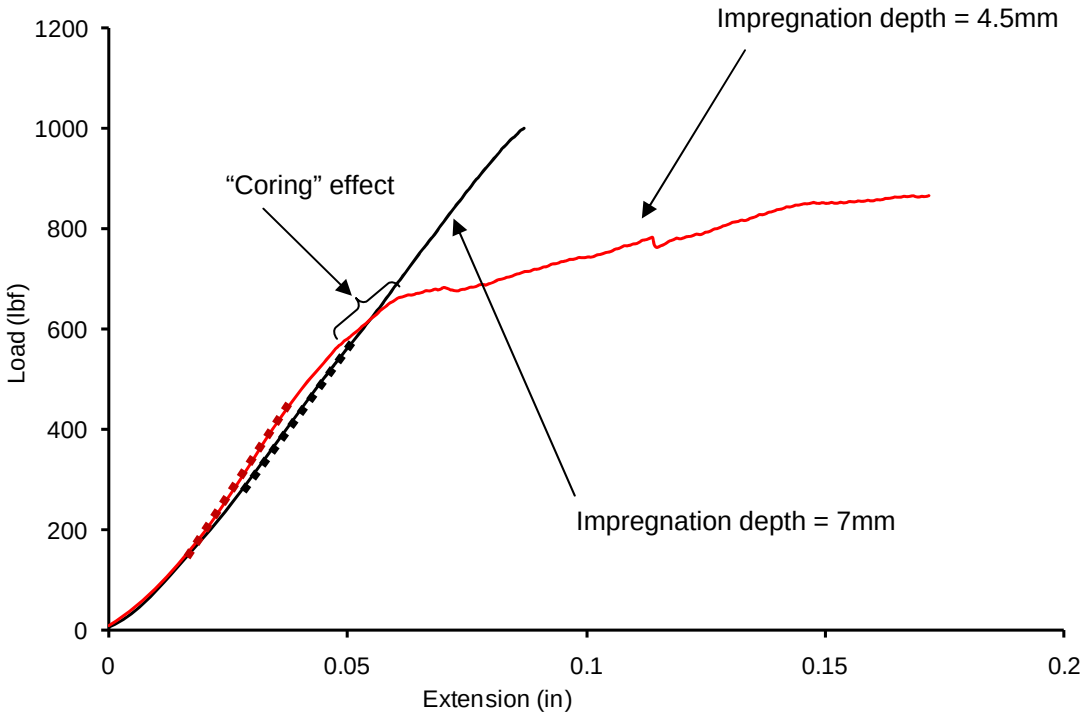

Figure 5-21. Data obtained from two hardness tests done on the same longleaf (large-block) SYP sample at areas where the impregnation depth varied significantly. Modulus area used for hardness determination is shown with dashed line.

As previously mentioned, the determination of hardness increase of impregnated samples was done by relating the results to data from unimpregnated blocks obtained from the

same wood specimen. Figure 5-22 and 5-23 present results of hardness and modulus obtained with unimpregnated samples of SYP shortleaf and SYP longleaf respectively.

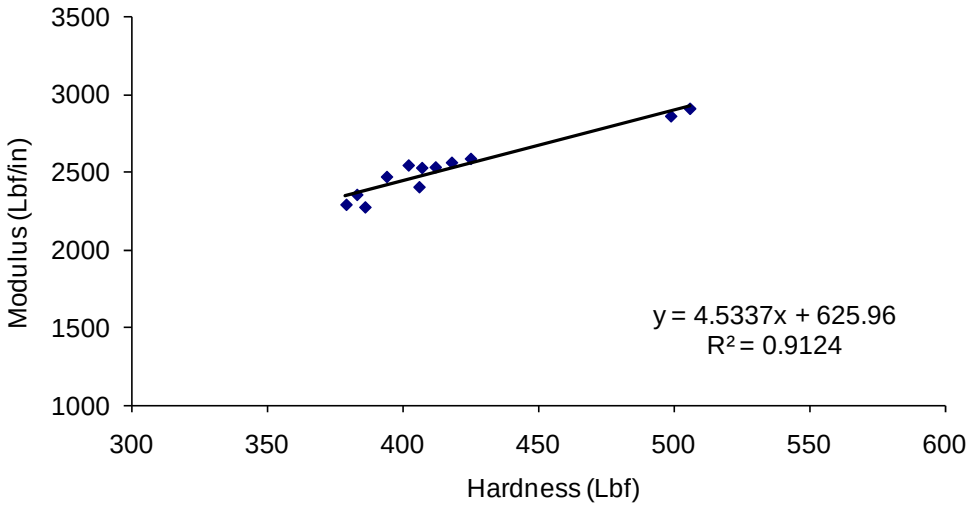

Figure 5-22. Linear fitting generated for relating the hardness to hardness modulus of shortleaf SYP.

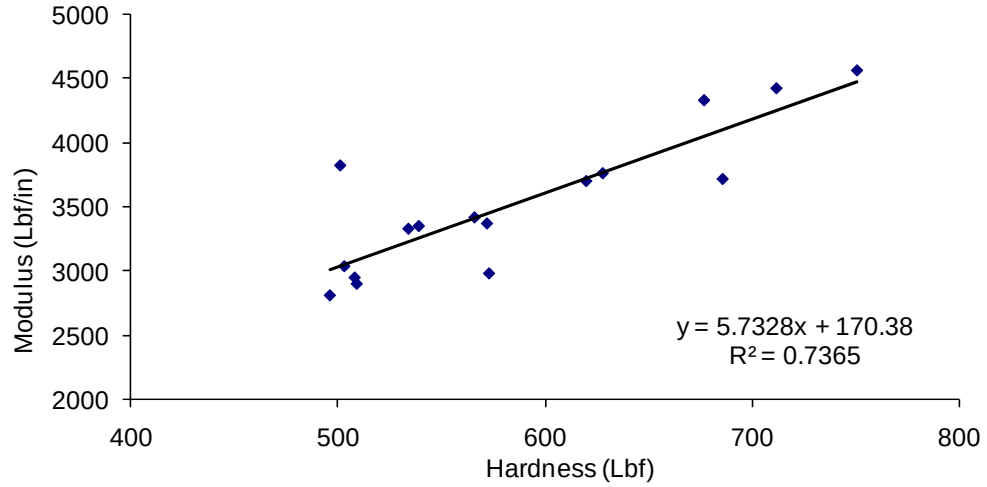

Figure 5-23. Linear fitting generated for relating the hardness to hardness modulus of longleaf SYP.

Variations in hardness between samples are common. The main reason is the variances of earlywood and latewood layers within the sample. Depending on where you test you may land on different layers. Furthermore, the thickness of these layers varies between wood pieces. Results reported on Figures 5-22 and 5-23 are hardness values obtained with the 11/32" ball size. In order to estimate the value that would be obtained using a 0.44" ball size a simple approximation may be done. Assuming a linear relationship between the projected areas of a 0.44" ball which is $100mm^2$ to that of an 11/32" ball ($60mm^2$), hardness results from the 11/32" ball may be multiplied by $1.\overline{66}$. By multiplying the 11/32" average hardness results for both shortleaf and longleaf specimens by $1.\overline{66}$ results in hardness values of 694lbf and 973lbf respectively. These results correlate very well with literature values for Janka hardness of shortleaf and longleaf SYP which are 690lbf and 870lbf respectively. Wood picked randomly is expected to have a hardness variation of up to 20% of the value reported in literature.

Hardness of impregnated samples was estimated by recording the modulus obtained with the hardness test, as shown by the dashed line on Figure 5-21. A value of hardness was then determined by using the linear fittings relations of hardness versus hardness modulus, shown on Figures 5-22 and 5-23. This would provide a value of hardness with the 11/32" ball which was then estimated to the Janka hardness (0.44") by use of our approximation. Figures 5-24 and 5-25 show the results obtained for the hardness increase of impregnated samples relative to depth of impregnation. Although there are large variations in the results, the dependency of the hardness to the impregnation depth may

be clearly seen. The hardness of the material increases drastically with impregnation up to a limit value.

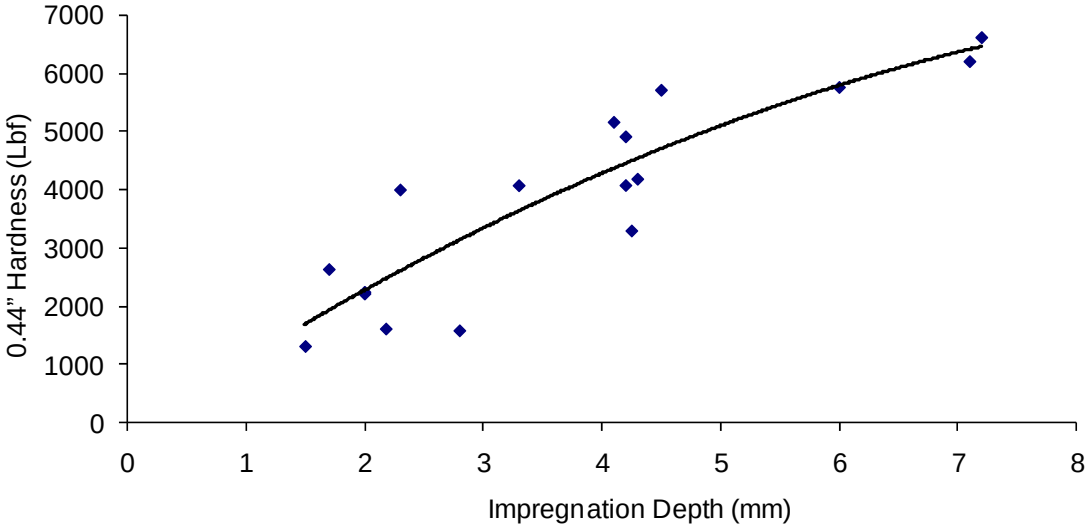

Figure 5-24. Fitting for variation in hardness with impregnation depth for shortleaf SYP.

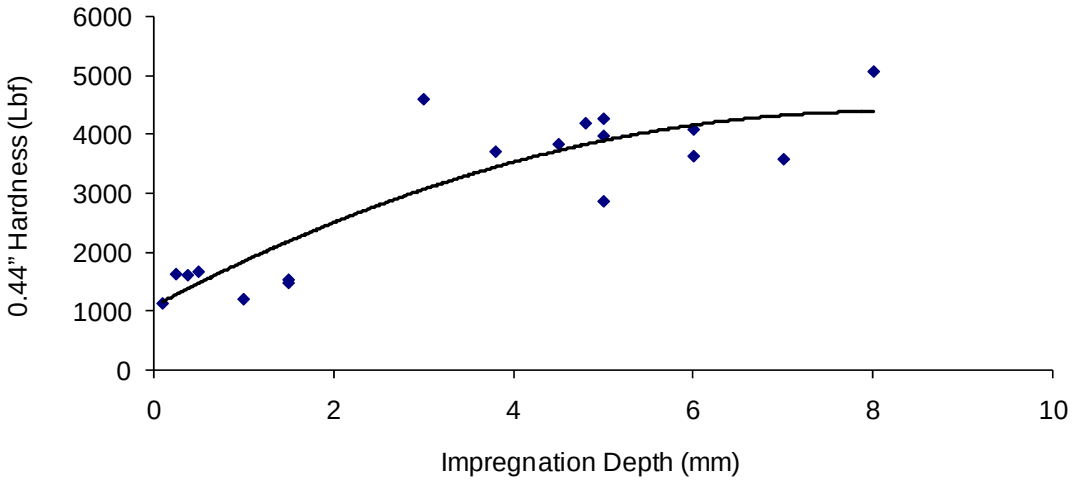

Figure 5-25. Fitting for variation in hardness with impregnation depth for longleaf SYP.

When comparing the value of hardness of impregnated samples to unimpregnated ones, the percent increase is extremely large. Tables 5-5 and 5-6 provide a summary of the results. Average 0.44” Janka hardness results shown on the tables were obtained from the fittings of Figures 5-24 and 5-25. According to these results even a slight impregnation will have a significant effect in the hardness of the material. An 8mm piece such as a flooring plank, fully impregnated, would have drastic hardness increases. Although more experiments have to be done to draw legitimate conclusions, results are favorable. Due to the drastic hardness increases in the wood, the impregnation application seems a reasonable process to consider.

Table 5-5. Results of hardness increase by impregnation for shortleaf SYP.

Depth (mm)	1	2	3	4	5	6	7	8
Avg. 0.44 HDNS (Lbf)	1075	2264	3330	4272	5090	5784	6355	6802
HDNS increase (%)	54.8	226.2	379.8	515.5	633.4	733.5	815.7	880.1
Avg. Unimpreganted SYP Shortleaf Janka HDNS				694				

Table 5-6. Results of hardness increase by impregnation for longleaf SYP.

Depth (mm)	1	2	3	4	5	6	7	8
Avg. 0.44 HDNS (Lbf)	1838	2500	3063	3526	3890	4155	4320	4386
HDNS increase (%)	88.9	157.0	214.8	262.4	299.8	327.0	344.0	350.7
Avg. Unimpreganted SYP Longleaf Janka HDNS				973				

5.5 Future Work

Impregnation is a process that has been used for many years to chemically treat wood. Great benefits in the degradation control of the wood and many other properties may be obtained through impregnation. Even so, due to the high viscosity of most thermoset resins this method is not common with resins. The presented linseed based epoxy provides an alternative for impregnation with a reduced viscosity and excellent properties. The results reported show that very positive outcomes are obtained from the impregnation process but efforts need to be continued in order to optimize the process. A responsive automated temperature control system is necessary to obtain consistent repeatable results. The application of pressure will also improve the impregnation process and should be further evaluated. Only two preliminary experiments were generated with pressure applied during impregnation. These are shown on the end of Table 5-4. The first pressure run did not offer positive results. The reason was that high enough vacuums were not applied. When pressure is applied entrapped air forms air-pockets that result in bubbles when the pressure is released and temperature increased. Since our current accelerator needs curing temperatures of 150°C, when the material is heated after impregnation expanded air and resin are pushed out of the wood. Very inconsistent impregnation depths are obtained, as shown on Figure 5-26 (a). A trace of the impregnation depth has been provided because the resin color is similar to the wood making the impregnation hard to see. Additionally, some deeper areas that have been impregnated appear to be impregnated with low resin quantity noticed by a slight increase in density—as if most of the resin had been pushed out of the wood.

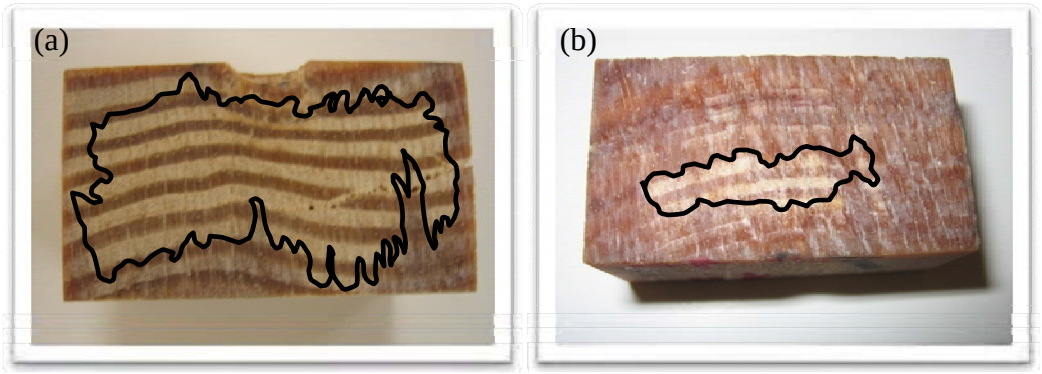

Figure 5-26. Pressure impregnations. (a) Inconsistent impregnation. (b) Deep pressure impregnation. Easily noticeable due to the dark resin color obtained with high humidity conditions.

On the contrary for the second pressure run, resin was maintained for a longer period of time curing at the lower impregnation temperature. This caused the resin's viscosity to increase so that it would not be easily removed from the wood. When this was done, as well as an appropriate vacuum, very deep impregnations were obtained as shown on Figure 5-26 (b).

In order to scale up the resin impregnation method, other variables have to be considered. Pressure application may induce extra costs therefore, studies targeting specific applications should be done and a minimum impregnation depth should be determined. Another important issue is that currently resin is cured by heat and all excess resin used during impregnation may not be reused. In order to account for this, UV-activated accelerators should be considered for resin impregnations. If the resin's viscosity may be increased by heat without inducing cure the material may be impregnated, all excess resin recollected, and the UV-light may be applied only to the samples to induce the curing.

Applying this material industrially requires much more variables to be analyzed. At the moment, the resin's color is affected by humidity. Figure 5-27 shows an example of material reacted at different humidity conditions. The possibility of using dyes to control or permit different wood finishes is something to consider. Thermal expansion coefficients between the resin and wood should be compared. Resistance to environmental conditions including, UV, water, and fungi should be studied. Finally, there is the possibility of a chemical interaction occurring between the wood and the resin which must be determined because such an interaction will greatly influence the final properties of the part. Systems such as IR and Raman may help in these analyses.

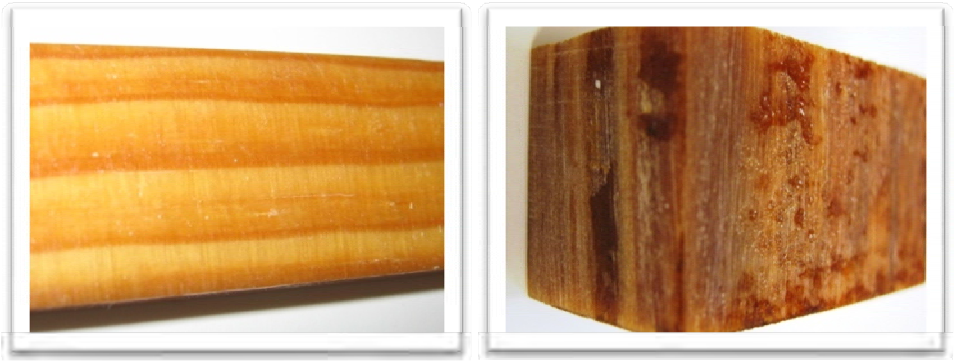

Figure 5-27. Difference in color due to humidity. 6% humidity (left). 40% humidity (right).

6 Conclusions

Numerous monitoring techniques are currently used to describe the curing behavior of thermosetting resins. Depending on the application and material being tested, each technique has its own benefits. A new cure monitoring system that incorporates the use of dispersive Raman with non-contact optics has been developed. It is demonstrated that dispersive Raman equipment may be used for online cure monitoring. Raman spectroscopy optics emitted through windows provide a “finger-print” of the molecular structure without ever having to be in contact or inside the resin’s cavity. By creating spectra in time, molecular changes that occur during the reaction are accurately monitored, and results used for the prediction of reaction rates and conversion. Actual material conversion is determined, with no need to normalize results with respect to a 100% conversion value. The laboratory scale reaction chamber constructed, to be used in conjunction with the Raman equipment, provided excellent results when monitoring thin accelerated *UP* resin samples. The high sensitivity temperature control system responds to direct sample temperature changes by use of a small thermocouple inserted in the middle of the sample. It was determined that DSC did not output the correct thermal behavior and was not able to control highly accelerated reactions. It was shown that there is a delay between the heating rate reported by the DSC and the real sample temperature due to heat transfer between surfaces and the low conductivity resin. The exothermic peak generated by the DSC was not coincident in time with the temperature rise of the sample during overheating, but was reported at a later time. The faster the heating rate the greater the delay. When high reaction rates occurred, overheating that was not shown in

the DSC heating rate output was observed in the actual sample temperature. Conversion curves of overheated samples also deviated from what was shown by Raman spectroscopy analysis. For samples with large overheating that were monitored with Raman, increases in reaction rates were comparable to DSC results but were maintained until a full conversion value was reached. Maximum conversion values never reach 100% conversion because some molecules end trapped between each other, never finding an active neighboring molecule. It was determined that for our particular resin, optimal thickness values that would allow monitoring reactions at constant heating rates were under 0.5mm for heating rates of 5-10K/min, and under 0.2mm for rates of 20K/min.

With the designed reaction chamber, pressure effects on the curing rate, reaction conversion, and mechanical properties were studied for pultrusion grade unsaturated polyester and coating grade epoxy. It was determined that a competing effect dominates highly accelerated unsaturated polyester curing reactions. Molecular mobility hinders the free-radical reaction, but pressure accelerates the reaction rate constants. With high enough pressure, the reaction rate constants may overcome molecular mobility effect. The addition cross-linking reaction of epoxy is accelerated by pressure. As pressure increases, reactive molecules are brought closer causing acceleration in the reaction rate. Final conversions were slightly higher for *UP* but no variation in final conversion could be determined for epoxy. Final mechanical properties of *UP* exhibit a maxima close to 1000psig. Hardness and modulus were found to increase with pressure until a certain value, where additional pressure would simply lower the properties. For the pressure

ranges studied, no definite conclusion could be obtained for changes in mechanical properties due to pressure on epoxy resin.

A wood-resin impregnation process was developed to improve the properties of lower cost softwoods. Optimal impregnation conditions can only be obtained with proper understanding of the curing behavior. Wood impregnation may be related to other composite preparation processes where fibers must be impregnated with resin. Viscosity and porosity are the main parameters that affect the impregnation process. A linseed based epoxy was used for impregnating thick sections of southern yellow pine. DSC experiments showed that a temperature of 80°C was adequate for impregnation. At this temperature, the resin would cure slow and allow enough preparation time for the impregnation process. Rheometry results showed that the lowest viscosity the material may be impregnated at, with our current process, is approximately 65mPa-s. The lowest viscosity attainable at a dynamic heating rate of 5K/min was found to be 18mPa-s. Therefore, with an automated process that reduces manual preparation steps impregnations at lower viscosities should be possible. Impregnation resulted in great enhancement in mechanical properties of the wood. DMA results showed that tension and compression modulus tripled. Hardness of the composite increased significantly. Depending on the depth of impregnation, values of hardness reached and surpassed 4500lbf, which is the estimated hardness of lignumvitae—one of the hardest woods available. Although more research has to be completed, impregnation of wood with linseed epoxy resin seems a viable technique to greatly improve properties of softwoods to the level of expensive hardwoods.

Appendix A

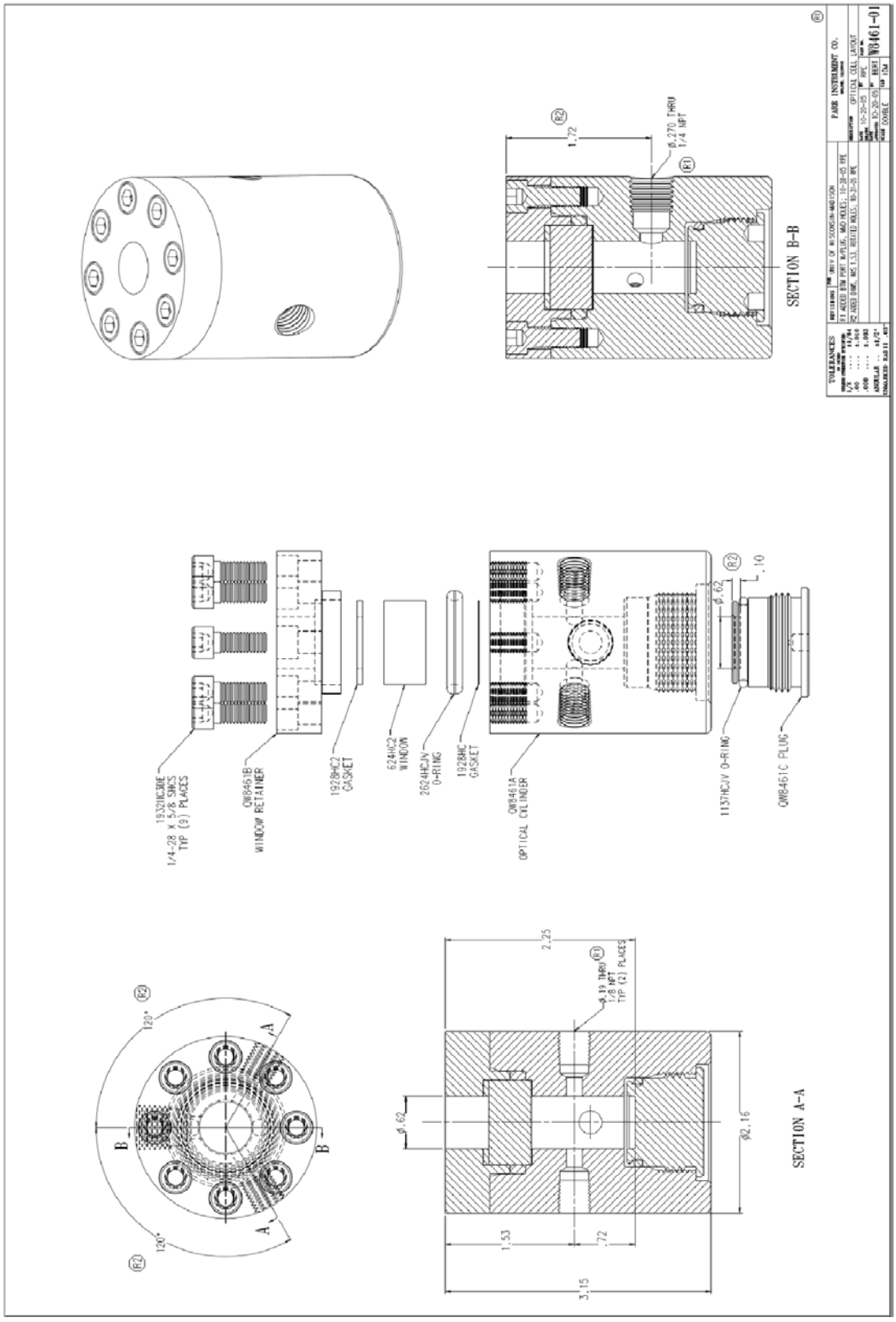
SECTION B-B
SECTION A-A
1932HC3DIE
1/4-28 X 5/8 SHCS
TYP (9) PLACES
QW8461B
WINDOW RETAINER
1928HC2
GASKET
624HC2
WINDOW
2624HCJV
O-RING
1928HC
GASKET
QW8461A
OPTICAL CYLINDER
1137HCJV O-RING
QW8461C PLUG
FARR INSTRUMENT CO.
W8461-01

Appendix B

Dimensional Analysis of the Impregnation Process

A dimensional analysis of the impregnation process was developed by Moritz Ruoff for this project. Dimensional analysis is used to reduce the number and complexity of variables in a process. Furthermore, dimensional analysis leads to dimensionless numbers that allow to easily scale the process. When dimensional analysis is used a system is adimensionalized by creating new dimensionless variables from groups of variables in the system. Physical problems are described by physical quantities. These quantities have respective dimensions, which can be shown in the basic quantities mass (M in kg), length (L in m), time (T in s) and temperature (Θ in K) for the SI-system.

The Π-theorem or Buckingham Π-theorem is a procedure to determine the dimensionless numbers out of the physical quantities which describe your process. The Π-theorem states that every system has m physical quantities. These are needed to describe the entire process. But these quantities can be reduced to a set of $m - n$ mutually independent dimensionless groups. In this case n is the number of basic quantities within the physical quantities. There are two ways to achieve the dimensionless Π-numbers. The first is via a linear system of equations, which becomes unclear with increasing physical quantities. The more common way is through a matrix transformation technique. In the dimensional matrix the SI quantities build the rows and the physical quantities build the columns. The matrix is then divided into a square core matrix with the repeating variables and a

residual matrix. During the analysis the core matrix is transformed into a unity matrix. The residual matrix performs exactly the same operations as the core matrix. Once the transformation is completed, the sets of dimensionless Π-numbers can be generated. For the impregnation process the following physical quantities were found to be most important in the process.

- Temperature ($\Delta\Theta$) – temperature directly affects the viscosity
- Time (t) – Infiltration depth is dependent on the time allotted for the material to be transported while viscosity will change in time due to cure and $\Delta\Theta$.
- Pressure (Δp) – the pressure difference drives the resin into the cavities.
- Permeability (P) – universal permeability, variable for wood type.
- Intrinsic permeability (κ) – the permeability properties of the wood in combination with the viscosity; relates to the ability of impregnating the wood.
- Viscosity (η) – Determinant factor in the infiltration process; $\eta=\eta(\Delta\Theta,t)$ and will have a great influence on the depth of impregnation.
- Temperature dependence of viscosity (a) = Relation that affects the processing times and variables and for a thermoset should include both the cure and temperature effect.
- Infiltration depth (δ) – the sought after quantity in the process. By working in the radial one-dimensional system, this quantity is simplified.
- Density (ρ) – the density of the wood combined with the permeability have an effect on the impregnation depth.

- Impregnation rate (u) – referent to the average flow rate of the resin into the solid. For the case of impregnation the value will be very small.

The core matrix for the infiltration process was set up with viscosity [η], density [ρ], time [t] and temperature [Δθ]. The residual matrix is made up of permeability [P], pressure difference [Δp], intrinsic permeability [κ], infiltration depth [δ], temperature dependence of viscosity [a] and the infiltration rate or flow rate [u]. This makes for $m = 10$ (physical quantities) and $n = 4$ (basic quantities) within the core and residual matrix:

$$\begin{array}{c|cccc|cccccc} & \eta & \rho & t & \Delta\Theta & P & \Delta p & \kappa & \delta & a & u \\ M & 1 & 1 & 0 & 0 & -1 & 1 & 0 & 0 & 0 & 0 \\ L & -1 & -3 & 0 & 0 & 3 & -1 & 2 & 1 & 0 & 1 \\ T & -1 & 0 & 1 & 0 & 1 & -2 & 0 & 0 & 0 & -1 \\ \Theta & 0 & 0 & 0 & 1 & 0 & 0 & 0 & 0 & -1 & 0 \end{array} \tag{A-1}$$

Therefore, six dimensionless numbers may be obtained with the dimensional analysis. The residual matrix after the transformation will then be:

$$\begin{array}{c|cccc|cccccc} & \eta & \rho & t & \Delta\Theta & P & \Delta p & \kappa & \delta & a & u \\ M & 1 & 0 & 0 & 0 & 0 & 1 & 1 & \frac{1}{2} & 0 & \frac{1}{2} \\ L & 0 & 1 & 0 & 0 & -1 & 0 & -1 & -\frac{1}{2} & 0 & -\frac{1}{2} \\ T & 0 & 0 & 1 & 0 & 1 & -1 & 1 & \frac{1}{2} & 0 & -\frac{1}{2} \\ \Theta & 0 & 0 & 0 & 1 & 0 & 0 & 0 & 0 & -1 & 0 \end{array} \tag{A-2}$$

The following dimensionless numbers are obtained: (A-3 to A-8)

$$\Pi_1=\frac{P}{\eta^0\cdot\rho^{-1}\cdot t^1\cdot\Delta\Theta^0}=\frac{P\cdot\rho}{t}\quad \Pi_2=\frac{\Delta p}{\eta^1\cdot\rho^0\cdot t^{-1}\cdot\Delta\Theta^0}=\frac{\Delta p\cdot t}{\eta}\quad \Pi_3=\frac{\kappa}{\eta^1\cdot\rho^{-1}\cdot t^1\cdot\Delta\Theta^0}=\frac{\kappa\cdot\rho}{\eta\cdot t}$$

$$\Pi_4=\frac{\delta}{\eta^{\frac{1}{2}}\cdot\rho^{-\frac{1}{2}}\cdot t^{\frac{1}{2}}\cdot\Delta\Theta^0}=\frac{\delta\cdot\sqrt{\rho}}{\sqrt{\eta}\cdot\sqrt{t}}\quad \Pi_5=\frac{a}{\eta^0\cdot\rho^0\cdot t^0\cdot\Delta\Theta^{-1}}=a\cdot\Delta\Theta\quad \Pi_6=\frac{u}{\eta^{\frac{1}{2}}\cdot\rho^{-\frac{1}{2}}\cdot t^{-\frac{1}{2}}\cdot\Delta\Theta^0}=\frac{u\cdot\sqrt{\rho}\cdot\sqrt{t}}{\sqrt{\eta}}$$

Π_5 is the dimensionless exponent of the equation for temperature dependence on viscosity.

$$\eta=\eta_0\cdot e^{-a\cdot\Delta\Theta} \tag{A-9}$$

where;

η: viscosity at the processing temperature

η_0: viscosity at Θ_0

ΔΘ: temperature difference between Θ_0 and processing temperature

a: coefficient of the temperature dependency

With Π_5 and Π_3 you can express a direct dimensionless relation between the infiltration depth and the porosity.

$$\frac{\Pi_5^{\,2}}{\Pi_3}=\frac{\delta^2\cdot\rho}{\eta\cdot t}\cdot\frac{\eta\cdot t}{\kappa\cdot\rho}=\frac{\delta^2}{\kappa} \tag{A-10}$$

This is a further dimensionless number called Π_7.

Due to the porous wood characteristics Darcy's law may be used for further calculations. Darcy's law (A-11) describes the flow of a fluid through a porous medium.

$$\bar{u} = -\frac{\kappa}{\eta}\frac{\partial p}{\partial x} \tag{A-11}$$

Where;

$\bar{u}$: the flux, the flow of fluid through an area in (l/t)

κ: permeability tensor of the porous medium

η: viscosity of the fluid

$\frac{\partial p}{\partial x}$: pressure gradient

In the case of the impregnation process, ∂x can be substituted with the infiltration depth in differential form ∂δ. Furthermore, the flux is the derivative of the infiltration depth over the time ∂t. Therefore, the adjusted form of Darcy's law for the infiltration process becomes:

$$\frac{\delta}{\partial t} = -\frac{\kappa}{\eta}\frac{\partial p}{\partial \delta} \tag{A-12}$$

For a short period of time during the impregnation which is done isothermally, and at low enough temperatures where the curing rate is very low, the viscosity may be assumed constant and the integration of equation A-12 leads to:

$$\frac{1}{2}\delta^2 = -\frac{\kappa}{\eta}\cdot\Delta p\cdot t \qquad \text{(A-13)}$$

A further transformation of equation (A-13) shows a relation between Π_7 and Π_2.

$$-\frac{1}{2}\frac{\delta^2}{\kappa} = \frac{\Delta p\cdot t}{\eta} \qquad \text{(A-14)}$$

with $\frac{\delta^2}{\kappa} = \Pi_7$ and $\frac{\Delta p\cdot t}{\eta} = \Pi_2$ equation (A-14) becomes:

$$-\frac{1}{2}\Pi_7 = \Pi_2 \qquad \text{(A-15)}$$

The permeability is related to the fluid and may be expressed with Π_1 and Π_3, which have been determined to be equal. The result is the relation between the intrinsic permeability and the viscosity of the fluid which is the term found in Darcy's law.

$$\Pi_1 = \Pi_3$$
$$\frac{P \cdot \rho}{t} = \frac{\kappa \cdot \rho}{\eta \cdot t}$$
$$P = \frac{\kappa}{\eta} \qquad \text{(A-16)}$$

Due to the fact that the flow rate is very low, other dimensionless numbers which might be actually necessary to describe a flow problem are negligible. For example the Reynolds number which can be described by;

$$Re = \Pi_4 \cdot \Pi_6 = \frac{\delta \cdot \sqrt{\rho}}{\sqrt{\eta} \cdot \sqrt{t}} \cdot \frac{u \cdot \sqrt{\rho} \cdot \sqrt{t}}{\sqrt{\eta}} = \frac{\delta \cdot \rho \cdot u}{\eta} \qquad \text{(A-17)}$$

$$with\, u \to 0\ follows\ Re \to 0$$

Other dimensionless numbers which are connected to the flow rate and are considered negligible as the Reynolds number are the Brinkmann, Euler, Eckert, and Froude number.

7 Bibliography

[1] Osswald, T. A., Baur, E., Brinkmann, S., Oberbach, K., and Schmachtenberg, E., "International Plastics Handbook", Hanser Gardner Publications, Inc., München, 902, (2006).

[2] Biron, M., "Thermosets and Composites: Technical Information for Plastics Users ", Elsevier, 536, (2003).

[3] Campbell, F. C., "Manufacturing Processes for Advanced Composites", Elsevier, 1, (2003).

[4] Davis, B. A., Gramman, P. J., Osswald, T. A., and Rios, A. C., "Compression Molding", Hanser Gardner Publications, Munich, 196, (2003).

[5] "IDES: The Plastics Web: Datasheets", *http://www.ides.com/*, (2008)

[6] Goodman, S. H., "Handbook of Thermoset Plastics", Second Edition, Noyes Publications, Westwood, New Jersey, 525, (1998).

[7] Koenig, J. L. and Shih, P. T. K., "Structure of Unsaturated Polyester Resins Cross-linked with Styrene as Studied by Raman Spectroscopy", *Journal of Polymer Science, A2*, **10**, 721, (1972).

[8] Osswald, T. A. and Menges, G., "Material Science of Polymers for Engineers", 2, Hanser Gardner Publications, Inc., Cincinnati, 334, (2003).

[9] Huang, Y.-J., Lu, T.-J., and Hwu, W., "Curing of Unsaturated Polyester Resins - Effects of Pressure", *Polymer Engineering and Science*, **33**, 1, 1, (1993).

[10] Gorovaya, T. A. and Korotkov, V. N., "Quick cure of thermosetting composites", *Composites Part A: Applied Science and Manufacturing (Incorporating Composites and Composites Manufacturing)*, **27**, 953, (1996).

[11] Huang, Y.-J. and Chen, C.-J., "Curing of unsaturated polyester resins: Effects of comonomer composition. II. High-temperature reactions", *Journal of Applied Polymer Science*, **47**, 9, 1533, (1993).

[12] Horie, K., Mita, I., and Kambe, H., "Calorimetric investigation of polymerization reactions. IV. Curing reaction of polyester fumarate with styrene", *Journal of Polymer Science Part A-1: Polymer Chemistry*, **8**, 10, 2839, (1970).

[13] Hill, R. R., Muzumdar, S. V., and Lee, J. L., "Analysis of Volumetric Changes of Unsaturated Polyester Resins During Curing", *Polymer Engineering and Science*, **35**, 10, 852, (1994).

[14] Yang, Y.-S. and Suspene, L., "Curing of Unsaturated Polyester Resin: Viscosity Studies and Simulations in Pre-Gel State", *Polymer Engineering and Science*, **31**, 5, 321, (1991).

[15] Young, R. A. and Lovell, P. A., "Introduction to Polymers", 2, Chapman and Hall, London, (1991).

[16] Felthouse, T. R., Burnett, J. C., Horrell, B., Mummey, M. J., and Kuo, Y.-J., "MALEIC ANHYDRIDE, MALEIC ACID, AND FUMARIC ACID", *http://www.huntsman.com/performance_products/Media/KOMaleic.pdf*, (2001)

[17] Hayes, B. T., Read, W. J., and Vaughan, L. H., "Some new chemical and physical aspects of polyester resin technology", *Chemistry and Industry*, 35, 1162, (1957).

[18] Cook, W. D. and Delatycki, O., "Re-examination of the Crosslinking Process in Styrene-Unsaturated Polyester Systems", *Journal of Macromolecular Science, Part A*, **12**, 5, 769 (1978).

[19] Skrifvars, M., Niemel, P., Koskinen, R., and Hormi, O., "Process Cure Monitoring of Unsaturated Polyester Resins,Vinyl Ester Resins, and Gel Coats by Raman Spectroscopy", *Journal of Applied Polymer Science*, **93**, 1285, (2004).

[20] Fink, J. K., "Reactive Polymers Fundamentals and Applications - A Concise Guide to Industrial Polymers", *3, Reactive Polymers Fundamentals and Applications - A Concise Guide to Industrial Polymers*, William Andrew Publishing Norwich, NY, 139, (2005).

[21] Hara, O., "Curing Agents for Epoxy Resin", *Three Bond Technical News*, 10, December 20 (1990)

[22] Lee, H. and Neville, K., "Handbook of Epoxy Resins", McGraw-Hill, New York, (1967).

[23] Fischer, W., Gabutti, C. A., Frischinger, I., and Wiesendanger., R., "Polymercaptopolyamines as epoxy resin hardeners", US Patent 6 759 506, Huntsman Advanced Materials Americas Inc., UT, USA, July 6, (2004)

[24] Miyashiro, J. J. and Seiling, A. W., "Epoxy compositions cured with carboxylic acid anhydrides and metallic salt of acetylacetone", US Patent 3 624 032 IL, USA, April 24, (1969)

[25] Decker, C., "The use of UV irradiation in polymerization", *Polymer International*, **45**, 2, 133, (1998).

[26] Cripps, D., "Guide to Composites-Epoxy Resins", *http://www.netcomposites.com/education.asp?sequence=11*,

[27] Naranjo, A., Noriega, M., Sierra, J. D., Roldán, A., and Osswald, T. A., "Testing and Characterization of Plastics - Industrial Applications", Hanser Publishers, Inc., Munich, (2008.).

[28] Dopico Garcia, M. S., Gonzalez Rodriguez, M. V., Diez Redondo, F. J., Lopez Lago, J., and Barrai Losada, L., "Kinetic of epoxy resin formation by high-performance liquid chromatography", *Journal of Applied Polymer Science*, **89**, 2, 497, (2003).

[29] Wu, L., Hoa, S. V., Minh, T., and Ton, T., "Effects of composition of hardener on the curing and aging for an epoxy resin system", *Journal of Applied Polymer Science*, **99**, 2, 580, (2006).

[30] Renault, T. and Ogale, A. A., "Photo dynamic mechanical analysis for cure monitoring of fiber reinforced photoresin composites", *Journal of Advanced Materials*, **28**, 1, 42, (1996).

[31] Maffezzoli, A., Quarta, E., Luprano, V. A. M., Montagna, G., and Nicolais, L., "Cure Monitoring of Epoxy Matrices for Composites by Ultrasonic Wave Propagation", *Journal of Applied Polymer Science*, **73**, 10, 1969, (1999).

[32] Cho, D., Choi, Y., and Drzal, L. T., "Simultaneous monitoring of the imidization and cure reactions of LaRC PETI-5 sized on a braided glass fabric substrate by dynamic mechanical analysis", *Polymer*, **42**, 4611, (2001).

[33] Lu, X.-D., Huang, Y.-D., Zhang, C.-H., and Sun, B.-H., "Investigation on curing kinetics and thermal properties of a novel epoxy resin system", *Guti Huojian Jishu/Journal of Solid Rocket Technology*, **30**, 2, 163, (2007).

[34] Gillham, J. K., "Review: Torsional Braid Analysis of Polymers",Defense Technical Information Center: Technical report, 41, (1973)

[35] Gillham, J. K., "The TBA torsion pendulum: a technique for characterizing the cure and properties of thermosetting systems", 262, (1997)

[36] Nunnery, L., "Tooling Innovations for Thermoset Molding",Technical Papers: Bulk Molding Compounds, Inc., 5,

[37] Kalenda, P., "Determination of the rate of hardening of unsaturated polyester by the measurement of the electric resistance", *Pigment and Resin Technology*, **33**, 1, 9, (2004).

[38] Kusterer, J. M., "What Wavelength Goes With a Color", *http://eosweb.larc.nasa.gov/EDDOCS/Wavelengths_for_Colors.html*, (2007)

[39] Dupuy, J., Adami, J., Maazouz, A., Sobotka, V., and Delaunay, D., "Kinetic Modeling of an Unsaturated Polyester Resin Using Two Complementary Techniques: Near-Infrared Spectroscopy and Heat Flux Sensors", *Polymer Engineering and Science*, **45**, 6, 846, (2005).

[40] Han, C. D. and Lem, K.-W., "Chemorheology of thermosetting resins. I. The chemorheology and curing kinetics of unsaturated polyester resin", *Journal of Applied Polymer Science*, **28**, 10, 3155, (1983).

[41] Yang, Y. S. and Lee, L. J., "Comparison of thermal and infrared spectroscopic analyses in the formation of polyurethane, unsaturated polyester, and their blends", *Journal of Applied Polymer Science*, **36**, 6, 1325, (1988).

[42] Penczek, P., Rudnik, E., Arczewska, B., and Ostrysz, R., "Curing of unsaturated polyester resins with low exotherm peak", *Die Angewandte Makromolekulare Chemie*, **229**, 1, 15, (1995).

[43] Zetterlund, P. B. and Johnson, A. F., "Free volume-based modelling of free radical crosslinking polymerisation of unsaturated polyesters", *Polymer*, **43**, 7, 2039, (2002).

[44] Prime, R. B., "Differential Scanning Calorimetry of The Epoxy Cure Reaction", *Polymer Engineering and Science*, **13**, 5, 365, (1973).

[45] Riccardi, C. C., Adabbo, H. E., and Williams, R. J. J., "Curing Reaction of Epoxy Resins with Diamines", *Journal of Applied Polymer Science*, **29**, 2481, (1984).

[46] Li, L., Cao, X., and Lee, J. L., "Kinetic Modeling of Unsaturated Polyester Resins at Low Temperatures", Center for Advanced Polymer and Composite Engineering (CAPCE), Ohio State University, Columbus, OH, 1, (2003)

[47] Kamal, M. R. and Sourour, S., "Kinetics and thermal characterization of thermoset cure", *Polymer Engineering and Science*, **13**, 1, 59, (1973).

[48] Huang, Y.-J. and Chen, C.-J., "Curing of unsaturated polyester resins - effects of comonomer composition. I. Low-temperature reactions", *Journal of Applied Polymer Science*, **46**, 9, 1573, (1992).

[49] Huang, Y.-J. and Chen, C.-J., "Curing of Unsaturated Polyester Resins--Effects of Comonomer Composition. III. Medium-Temperature Reactions", *Journal of Applied Polymer Science*, **48**, 151, (1993).

[50] Bilyeu, B., Brostow, W., Keselman, M., and Menard, K. P., "Characterization of Epoxy Curing Using High Heating Rate DSC", *Proceedings of the Society of Plastic Engineers ANTEC*, 1876, (2003).

[51] Costa, M. L., Pardini, L. C., and Rezende, M. C., "Influence of aromatic amine hardeners in the cure kinetics of an epoxy resin used in advanced composites ", *Materials Research*, **8**, 1, 65, (2005).

[52] Kiaee, L., Yang, Y. S., and Lee, L. J., "Effect of Low Profile Additives on the Morphology and Curing of Unsaturated Polyester Resins", *American Institute of Chemical Engineers, Symposium Series*, 52, (1988).

[53] Barbadillo, F., Losada, R., Suarez, M., Mier, J. L., Garcia, L., and Naya, S., "Study of a curing reaction of an epoxy resin", Leganes, Madrid, Spain, 2163, (2003).

[54] Barone, M. R. and Caulk, D. A., "The effect of deformation and thermoset cure on heat conduction in a chopped-fiber reinforced polyester during", *International Journal of Heat and Mass Transfer*, **22**, 7, 1021, (1979).

[55] Salla, J. M. and Ramis, X., "Comparative study of the cure kinetics of an unsaturated polyester resin using different procedures", *Polymer Engineering and Science*, **36**, 6, 835, (1996).

[56] Losada, R., Mier, J. L., Barbadillo, F., Artiaga, R., Varela, A., and Naya, S., "Study of the cure of a diglycidyl-ether of bisphenol-a (DGEBA)/ Triethylenetetramine (TETA) epoxy system by non-isothermal differential scanning calorimetry (DSC)", Aveiro, Portugal, 1094, (2006).

[57] Janeschitz-Kriegl, H., Wippel, H., Paulik, C., and Eder, G., "Polymer crystallization dynamics, as reflected by differential scanning calorimetry. Part 1: On the calibration of the apparatus", *Colloid & Polymer Science*, **271**, 12, 1107, (1993).

[58] Wu, C. H., Eder, G., and Janeschitz-Kriegl, H., "Polymer crystallization dynamics, as reflected by differential scanning calorimetry. Part 2: Numerical simulations", *Colloid & Polymer Science*, **271**, 12, 1116, (1993).

[59] Brame, J. E. G. and Graselli, J. G., *Infrared and Raman Spectroscopy*, Marcel Dekker, NewYork, 873, (1977).

[60] Pelletier, M. J., "Analytical Applications of Raman Spectroscopy", Blackwell Science, MA, 476, (1999).

[61] Lewis, I. R. and Edwards, H. G., "Handbook of Raman Spectroscopy: From the Research Laboratory to the Process Line", Marcel Dekker, Inc., New York, 1076, (2001).

[62] Farquharson, S., Bhat, S., Osbaldiston, R., DiTaranto, M., Smith, W., Rose, J., Liu, Y.-M., and Shaw, M., "Characterization of polymer composites by fiber optic Fourier transform Raman spectroscopy", *Proceedings of SPIE - The International Society for Optical Engineering*, **3535**, 303, (1999).

[63] Farquharson, S., Carignan, J., Khitrov, V., Senador, A., and Shaw, M., "Development of a phase diagram to control composite manufacturing using Raman spectroscopy", Providence, RI, United States, 19, (2004).

[64] Farquharson, S., Smith, W., Rigas, E., and Granville, D., "Characterization of polymer composites during autoclave manufacturing by Fourier transform Raman spectroscopy", Boston, MA, 103, (2001).

[65] Hong, K. C., Vess, T. M., Lyon, R. E., Chike, K. E., Aust, J. F., and Myrick, M. L., "Remote cure monitoring of polymeric resins by laser Raman spectroscopy", Anaheim, CA, USA, 427, (1993).

[66] Seo, Y., Lee, S. M., Kim, D. Y., and Kim, K. U., "Kinetic study of the imidization of a poly(ester amic acid) by FT-Raman spectroscopy", *Macromolecules*, **30**, 13, 3747, (1997).

[67] Younes, M., Wartewig, S., Lellinger, D., Strehmel, B., and Strehmel, V., "Curing of epoxy resins as studied by various methods", *Polymer*, **35**, 24, 5269, (1994).

[68] Lu, C. S. and Koenig, J. L., " Raman Spectra of Epoxy Resins", *American Chemical Society, Division of Organic Coatings and Plastic Chemistry*, **32**, 1, 112, (1972).

[69] Aust, J. F., Booksh, K. S., Stellman, C. M., Parnas, R. S., and Myrick, M. L., "Precise Determination of Percent Cure of Epoxide Polymers and Composites via Fiber-Optic Raman Spectroscopy and Multivariate Analysis", *Applied Spectroscopy*, **51**, 2, 247, (1997).

[70] Lyon, R. E., Chike, K. E., and Angel, S. M., "In situ cure monitoring of epoxy resins using fiber-optic Raman spectroscopy", *Journal of Applied Polymer Science*, **53**, 13, 1805, (1994).

[71] Rose, H., "In-situ cure monitoring of epoxy resin using Fiber Optic Raman Spectroscopy (FORS)", Anaheim, CA, USA, 277, (1998).

[72] Soares, L. E. S., Martin, A. A., and Pinheiro, A. L. B., "Degree of Conversion of Composite Resin: A Raman Study", *Journal of Clinical Laser Medicine and Surgery*, **21**, 6, 357, (2003).

[73] Musto, P., Abbate, M., Ragosta, G., and Scarinzi, G., "A study by Raman, near-infrared and dynamic-mechanical spectroscopies on the curing behaviour, molecular structure and viscoelastic properties of epoxy/anhydride networks", *Polymer*, **48**, 13, 3703, (2007).

[74] Gauthier, M. A., Stangel, I., Ellis, T. H., and Zhu, J. X., "New Method for Quantifying the Intensity of the C=C Band of Dimethacrylate Dental Monomers in their FTIR and Raman Spectra", *Polymeric Materials: Science & Engineering*, **93**, 630, (2005).

[75] Musick, J., Popp, J., Trunk, M., and Kiefer, W., "Investigations of Radical Polymerization and Copolymerization Reactions in Optically Levitated Microdroplets by Simultaneous Raman Spectroscopy, Mie Scattering, and Radiation Pressure Measurements", *Applied Spectroscopy*, **52**, 5, 692, (1998).

[76] Rose, J., Osbaldiston, R., Smith, W., Farquharson, S., and Shaw, M. T., "In-situ Monitoring of a Polymer Cure Using Dynamic Rheometry and Raman Spectroscopy", 714, (1998).

[77] Enns., J. B. and Gillham, J. K., "Time-Temperature-Transformation (TTT) Cure Diagram: Modeling the Cure Behavior of Thermosets", *J. Appl. Polym. Sci.*, **28**, 2567, (1983).

[78] Gilham, J. K., "Molecular Design of Thermosetting Systems: Evolution of Properties During Cure in Terms of Transitions", *Proceedings of the Society of Plastic Engineers ANTEC*, 0954, (2000).

[79] Atarsia, A. and Boukhili, R., "Relationship Between Isothermal and Dynamic Cure of Thermosets Via the Isoconversion Representation", *Polymer Engineering and Science*, **40**, 3, 607, (2000).

[80] Mele, V. B., Assche, V. G., and Hemelrijck, V. A., "Modulated Differential Scanning Calorimetry to Study Reacting Polymer Systems", *Proceedings of the Society of Plastic Engineers ANTEC*, 0363, (1998)

[81] Bilyeu, B. and Brostow, W., "Use of the Temperature-Modulated and Step-Scan DSC and DMA to Study Curing in an Epoxy Composite", *Proceedings of the Society of Plastic Engineers ANTEC*, 0852, (2001).

[82] Ramis, X. and Salla, J. M., "Time-temperature transformation (TTT) cure diagram of an unsaturated polyester resin", *Journal of Polymer Science, Part B: Polymer Physics*, **35**, 2, 371, (1997).

[83] Wacker, M. and Ehrenstein, G. W., "Investigations for the Numerical Determination of the TTT-Diagram for Unsaturated Polyester Resin Systems", *Proceedings of the Society of Plastic Engineers ANTEC*, 0081, (2001).

[84] Sbirrazzuoli, N., Vyazovkin, S., Mititelu, A., Sladic, C., and Vincent, L., "A Study of Epoxy-Amine Cure Kinetics by Combining Isoconversional Analysis with Temperature Modulated DSC and Dynamic Rheometry", *Macromolecular Chemistry and Physics*, **204**, 15, 1815, (2003).

[85] Hadiprajitno, S., Hernandez, J. P., and Osswald, T. A., "Developing Time-Temperature-Transformation Diagrams for Unsaturated Polyester using DSC Data", *Proceedings of the Society of Plastic Engineers ANTEC*, 1530, (2003).

[86] Dusek, K., Galina, H., and Mikes, J., "Features of network formation in the chain crosslinking (co)polymerization", *Polymer Bulletin*, **3**, 19, (1980).

[87] Yang, Y. S. and Lee, L. J., "Microstructure Formation in the Cure of Unsaturated Polyester Resins", *Polymer*, **29**, 10, 1793, (1988).

[88] Lohse, F., Schmid, R., Batzer, H., and Fisch, W., "Influence of Chemical Structure on the Morphology and Physical Properties of Cross-linked Macromolecules Synthesized by Polyaddition Reaction", **1**, 3, 110, (1969).

[89] Schmid, R., Lohse, F., Fisch, W., and Batzer, H., "Influence of the chemical structure on the morphology and physical properties of crosslinked macromolecules synthesized by polyaddition reaction", 30, 339, (1970).

[90] Skrifvars, M., Niemelä, P., Koskinen, R., and Hormi, O., "Process Cure Monitoring of Unsaturated Polyester Resins,Vinyl Ester Resins, and Gel Coats by Raman Spectroscopy", *Journal of Applied Polymer Science*, **93**, 1285, (2004).

[91] Boey, F. Y. C. and Lye, S. W., "Effects of vacuum and pressure in an autoclave curing process for a thermosetting fibre-reinforced composite", *Journal of Materials Processing Technology*, **23**, 2, 121, (1990)

[92] Lee, J. K. and Pae, K. D., "Effects of hydrostatic pressure on isothermal curing of an epoxy resin-amine system", **28**, 11, 323, (1990).

[93] Lee, J. K. and Pae, K. D., "Effects of hydrostatic Pressure on Curing of a DGEBA-DDS System", *Journal of Macromolecular Science, Part B: Physics*, **B32**, 1, 79, (1993).

[94] Odian, G. G., *Principles of Polymerization*, 3rd Edition, Wiley-Interscience, New York, 283, (1991).

[95] Baltá-Calleja, F. J. and Fakirov, S., "Microhardness of Polymers", 1, Cambridge University Press, 251, (2007).

[96] Low, I. M. and Shi, C., "Vickers indentation responses of epoxy polymers", *Journal of Materials Science Letters*, **17**, 14, 1181, (1998).

[97] Suwanprateeb, J., "A comparison of different methods in determining load- and time-dependence of Vickers hardness in polymers", *Polymer Testing*, **17**, 7, 495, (1998).

[98] Barbadillo, F., Losada, R., Suarez, M., Mier, J. L., Garcia, L., and Naya, S., "Study of a curing reaction of an epoxy resin", Madrid, Spain, 2163, (2003).

[99] Low, I. M., Paglia, G., and Shi, C., "Indentation responses of viscoelastic materials", *Journal of Applied Polymer Science*, **70**, 12, 2349, (1998).

[100] Olivier, L., Ho, N. Q., Grandidier, J. C., and Lafarie-Frenot, M. C., "Characterization by ultra-micro indentation of an oxidized epoxy polymer: Correlations with the prediction of a kinetic model of oxidation", *Polymer Degradation and Stability*, **93**, 489, (2008).

[101] Spychaj, S. and Balta Calleja, F. J., "Mechanical properties of hardened unsaturated polyester resins thickened with magnesium oxide", *Journal of Materials Science Letters*, **12**, 16, 1255, (1993).

[102] Clemons, C. M., "Woodfiber-Plastic Composites in the United States - History and Current and Future Markets", *3rd International Wood and Natural Fibre Composites Symposium*, Kassel / Germany, (2000).

[103] Rowell, R. M., "Handbook of Wood Chemistry and Wood Composites", CRC Press, Boca Raton, 487, (2005).

[104] Moustafa, A. B., Kandil, E. E., Hady, B. A., and Ghanem, N. A., "Some wood polymer composites ii", *Die Angewandte Makromolekulare Chemie*, **65**, 1, 121, (1977).

[105] West, J., William O., "Hardened wood flooring product", US Patent 6194078 Triangle Pacific Corporation, 1999

[106] Deka, M., Gindl, W., Wimmerb, R., and Christian, H., "Chemical modification of Norway spruce (Picea abies (L) Karst) wood with melamine formaldehyde resin", *Indian Journal of Chemical Technology*, **14**, 2, 134, (2007).

[107] Deka, M. and Saikia, C. N., "Chemical modification of wood with thermosetting resin: Effect on dimensional stability and strength property", *Bioresource Technology*, **73**, 2, 179, (2000).

[108] Gindl, W., Hansmann, C., Gierlinger, N., Schwanninger, M., Hinterstoisser, B., and Jeronimidis, G., "Using a water-soluble melamine-formaldehyde resin to improve the hardness of Norway spruce wood", *Journal of Applied Polymer Science*, **93**, 4, 1900, (2004).

[109] Mahmoud, A. A., Eissa, A. M. F., Omar, M. S., El-Sawy, A. A., and Shaaban, A. F., "Improvement of white pinewood properties by impregnation with thiourea-formaldehyde resin and orthophosphoric acid", *Journal of Applied Polymer Science*, **77**, 2, 390, (2000).

[110] Mourant, D., Yang, D.-Q., and Roy, C., "Decay resistance of pf-pyrolytic oil resin-treated wood", *Forest Products Journal*, **57**, 5, 30, (2007).

[111] Pittman, C. U., Jr., Kim, M. G., Nicholas, D. D., Wang, L., Ahmed Kabir, F. R., Schultz, T. P., and Ingram, L. L., Jr., "Wood enhancement treatments I. Impregnation of southern yellow pine with melamine-formaldehyde and melamine-ammeline-formaldehyde resins", *Journal of Wood Chemistry and Technology*, **14**, 4, 577, (1994).

[112] Shams, M. I., Kagemori, N., and Yano, H., "Compressive deformation of wood impregnated with low molecular weight phenol formaldehyde (PF) resin IV: Species dependency", *Journal of Wood Science*, **52**, 2, 179, (2006).

[113] Shams, M. I., Morooka, T., and Yano, H., "Compressive deformation of wood impregnated with low molecular weight phenol formaldehyde (PF) resin V: Effects of steam pretreatment", *Journal of Wood Science*, **52**, 5, 389, (2006

[114] Shams, M. I. and Yano, H., "Compressive deformation of wood impregnated with low molecular weight phenol formaldehyde (PF) resin II: Effects of processing parameters", *Journal of Wood Science*, **50**, 4, 343, (2004).

[115] Shams, M. I., Yano, H., and Endou, K., "Compressive deformation of wood impregnated with low molecular weight phenol formaldehyde (PF) resin I: Effects of pressing pressure and pressure holding", *Journal of Wood Science*, **50**, 4, 337, (2004).

[116] Shams, M. I., Yano, H., and Endou, K., "Compressive deformation of wood impregnated with low molecular weight phenol formaldehyde (PF) resin III: Effects of sodium chlorite treatment", *Journal of Wood Science*, **51**, 3, 234, (2005).

[117] Shi, J.-S., Li, J.-Z., Zhou, W.-R., and Zhang, D.-R., "Improvement of wood properties by urea-formaldehyde resin and nano-SiO2", *Beijing Linye Daxue Xuebao/Journal of Beijing Forestry University*, **28**, 2, 123, (2006).

[118] Wan, H. and Kim, M. G., "Impregnation of southern pine wood and strands with low molecular weight phenol-formaldehyde resins for stabilization of oriented strandboard", *Wood and Fiber Science*, **38**, 2, 314, (2006).

[119] Yano, H., Mori, K., Collins, P. J., and Yazaki, Y., "Effects of element size and orientation in the production of high strength resin impregnated wood based materials", *Holzforschung*, **54**, 4, 443, (2000).

[120] Moore, G. R., Kline, D. E., and Blankenhorn, P. R., "Impregnation of Wood with a High Viscosity Epoxy Resin", *Wood and Fiber Science*, **15**, 3, 223, (1983).

[121] Ibach, R. E., "Wood Handbook: Wood as an Engineering Material", *14*, *Wood Preservation*, U.S. Department of Agriculture, Madison, 26, (1999).

[122] Meylan, B. A. and Butterfield, B. G., "Three-Dimensional Structure of Wood; A Scanning Electron Microscope Study", 1rst, Syracuse University Press, Syracuse, NY, 80, (1972).

[123] "Wood Handbook: Wood as an Engineering Material", Forest Products Laboratory, U.S. Department of Agriculture, Madison, 26, (1999).

[124] Lu, J. and Wool, R. P., "Novel thermosetting resins for SMC applications from linseed oil: Synthesis, characterization, and properties", *Journal of Applied Polymer Science*, **99**, 5, 2481, (2006).

[125] Mosiewicki, M., Borrajo, J., and Aranguren, M. I., "Mechanical properties of woodflour/linseed oil resin composites", *Polymer International*, **54**, 5, 829, (2005).

[126] Mosiewicki, M., Aranguren, M. I., and Borrajo, J., "Síntesis y Polimerización de Maleatos Monoglicéridos a partir de Aceite de Lino", *Argentine-Chilean Polymer Symposium*, 142, (2003).

[127] Can, E., Küsefoglu, S., and Wool, R. P., "Rigid, thermosetting liquid molding resins from renewable resources. I. Synthesis and polymerization of soy oil monoglyceride maleates", *Journal of Applied Polymer Science*, **81**, 1, 69, (2001).

[128] Green, D. W., Begel, M., and Nelson, W., "Janka Hardness Using Nonstandard Specimens", *Forest Products Laboratory Research Note FPL–RN–0303*, (2006).